

Hobby

Ionospheric and Tropospheric Corrections for the DeltaT File

Anthony Minter

96 May 14

OVLBI-ES MEMO NO. 62

ABSTRACT

In this memo we review the corrections for ionospheric and tropospheric propagation effects that need to be applied to the DELTAT data. TEC data collected at Boulder, Co. from 1980 through 1992 is used to illustrate the range and variations of the ionospheric corrections which need to be made to the DELTAT file. We also use this TEC data to compare the performance of two ionospheric models which could be used in the DELTAT program if no TEC data is available to the GBES. A review of the methods presented by L. D'Addario and J. Springett for making the DeltaT corrections is also presented. It is found that corrections for the non-reciprocity of the ionosphere and troposphere need to be made in order to produce the best coherence factors possible.

Overview

At the GBES the TWT subsystem will measure the residual phase in the two way signal from the GBES to VSOP and back to the GBES. These residual phases arise mainly due to three factors: 1) tropospheric propagation effects 2) ionospheric propagation effects and 3) errors in the predicted orbit. The timing errors that need to be corrected for at the spacecraft are the result of the phase residuals on the uplink signal path, which to first order is half of the total round trip phase residual. Since the ionosphere and troposphere create different phase residuals for the uplink and downlink signal we must correct for these non-reciprocities in order to determine the true timing corrections at the spacecraft.

Desired Accuracy of Corrections

It is desirable to produce the longest possible coherence times at the correlator. This results in having as small an RMS in the spacecraft timing errors as possible. In order to achieve a coherence factor of 99% at 22 GHz, the timing RMS variations must be less than 6 psec.

Ionospheric Corrections

Ground based VLBI observations can ignore ionospheric delay effects which create phase errors when correlating the data. For the observations with VSOP and RadioAstron, however, the effects of the ionosphere, at least for the data from the satellites, must be removed in order to maintain the coherence times obtained with ground based VLBI on baselines involving the satellite. The special treatment for the ground telescope to the spacecraft baselines (ground-space baselines) arises from the structure of the ionosphere.

We now introduce the following picture of the ionosphere in order to help us understand

why we need to correct the ground-space baselines. Since the sun is the dominant source of ionization in the ionosphere, the ionosphere can be thought of as being static (for short time periods - generally a few days) in a reference frame where the x axis extends from the Earth to the Sun, the z axis points towards the North ecliptic pole and the y axis lies in the plane of the ecliptic. In this reference frame the electron density in the ionosphere is constant with time at any given point. Since the Earth rotates in this reference frame, a person on the Earth will observe changes in the ionosphere when looking at a constant azimuth and elevation as the Earth rotates and different parts of the ionosphere are observed. This view of the ionosphere is the same as saying that the ionosphere is attached to the celestial sphere (to first order) and is constant over several days time.

We have used the term constant rather loosely in the above description of the ionosphere with the intention of meaning that the general characteristics of the ionosphere are not quickly changing. There will be short-lived events which will cause small changes in the ionosphere such as traveling ionospheric disturbances (TIDS). Typically TIDS are acoustic-gravity waves in the upper atmosphere. These TIDS generally have length scales of 100-200 km, time scales of 10-20 minutes and cause variations in the total electron content (TEC) of the ionosphere from 0.5% up to 5%. During times when there are storms in the ionosphere and during periods after solar flaring events the ionosphere can be even more dynamic.

A ground based telescope which looks at one astronomical source for a length of time will see very little change in the ionosphere for a given 5-10 minute period of time. Thus the ionosphere produces a nearly constant phase error during this time. This is because the ionosphere rotates with the celestial sphere and the ground based telescope will be looking through the same part of the ionosphere for the duration of the observations. Thus, to first order the ionosphere is constant during this period for a ground based telescope. The only changes in the ionosphere that the telescope will see will be due such phenomena as TIDS propagating past the line of sight.

For the tracking of the spacecraft things will be different. The spacecraft will move across the celestial sphere during the observations. The ground tracking stations will therefore observe the spacecraft moving through different parts and structures of the ionosphere, such as the sudden decline of the ionosphere after sunset. If no ionospheric corrections are applied to the spacecraft data, this will result in spacecraft timing errors which can also be viewed, to first order, as phase errors in the spacecraft data. These phase errors will be rapidly varying due to the spacecraft's motion. The coherence time for the ground-space baselines will thus be shorter than the ground-ground baselines if the ionospheric effects are not corrected for in the spacecraft timing. This results from the fact that the ionosphere observed from the ground station to the spacecraft will vary more rapidly than will the ionosphere observed by a ground based antenna looking at an astronomical source. If the line of sight from the ground station to the spacecraft happens to enter sunset in the ionosphere during only part of an observation, then variations of ~ 10 psec in the spacecraft timing occur if no corrections are applied to the TWT data. This results in a coherence factor of 97% at 22 GHz. These fluctuations arise from structures which can easily be model and can thus the fluctuations can easily be removed from the spacecraft timing. *It is thus imperative that the ionospheric effects be corrected for in the DELTAT file in order to produce the best possible coherence factors.*

Fluctuations in the spacecraft timing due to TIDS are uncorrectable since the TIDS cannot be

modeled. We can, however, estimate their effect on the coherence of ground-space baselines. Consider the worst case tracking pass were VSOP reaches perigee at the zenith. VSOP can move ~ 900 km perpendicular to the line of sight in 100 seconds. This corresponds to the line of sight vector from the ground station to VSOP having moved through ~ 300 km in the ionosphere in 100 seconds. Thus VSOP may have moved through several TIDS during a period while ground based observations have remained coherent. With the ionosphere creating timing corrections due to non-reciprocity in the most active ionosphere of up to 600 psec (see below), this results in variations of up to 30 psec in the spacecraft timing by quickly passing through these TIDS (which have been assumed to create 5% fluctuations). A 30 psec RMS error in the timing corresponds to a coherence factor at 22 GHz of only 80% at the correlator. Under more common circumstances were the satellite is not at perigee at zenith and the non-reciprocity of the ionosphere creates a timing correction of 100 psec, the RMS error in the spacecraft timing will be 0.5 – 5 psec due to fluctuations in the ionosphere.

Non-Reciprocity of the Ionosphere

In OVLBI-ES memo 38 a correction for the DELTAT file is outlined which is due to the non-reciprocity of the ionosphere for the uplink and downlink signals when communicating with the satellite. We will now briefly review this correction.

For a signal propagating one way through the ionosphere at a frequency ν , the ionosphere adds an extra path length of

$$L = \frac{e^2}{8\pi^2\epsilon_0 m_e \nu^2} N \quad 1$$

where e and m_e are the electron's charge and mass respectively, ϵ_0 is the permittivity of free space and N is the line of sight total electron content. A round trip signal from the GBES to the spacecraft and back to the GBES will use different frequencies for the uplink and downlink signal so that the round trip delay, in terms of the extra pathlength, due to the ionosphere is

$$L_i = \frac{e^2}{8\pi^2\epsilon_0 m_e} \left(\frac{N^{up}}{\nu_{up}^2} + \frac{N^{down}}{\nu_{down}^2} \right) = 40.3 \left(\frac{N^{up}}{\nu_{up}^2} + \frac{N^{down}}{\nu_{down}^2} \right) \text{ meters} \quad 2$$

where the frequencies are given in Hz and N^{up} and N^{down} are the total electron contents in m^{-2} on the uplink and downlink paths, respectively. The total round trip delay is measured by the TWT subsystem. The correction that is inserted into the DELTAT file is the delay for the uplink signal. To first order this value is half of the measured delay from the TWT subsystem for the two way signal. However, a correction to this needs to be made since the ionosphere produces different delays for the uplink and the downlink signals. This correction (ϵ_i) amounts to being half of the difference in the ionospheric uplink and downlink delays:

$$\epsilon_i = \frac{40.3}{2c} \left(\frac{N^{up}}{\nu_{up}^2} - \frac{N^{down}}{\nu_{down}^2} \right) \text{ seconds} \quad 3$$

where c is the speed of light.

Elevation Dependence of $N(z)$

During the round trip time of the two-way phase transfer (< 1 sec) we can consider the ionosphere to be "frozen" so that a simple model of the zenith angle dependence N can be

used. Since the peak densities in the ionosphere occur at heights from 200 to 400 km above the Earth's surface, a simple $\sec z$ law for $N(z)$ does not work well near the horizon. A modified version of the $\sec z$ law which takes into account the Earth's curvature and the height of the ionospheric slab (the height of the peak densities) works quite well. This model has the following form

$$N(z) = N(z = 0^\circ) \sec z_i \quad 4$$

where $\sec z_i$ is the elevation angle of the line of sight relative to the ionospheric slab and is given by

$$\sin e_i = \left(\frac{R_\oplus}{R_\oplus + h_i} \right) \sin e \quad 5$$

where R_\oplus is the Earth's radius and h_i is the height of the ionospheric slab. Thompson, Moran and Swenson (1986) compare this model for the elevation dependence of the line of sight TEC versus ray-tracing calculations in their figure 13.13. For elevations above ten degrees this model works extremely well. There is a slight deviation between the model and the ray-tracing below ten degrees and only amounts to a $\sim 6\%$ error at the horizon. This model of the elevation dependence of $N(z)$ will be applied to the zenith TEC values predicted by the various ionospheric models.

Tropospheric Corrections

The GBES weather station periodically measures the temperature (T), dew point (D) and pressure (P) at the GBES. These values can then be used with a model of the troposphere to estimate the tropospheric non-reciprocity DELTAT correction outlined in OVLBI-ES memo 38. The water vapor pressure (P_w) at the GBES can be determined as follows:

$$P_w = \exp \left[\frac{17.27 * D}{237.3 + D} + 1.81 \right] \text{ mb} \quad 6$$

where D is in Centigrade. The excess path length along the line of sight to the satellite due to the troposphere is then given by the Smith-Weintraub equation in conjunction with a cubic $\sec z$ correction (Thompson et al. 1986):

$$L_t = \frac{75000 P_w \sec z}{T^2} (1 - 0.0003 \tan^2 z) + 0.228 P \sec z (1 - 0.0013 \tan^2 z) \text{ cm} \quad 7$$

where T is in Kelvin, P and P_w are in millibars. This equation is accurate to $z \sim 80^\circ$ (Thompson et al. 1986). This model for the troposphere will not be able to make corrections for such tropospheric features as thunderstorms and weather fronts.

The tropospheric correction to the DELTAT file (ϵ_t) arises from the fact that the satellite's elevation axis changes during the time that it takes the signal to propagate from the GBES to the satellite and back to the GBES. This correction is given by the total tropospheric delay times the time derivative of the tropospheric delay:

$$\epsilon_t = \frac{L}{c} \frac{dL_t}{dt} = \frac{L}{c^2} L_t(z = 0^\circ) \frac{\sin z}{\cos^2 z} \frac{dz}{dt} = \frac{L_t^{up} - L_t^{down}}{2c}. \quad 8$$

Under the worst weather conditions at Green Bank, $T = 21^\circ C$ and 100% humidity and $P = 920 \text{ mb}$, the total tropospheric delay is $\sim 74.6 \text{ nsec}$. This is a factor of 100 greater than

the delay claimed in OVLBI-ES memo 38 and is possibly explained by the exclusion of the dry tropospheric path length from the calculations in OVLBI-ES memo 38. For the worst case scenario, VSOP passing directly overhead with perigee occurring at the horizon, this correction corresponds to

$$\epsilon_t < 8.0 \text{ psec.} \quad 9$$

The weather station data from the GBES will allow the tropospheric correction term to be known to within 10%. This corresponds to an error of $< 0.8 \text{ psec}$ due to the wet troposphere and a coherence factor $> 99.98\%$. The 1% accuracy of the Smith-Weintraub equation (Thompson et al. 1986) results in an error of $< 1 \text{ psec}$ in the tropospheric correction term. Under normal circumstances, the spacecraft will not be observed near perigee and the tropospheric correction term will be $\leq 2 \text{ psec}$, with corresponding errors being $\leq 1 \text{ psec}$.

Ionospheric Data Sources

Ionosphere corrections to the DELTAT file will be made using various models. These models can be classified into several groups depending on the level of sophistication of the model. All of these models, however, require some input describing the state of the ionosphere.

Ionospheric data for use at the GBES will possibly be obtained from JPL. In this model, a global map of TEC versus geographic latitude and fixed solar longitude will be produced at regular intervals. The line of sight TEC value (N) to the satellite is found from these maps by approximating the ionosphere as a thin slab at a given height. Determining the sub-ionospheric point on the path from the ground station to the satellite, the zenith TEC value at the sub-ionospheric point is readily measured from the map. A correction for the elevation of the line of sight through the thin slab will then give the line of sight TEC value. The ionospheric data from JPL will arise from global GPS ionospheric measurements and not having a GPS receiver in Green Bank capable of making these measurements will have no effect on the results. These ionospheric measurements will be good to better than $5 \times 10^{16} \text{ m}^{-2}$. This is the most sophisticated model being considered and provides for the effects of non-local ionospheric effects via the global GPS measurements.

Another possible source of ionospheric TEC data is from pulsar monitoring programs. The 85-3 telescope in Green Bank is used to monitor pulsars on a daily basis. From pulsar rotation measure observations it should be possible to determine the ionospheric rotation measure along the line of sight to the pulsar. The ionospheric zenith TEC in Green Bank can then be determined from this data allowing the line of sight TEC to the spacecraft to be estimated. This method should produce TEC values with errors of $\leq 10^{16} \text{ m}^{-2}$. Although this method provides real time measurements of the ionosphere at Green Bank, it does not allow for the determination of other non-local ionospheric structures due to the lack of global measurements. However, the error in not being able to determine the non-local structure of the ionosphere is small ($< 5\%$). Therefore, obtaining data on the ionosphere from a global network of GPS receivers only provides a marginal gain over determining the TEC from the pulsar monitoring.

If ionospheric measurements are not available to the GBES then the corrections must be made relying on simplistic models of the ionosphere that generally have only the average sunspot number as an input. These models typically are good to within $2 \times 10^{17} \text{ m}^{-2}$, four times worse than the accuracy of the GPS measurements. There are typically two types

of these simplistic ionospheric models. The first predicts the zenith TEC value for a given geographical location. The second produces predicted ionospheric electron density profiles versus height for a given geographical location.

The tropospheric data will arise from measurements of the temperature, pressure and dewpoint made at the GBES. These values can easily be used to calculate the water vapor pressure at the GBES, allowing tropospheric corrections to be modeled. Non-local tropospheric effects can not be corrected for in this model due to the lack of non-local measurements. The weather measurements are currently made every ten minutes at the GBES.

Ionospheric Measurements at Boulder, Co. 1980-1992

Zenith TEC values were provided to NRAO for use in calibration of VLA data from Boulder, Colorado from 1980 through 1992. Boulder, Co. has almost the same latitude as Green Bank so these ionospheric data should represent the ionosphere seen from Green Bank reasonably well. These data consist of hourly measurements of the zenith TEC. These hourly measurements have been averaged for each month of each year and are presented in Figure 1. The inner error bars in Figure 1 represent the standard deviation of the daily values while the outer error bars represent the extremum for that month. The right side of these graphs presents the corresponding ionospheric DELTAT correction due to non-reciprocity at the horizon for VSOP in psec. For VSOP, the ionospheric non-reciprocity DELTAT correction at the horizon is

$$\epsilon_i \sim 3.0 \frac{N(e = 90^\circ)}{10^{16} m^{-2}} psec \quad 10$$

while the correction at the zenith is

$$\epsilon_i \sim 0.92 \frac{N(\bar{e} = 90^\circ)}{10^{16} m^{-2}} psec. \quad 11$$

Since the state of the ionosphere depends on the amount of solar activity, which is tied to the sunspot cycle, the TEC data for 1986 should be representative of how the ionosphere will appear in 1997 during VSOP's first year of astronomical observations.

An error of $5 \times 10^{16} m^{-2}$ in the zenith TEC thus results in an error of 15 psec at the horizon and 4.6 psec at the zenith for VSOP. The $\sim 6\%$ error in using the sec z_i law at the horizon can give rise to another 1 psec error.

Evaluation of Ionospheric Models

We have chosen two ionospheric models for comparison with the measured Boulder, Co. TEC data. The first model was developed by Chiu (1975) and predicts the zenith TEC value for a given sunspot number, time and geographic location. The second model is the International Reference Ionosphere (IRI) which produces a predicted electron density profile of the ionosphere for a given sunspot number, time and geographic location (Bilitza 1985). The TEC is then found by integrating over this electron density profile. In Table 1 we present a comparison of the IRI model with the measured TEC values and in Table 2 we present a comparison of the Chiu model with the measured TEC values. The data were compared for every hour of every day for a single year. In the tables, the first column is the year. The

second column give the average deviation of the model from the measured data:

$$\alpha = \frac{1}{N} \sum_1^N [TEC(measured) - TEC(model)] , \quad 12$$

where N is the number of data points. A nonzero value of α indicates a systematic error in the model estimate of the TEC. The third column gives the standard deviation of the mean

$$\sigma = \sqrt{\frac{\sum_1^N [TEC(measured) - TEC(model)]^2}{N - 1}} \quad 13$$

between the model and the data. The fourth, fifth and sixth columns list the fractional error below which 50% (ϵ_{50}), 75% (ϵ_{75}), and 90% (ϵ_{90}) of the data occur. The fractional error is defined as

$$\epsilon = \frac{|TEC(model) - TEC(measured)|}{TEC(measured)} . \quad 14$$

The seventh column lists the Kolmogorov-Smirnov statistic which is a measure of the greatest distance between the distributions of TEC in the measured data and the modeled data (Press *et al.* 1989). The eighth column gives the linear correlation coefficient (γ) between the model TEC values and the measured TEC values.

As can be seen from Tables 1 and 2, the IRI model provides a better prediction of the ionospheric TEC than does the Chiu model. The TEC values predicted by the IRI model have a higher correlation with the measured TEC values than do the Chiu TEC values in all years except one. In 1984 the Chiu model and the IRI model had the same correlation coefficient. In all cases the IRI model had a smaller standard deviation than did the Chiu model. During periods of enhanced solar activity the IRI model performs significantly better than the Chiu ionospheric model. At solar minimum the two models become comparable although the IRI model still generally has a smaller standard deviation and larger correlation coefficients than the Chiu model. The IRI model, however, requires up to 1000 times the computational time that the Chiu model requires.

Total Error Budget

As discussed above, the ionospheric TEC values can fluctuate by 0.5 – 5%. Thus the ionospheric correction term will have the 0.5 – 5% fluctuations in it. This is presumably the limiting factor in determining the TEC through GPS receivers. We can thus expect under normal circumstances an RMS in the timing of < 1.5 – 15 *psec* at the horizon and < 0.5 – 5 *psec* at the zenith if TEC measurements are used. We thus expect a coherence factor at 22 GHz of 95% (99%) due to the ionosphere at the horizon (zenith) when TEC measurements are available. We are assuming the coherence factor is given by

$$e^{-\frac{\tau_{RMS}^2 \nu^2}{2}} \quad 15$$

where τ_{RMS} is RMS fluctuations in the time corrections. All listed coherence factors will be for 22 GHz unless otherwise stated. If measured TEC values are not available, we can estimate the worst case coherence factor using a TEC value of $5 \times 10^{18} m^{-2}$. The 5% fluctuations result in a timing RMS of 75 *psec* at the horizon and 23 *psec* at the zenith.

Table 1: Comparison of predicted TEC from the IRI ionospheric model with the measured TEC values at Boulder, Co.

Year	α (10^{13}cm^{-2})	σ (10^{13}cm^{-2})	ϵ_{50}	ϵ_{75}	ϵ_{90}	K-S	γ
1980	0.10	0.80	0.18	0.32	0.47	0.07	0.90
1981	0.10	0.88	0.24	0.42	0.60	0.13	0.90
1982	0.17	0.72	0.22	0.40	0.58	0.07	0.91
1983	0.17	0.49	0.30	0.51	0.75	0.13	0.85
1984	-0.01	0.41	0.27	0.44	0.65	0.08	0.85
1985	0.10	0.26	0.31	0.58	1.13	0.20	0.78
1986	0.19	0.25	0.39	0.77	1.25	0.26	0.83
1987	-0.03	0.23	0.23	0.43	0.62	0.09	0.85
1988	-0.20	0.59	0.27	0.44	0.61	0.18	0.89
1989	-0.03	0.85	0.24	0.42	0.60	0.18	0.91

Table 2: Comparison of predicted TEC from the Chiu ionospheric model with the measured TEC values at Boulder, Co.

Year	α (10^{13}cm^{-2})	σ (10^{13}cm^{-2})	ϵ_{50}	ϵ_{75}	ϵ_{90}	K-S	γ
1980	0.36	1.03	0.31	0.54	0.84	0.11	0.82
1981	0.52	1.08	0.34	0.58	0.91	0.14	0.86
1982	0.48	0.91	0.32	0.58	0.93	0.12	0.87
1983	0.17	0.57	0.36	0.59	0.87	0.12	0.77
1984	-0.01	0.41	0.29	0.48	0.73	0.13	0.85
1985	0.06	0.30	0.36	0.64	1.04	0.11	0.71
1986	0.14	0.28	0.38	0.69	1.10	0.22	0.74
1987	-0.04	0.25	0.28	0.51	0.72	0.14	0.83
1988	-0.05	0.68	0.28	0.47	0.65	0.17	0.84
1989	0.22	1.15	0.36	0.62	0.89	0.14	0.81

The coherence factors are then 88% at the zenith and 26% at the horizon. The ionosphere, however, only rarely exceeds a TEC of $1 \times 10^{18} \text{ m}^{-2}$ which results in an RMS of 25 *psec* at the horizon with a coherence factor of 86%. *Measured TEC values thus greatly increases the coherence of the data obtained with VSOP.*

The worst case tropospheric timing fluctuation would occur when either the uplink (downlink) path passed through a thunderstorm while the downlink (uplink) did not. A 1 *km* cloud with a water vapor density of 1 g m^{-3} results in an excess wet path length of 4 *mm* (Thompson, Moran and Swenson). A typical thunderstorm can reach altitudes of 30000 *ft* (9 *km*) so that that a timing error of 60 *psec* occurs in the troposphere giving a coherence factor of only 42%. Typically, such an occurrence will be very rare. Tropospheric fluctuations are generally of the order of 0.01% which results in an RMS timing error of $\sim 0.5 \text{ psec}$ and a coherence factor $> 99\%$.

It should thus be possible to provide timing corrections such that the coherence factor for the spacecraft data greater than 0.95 except under extreme conditions.

Methods of Implementation of DELTAT Corrections

Two different methods of computing the DELTAT corrections have been proposed by L. D'Addario and J. Springett. We now briefly review these different methods and how they will be implemented.

Springett's Correction

In the correction proposed by J. Springett, no time dependent corrections are applied to the TWT residual phase data. The TWT phase residuals are split into a slowly varying and a rapidly varying component. The DELTAT value is then calculated as

$$\Delta T = \frac{\tau_{TWT}^{slow}}{2} + \mu \tau_{TWT}^{fast} \quad 16$$

where τ_{TWT} is the TWT residual time and μ is the constant which maximizes the coherence factor. This correction assumes that the slowly time varying propagation effects can be modeled as a polynomial up to a quadratic term. The time varying effects include changes due to the spacecraft's motion and also due to variations in the ionosphere and troposphere. The correlator is capable of fitting for a constant time offset and a term which changes linearly with time. It is assumed that any changes in the spacecraft timing due to the spacecraft's motion are linear during the integration time. However, since the changes in the spacecraft's motions produce quadratic and higher order terms in the DELTAT corrections, this approach introduces an unnatural upper limit to the coherence time of the spacecraft's observations. This process also provides the formidable task of splitting the TWT phase residuals into slow varying and rapidly varying components.

D'Addario's Correction

In the correction proposed by L. D'Addario, time dependent corrections due to the satellite's motion will be applied to the TWT residual phase data. These corrections are those discussed in this memo and in OVLBI-ES memo 38. In applying these corrections to the TWT phase residual data, the unnatural upper limit to the coherence time for the spacecraft

Table 3: Ionospheric and Tropospheric Delays and Corrections for VSOP

Observing Conditions					Delays		Corrections	
TEC	P	T	D	elevation	L_t^{up}	L_i^{up}	ϵ_t^{max}	ϵ_i
$10^{16} m^{-2}$	mb	C	C	deg	nsec	psec	psec	psec
10	920	21	15	5	86.1	186.7	7.5	30.0
10	920	21	15	30	15.0	102.2		16.4
10	920	21	15	60	8.7	65.3		10.5
10	920	21	15	90	7.5	57.4		9.2
50	920	0	-10	5	81.5	934	7.1	150
50	920	0	-10	30	14.2	511		82
50	920	0	-10	60	8.2	327		53
50	920	0	-10	90	7.1	287		46
100	920	-20	-25	5	80.4	1867	7.0	300
100	920	-20	-25	30	14.0	1022		164
100	920	-20	-25	60	8.1	653		105
100	920	-20	-25	90	7.0	574		92
200	910	-20	-25	5	79.3	3734	6.9	600
200	910	-20	-25	30	13.8	2044		328
200	910	-20	-25	60	8.0	1306		210
200	910	-20	-25	90	6.9	1148		184

data in Springett's method is removed. Thus the coherence time is naturally limited by the fluctuations in the troposphere and ionosphere. Also, the TWT timing residuals need not be split into various components.

In Table 3 we present estimates of the propagation effects due to the troposphere and the ionosphere under varying conditions. The observing conditions are given by the TEC, total atmospheric pressure, temperature, dewpoint and elevation angle of the satellite which are listed in columns one through five. The uplink delay introduced by the troposphere is listed in column 6 while the uplink delay for the ionosphere is listed in column 7. The non-reciprocity corrections for the troposphere and the ionosphere are listed in columns 8 and 9 respectively. It is seen that not correcting for these changes could limit the coherence of the observations.

How the GBES will apply the active corrections

The application of the non-reciprocity corrections is performed via a simple calculation. Since the ionosphere and troposphere are much closer to the GBES than the spacecraft, the ionospheric and tropospheric delays can be modeled as occurring at the uplink transmission time for the uplink signal and the downlink reception time for the downlink signal. The elevation angle of the spacecraft at the uplink and downlink times are easily determined from the "orbit file". The uplink and downlink delays for the troposphere and the ionosphere can then be easily determined from the available weather and ionospheric data. The non-reciprocity corrections are then easily determined by looking at the difference in the uplink and downlink delays for the troposphere and the ionosphere.

References

GBES memo 38, "Post-Pass Processing of Two-Way Timing Measurements" by Larry D'Addario

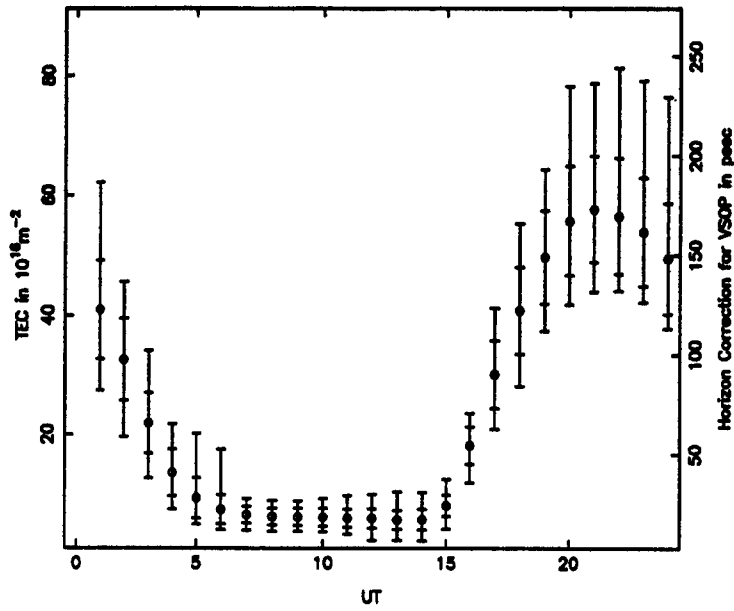
Thompson, Moran and Swenson, "Interferometry and Synthesis in Radio Astronomy", 1986, Krieger Publishing Company.

Chiu, Y.T. 1975, J. Atm. Terr. Phys., 35, 1615

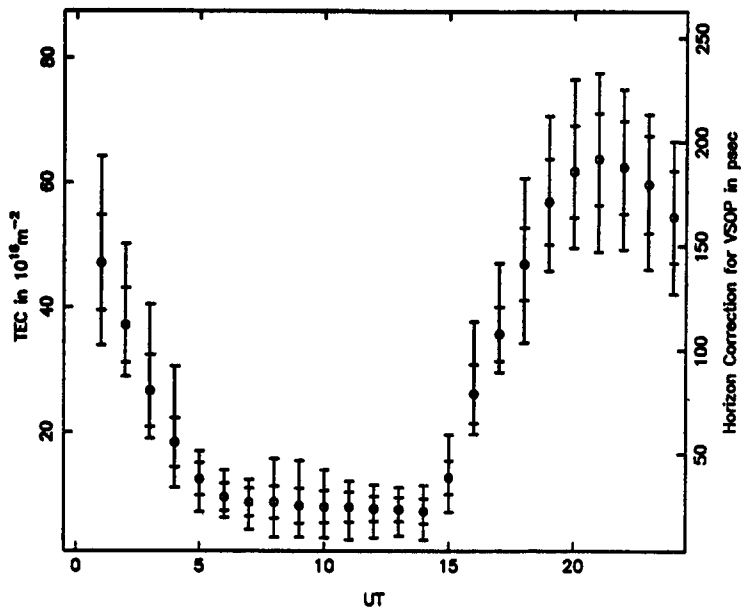
Bilitza, D. 1985, Adv. Space Res. 5, 15

Press, W.H., Flannery, B.P., Teulolsy, S.A. and Vetterling, W.T. 1989, "Numerical Recipes", Cambridge University Press

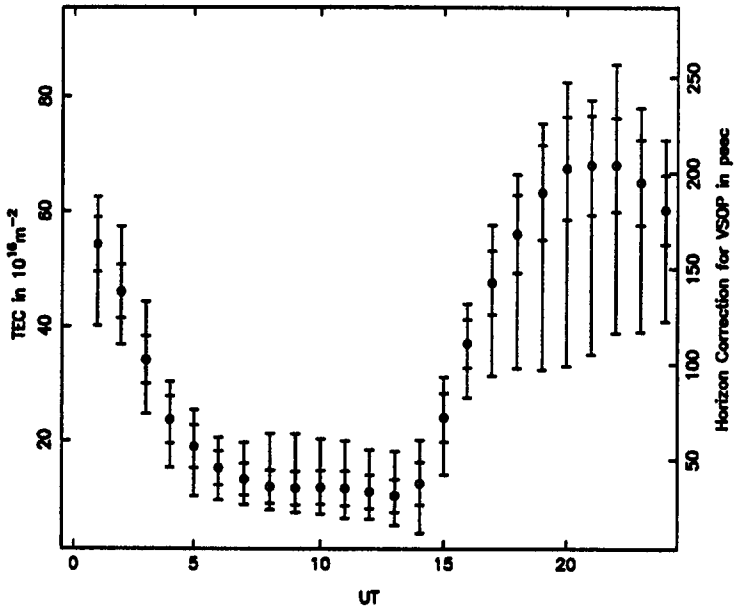
Monthly Averaged Boulder Zenith TEC: January 1980



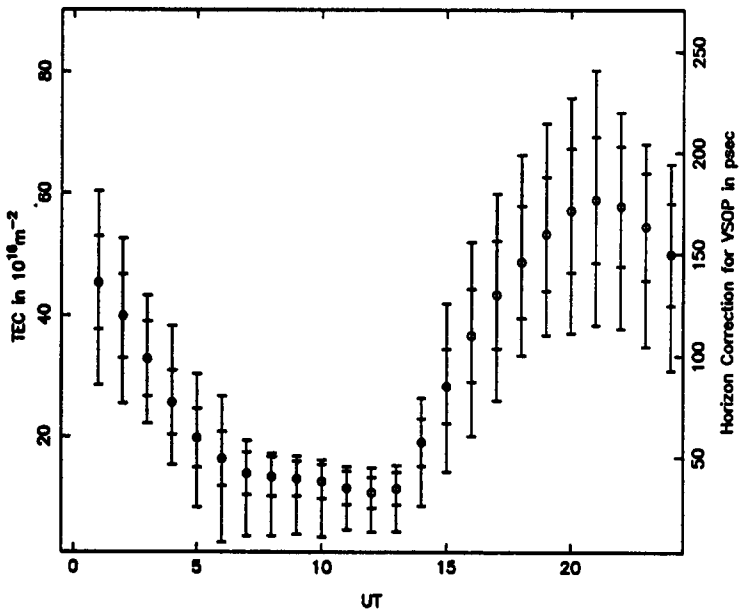
Monthly Averaged Boulder Zenith TEC: February 1980



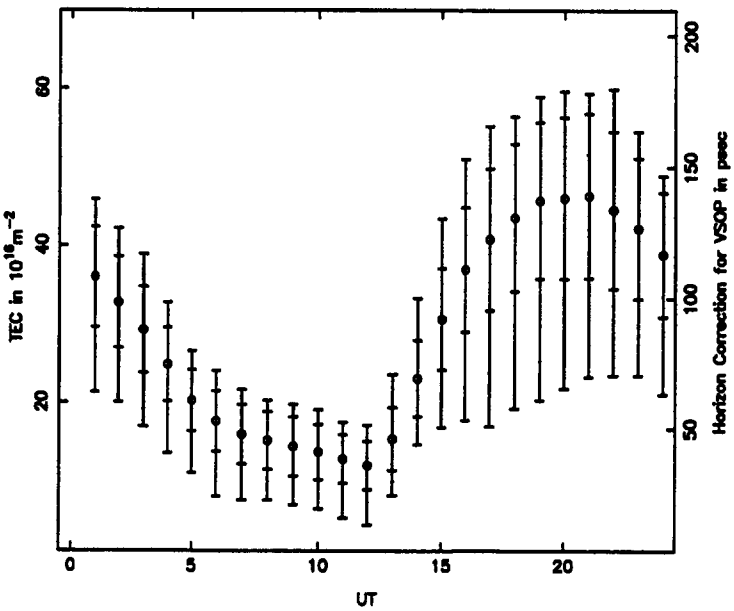
Monthly Averaged Boulder Zenith TEC: March 1980



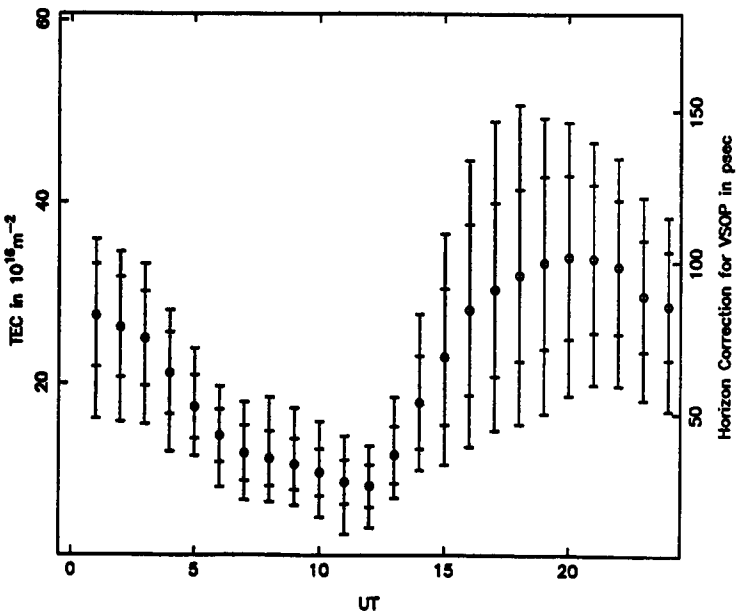
Monthly Averaged Boulder Zenith TEC: April 1980



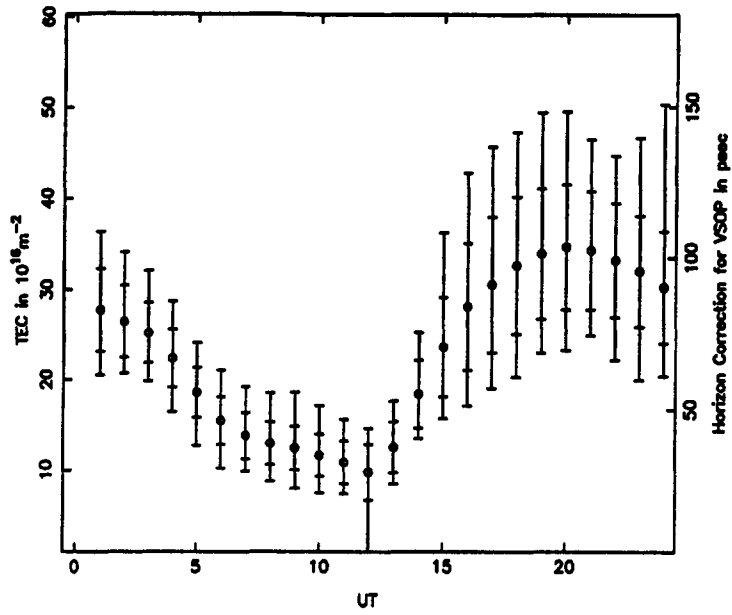
Monthly Averaged Boulder Zenith TEC: May 1980



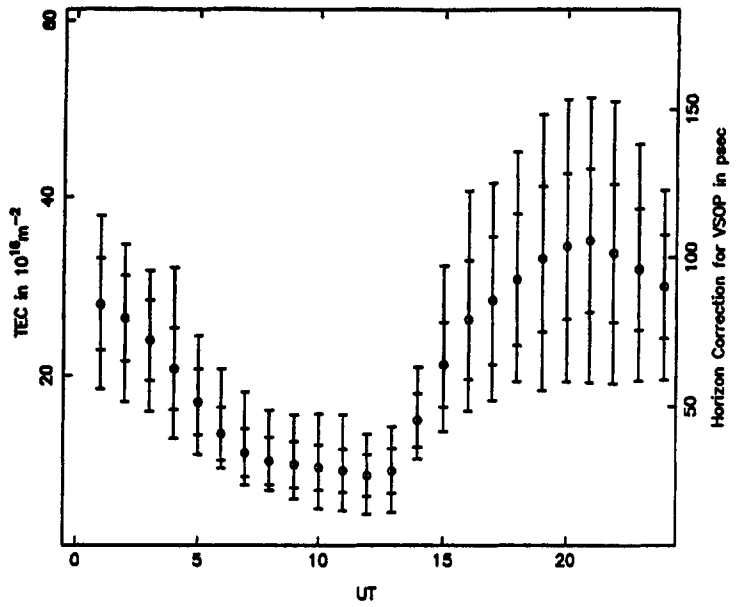
Monthly Averaged Boulder Zenith TEC: June 1980



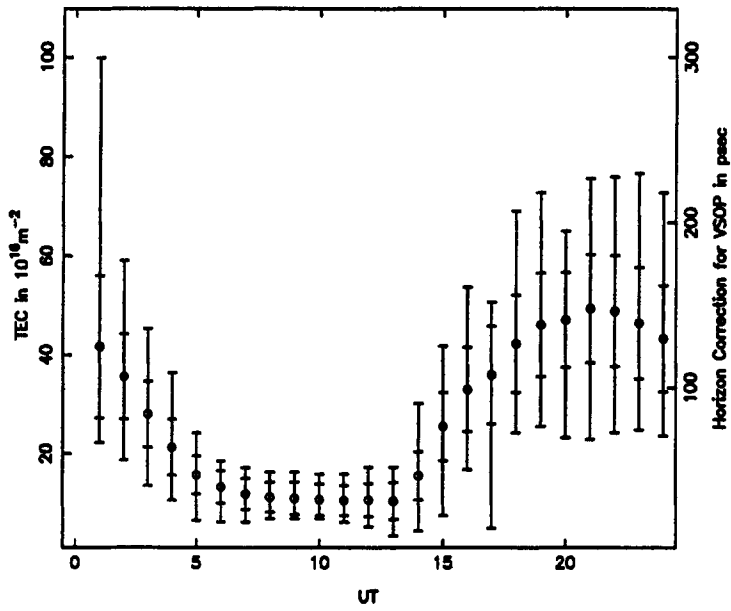
Monthly Averaged Boulder Zentith TEC: July 1980



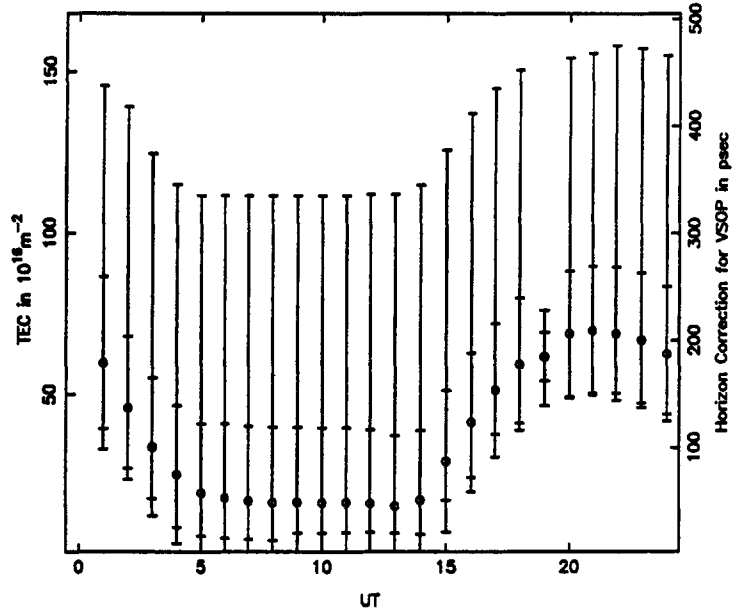
Monthly Averaged Boulder Zentith TEC: August 1980



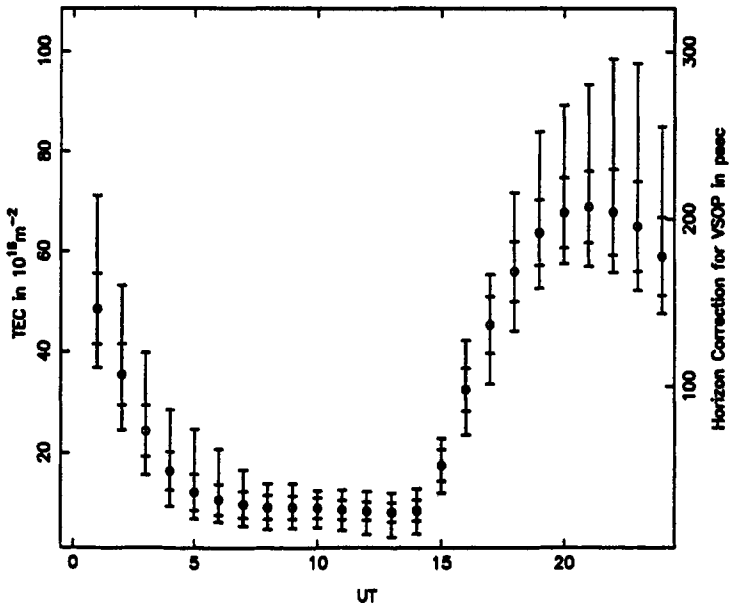
Monthly Averaged Boulder Zentith TEC: September 1980



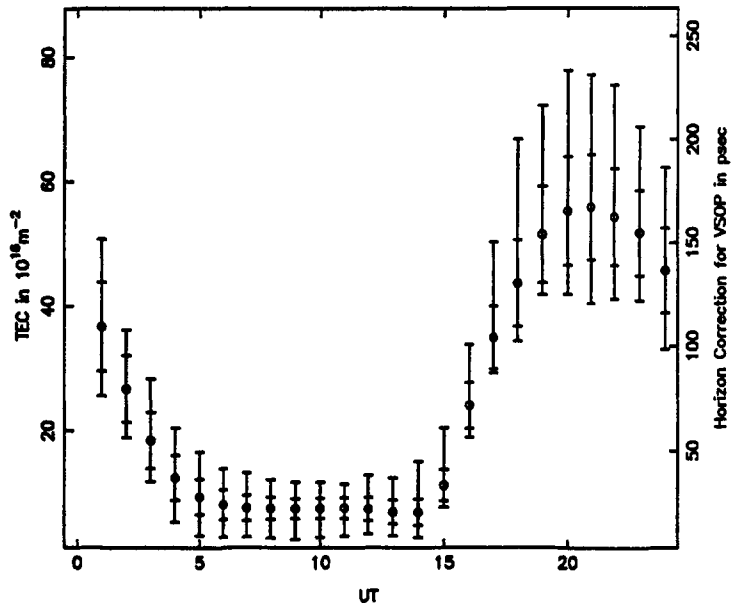
Monthly Averaged Boulder Zentith TEC: October 1980



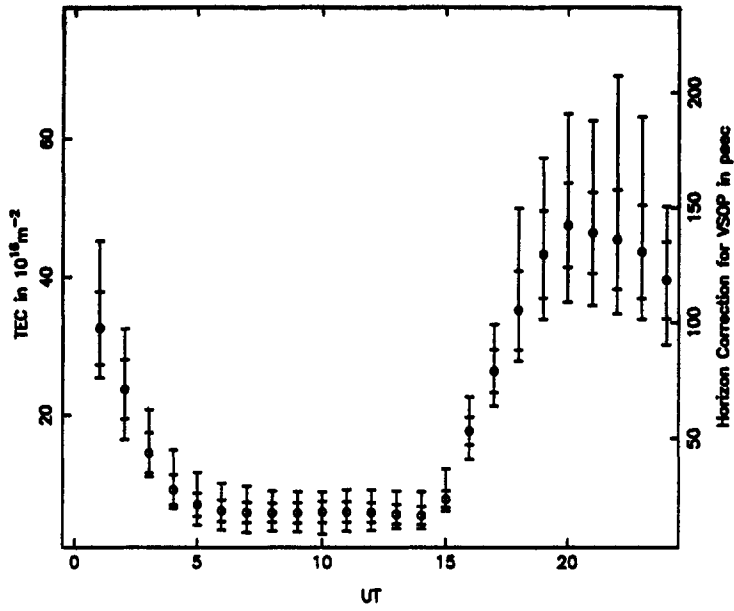
Monthly Averaged Boulder Zentith TEC: November 1980



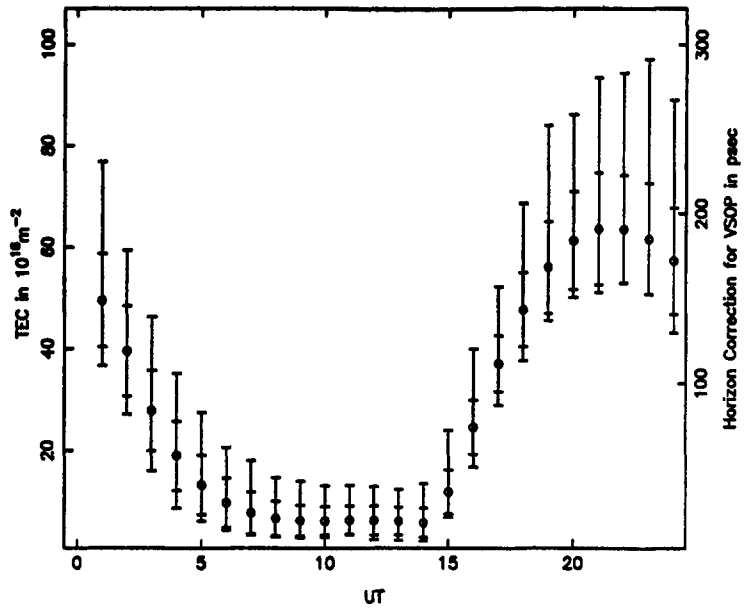
Monthly Averaged Boulder Zentith TEC: December 1980



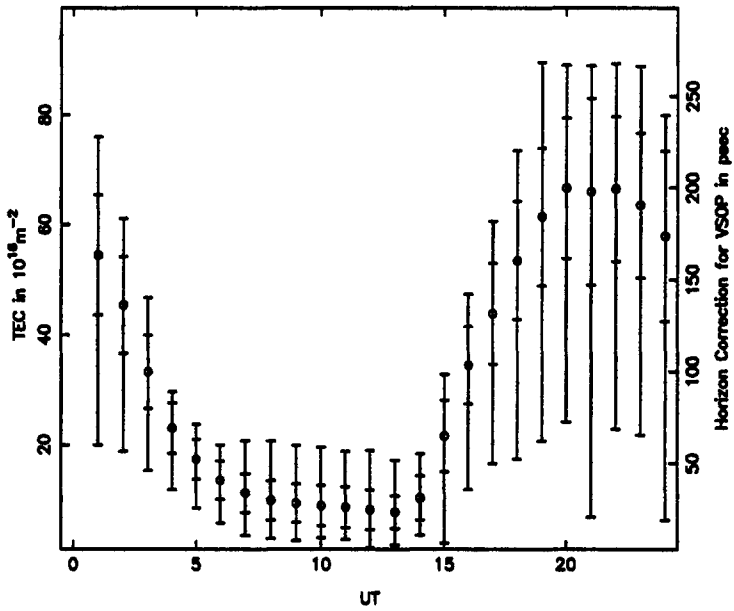
Monthly Averaged Boulder Zentith TEC: January 1981



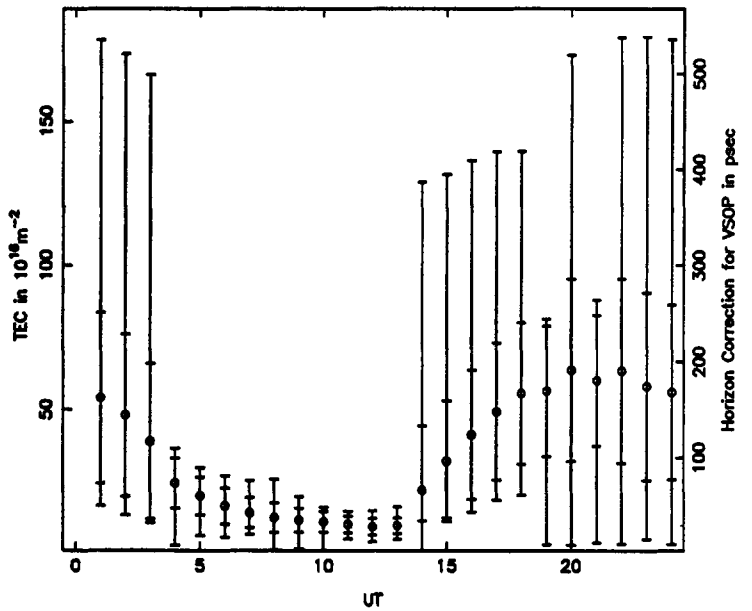
Monthly Averaged Boulder Zentith TEC: February 1981



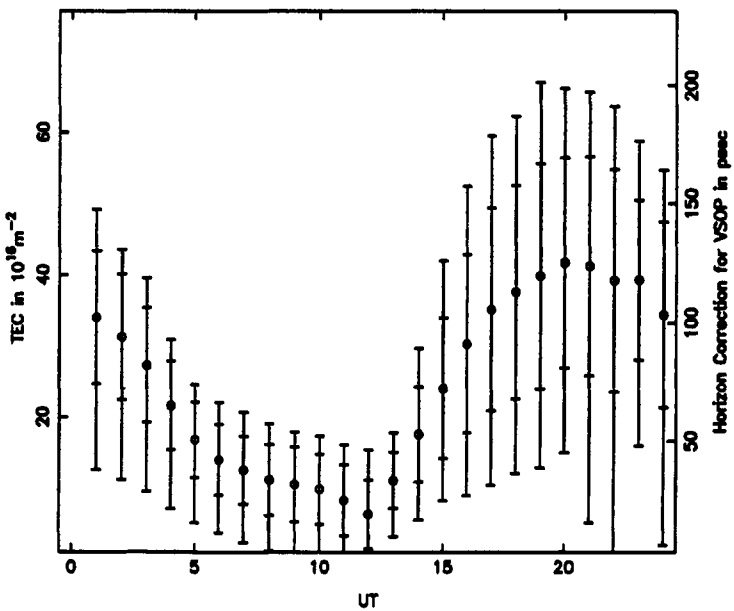
Monthly Averaged Boulder Zentith TEC: March 1981



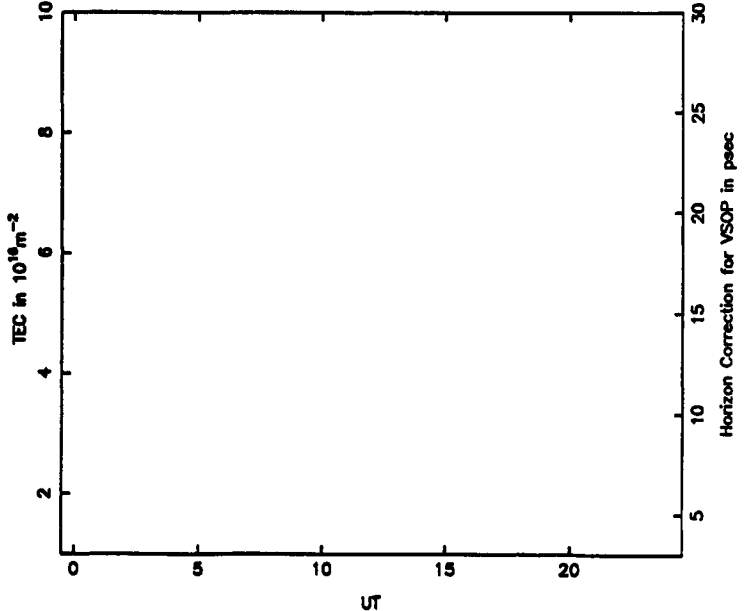
Monthly Averaged Boulder Zentith TEC: April 1981



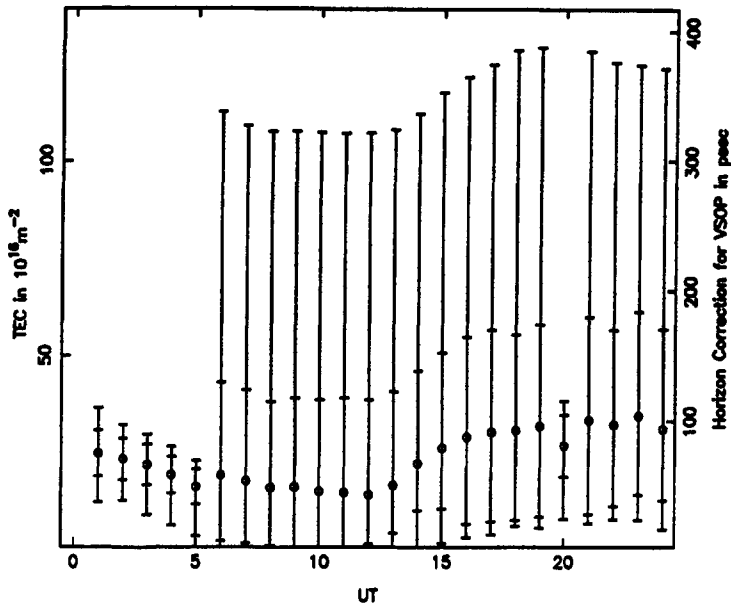
Monthly Averaged Boulder Zentith TEC: May 1981



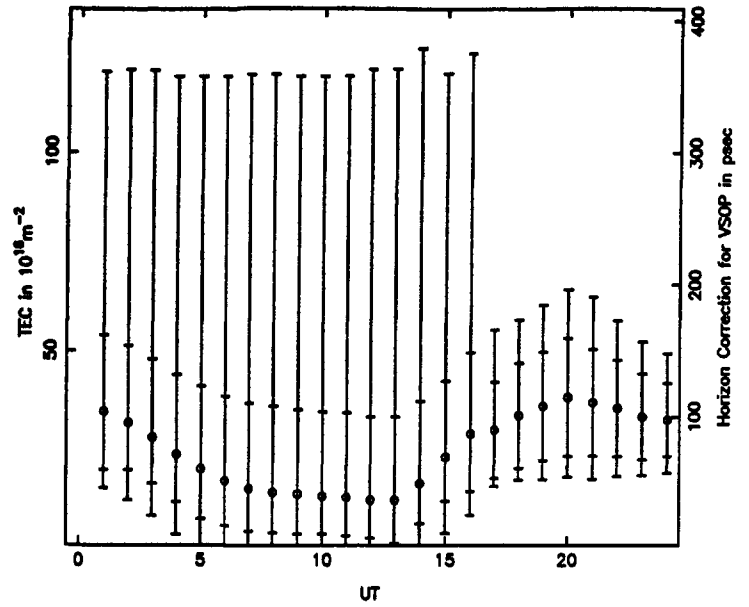
Monthly Averaged Boulder Zentith TEC: June 1981



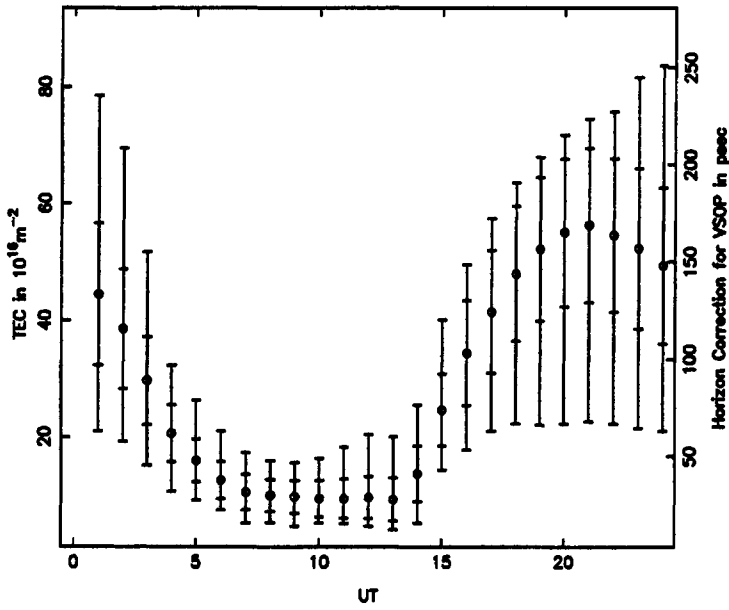
Monthly Averaged Boulder Zenith TEC: July 1981



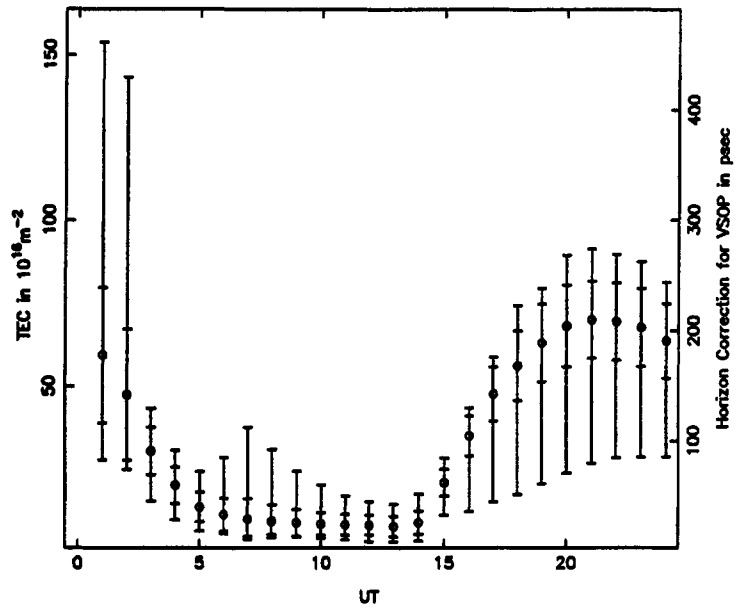
Monthly Averaged Boulder Zenith TEC: August 1981



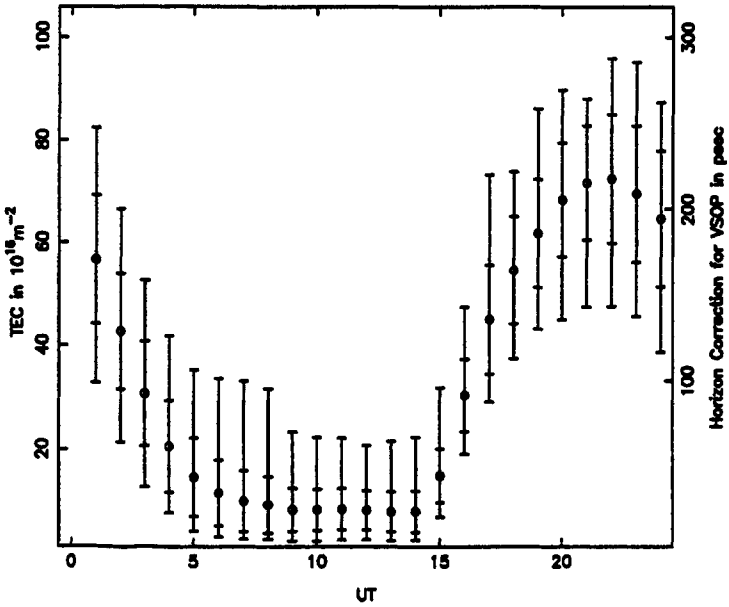
Monthly Averaged Boulder Zenith TEC: September 1981



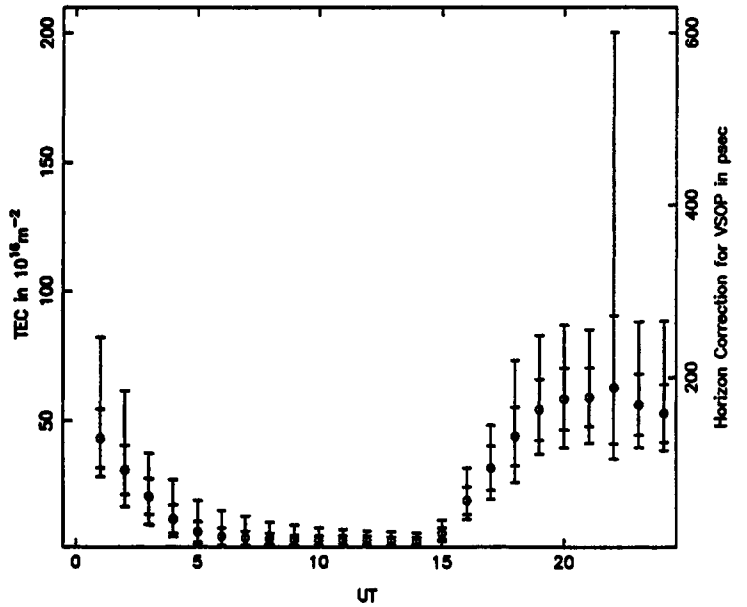
Monthly Averaged Boulder Zenith TEC: October 1981



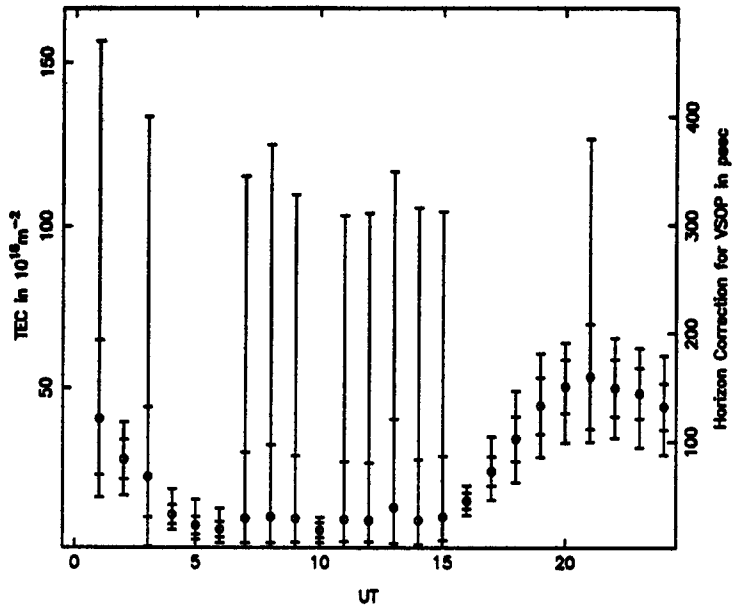
Monthly Averaged Boulder Zenith TEC: November 1981



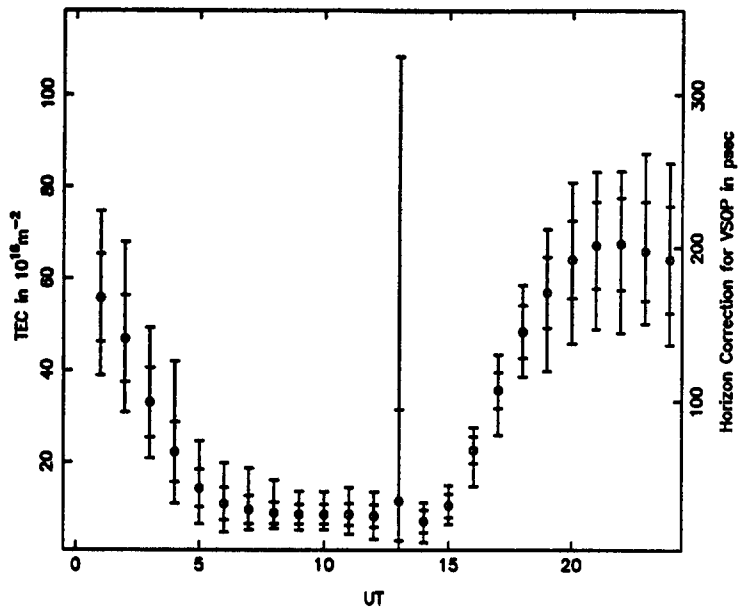
Monthly Averaged Boulder Zenith TEC: December 1981



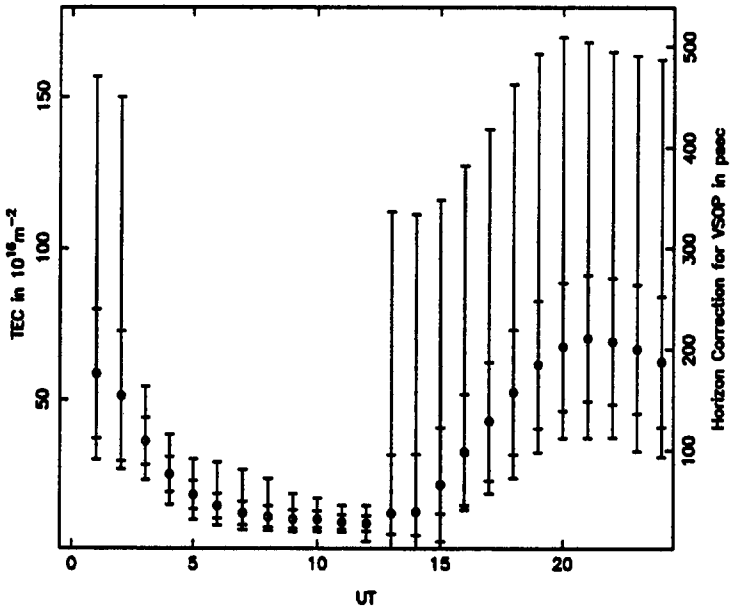
Monthly Averaged Boulder Zentith TEC: January 1982



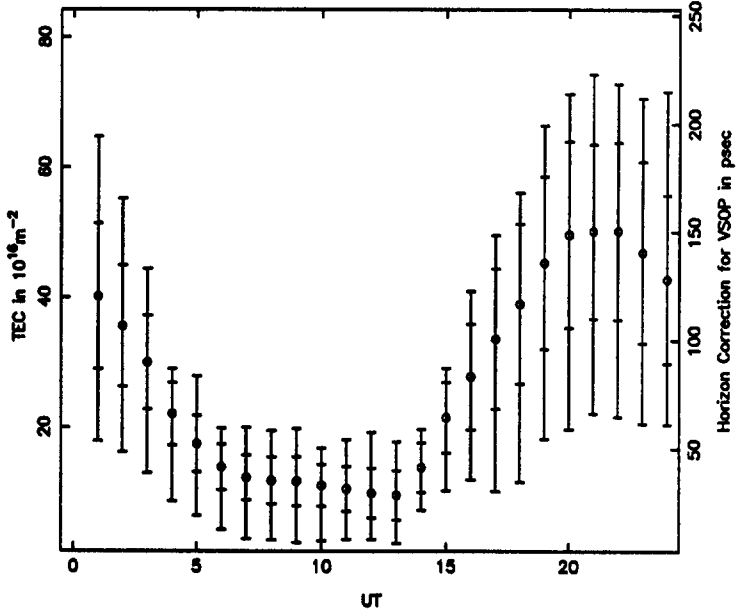
Monthly Averaged Boulder Zentith TEC: February 1982



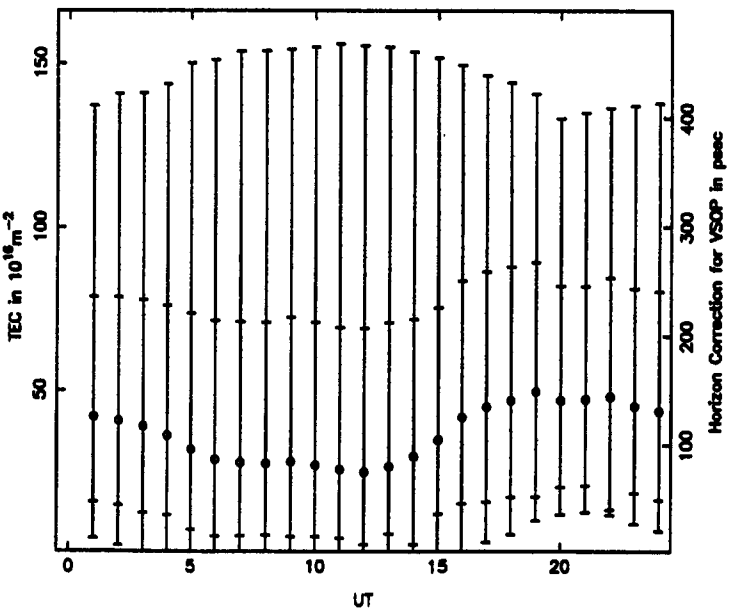
Monthly Averaged Boulder Zentith TEC: March 1982



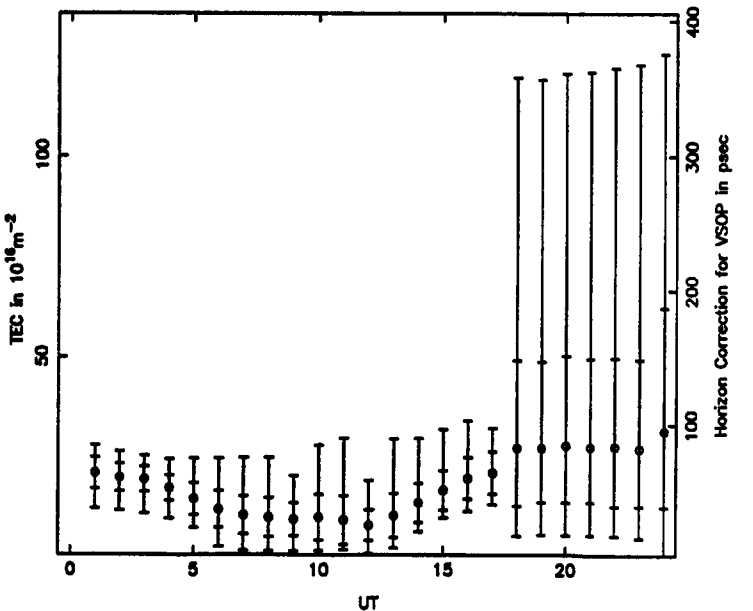
Monthly Averaged Boulder Zentith TEC: April 1982



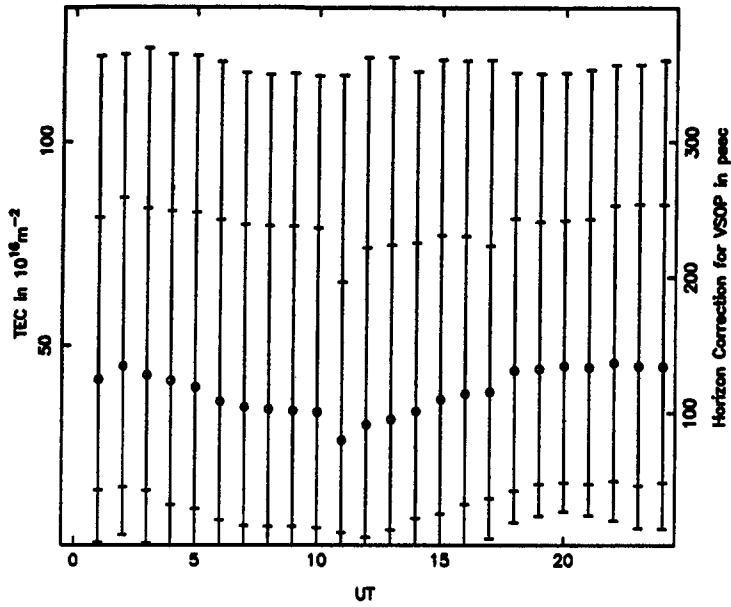
Monthly Averaged Boulder Zentith TEC: May 1982



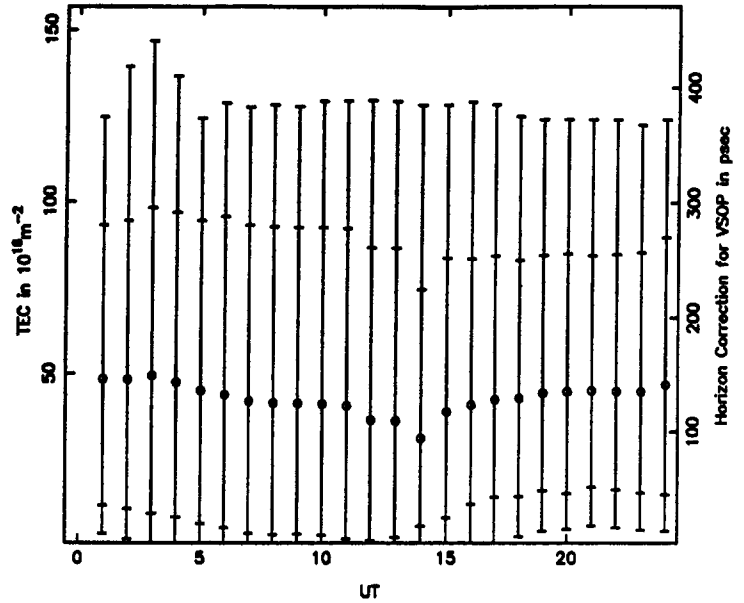
Monthly Averaged Boulder Zentith TEC: June 1982



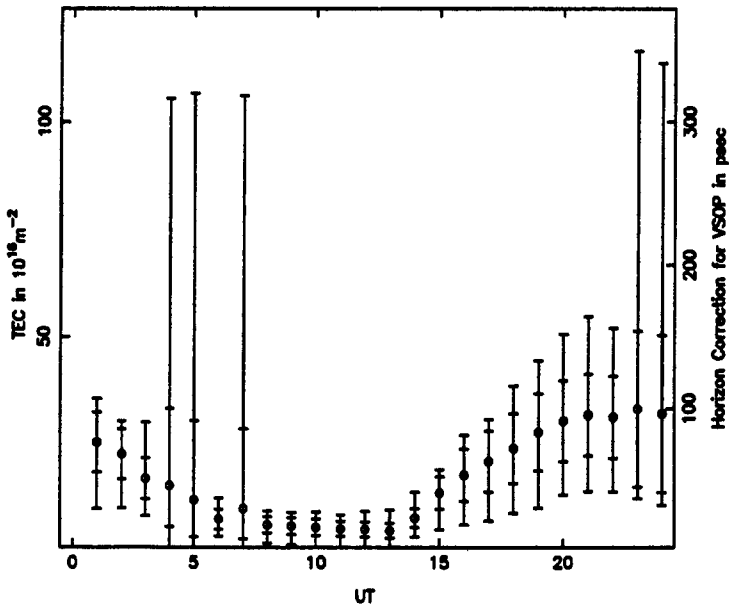
Monthly Averaged Boulder Zenith TEC: July 1982



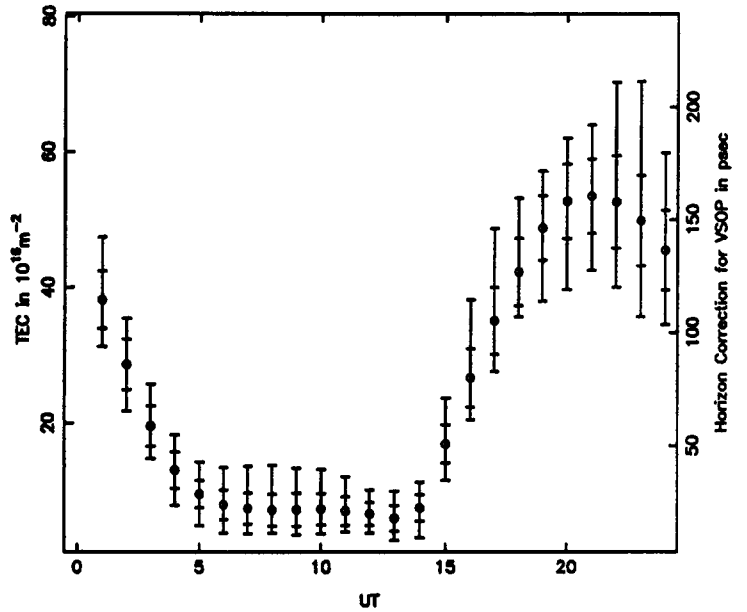
Monthly Averaged Boulder Zenith TEC: August 1982



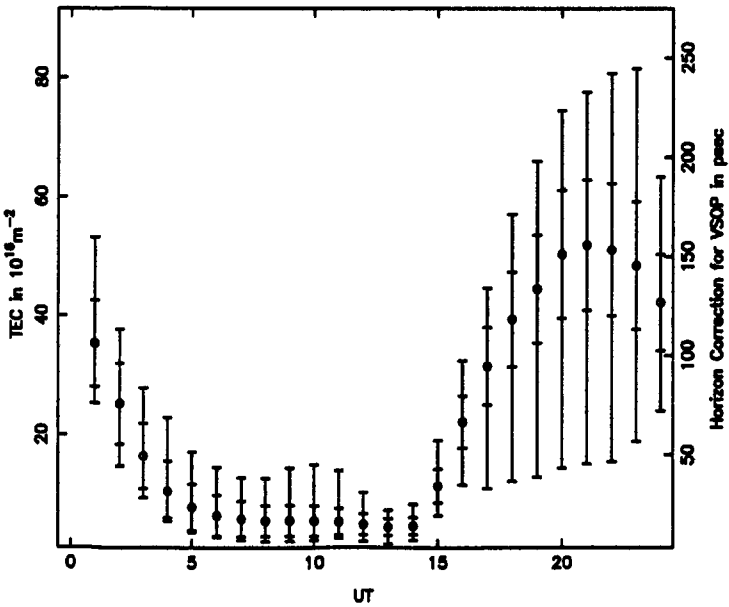
Monthly Averaged Boulder Zenith TEC: September 1982



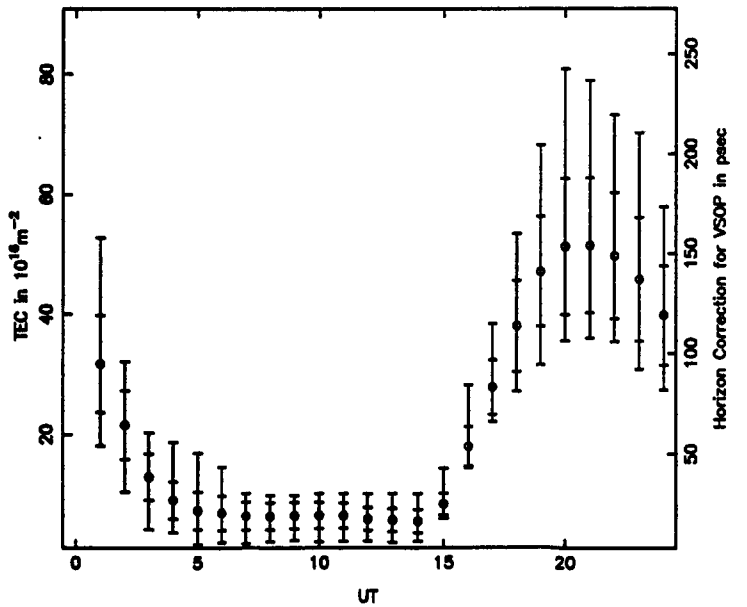
Monthly Averaged Boulder Zenith TEC: October 1982



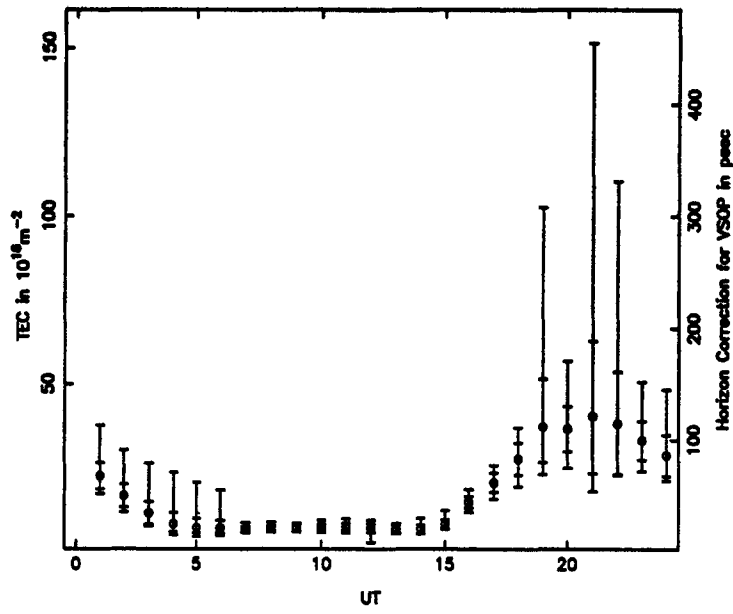
Monthly Averaged Boulder Zenith TEC: November 1982



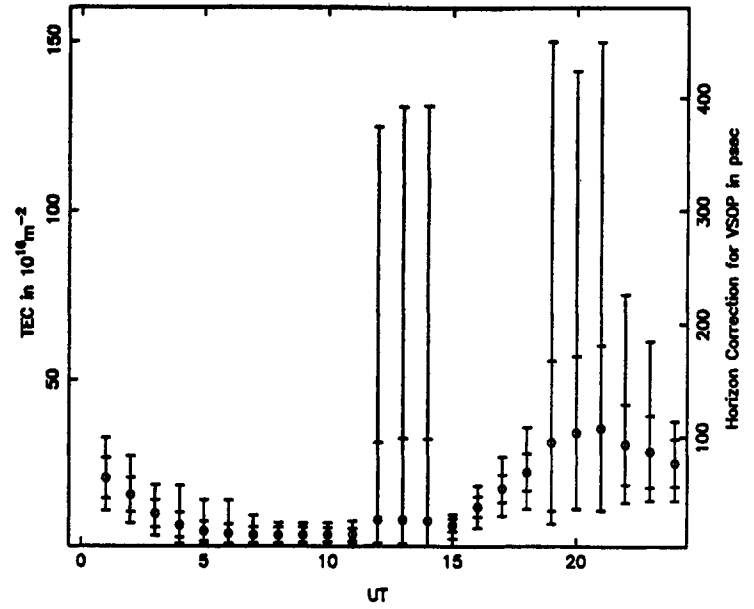
Monthly Averaged Boulder Zenith TEC: December 1982



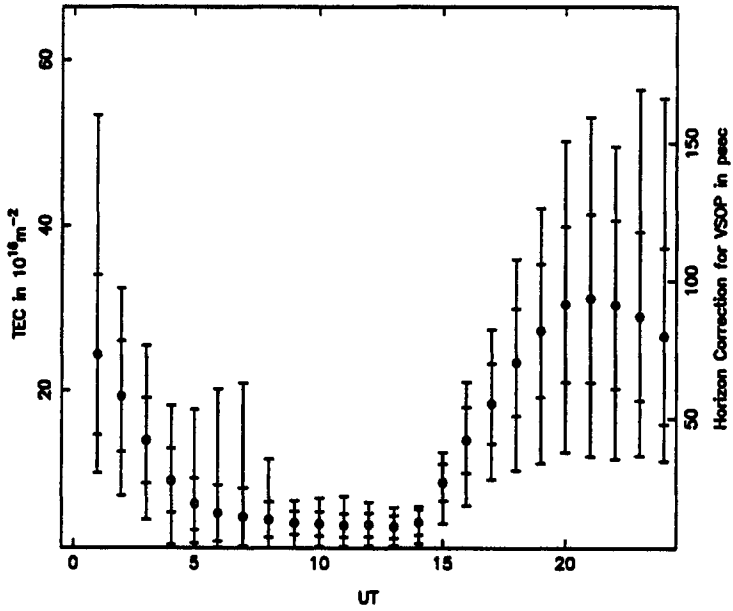
Monthly Averaged Boulder Zenth TEC: January 1983



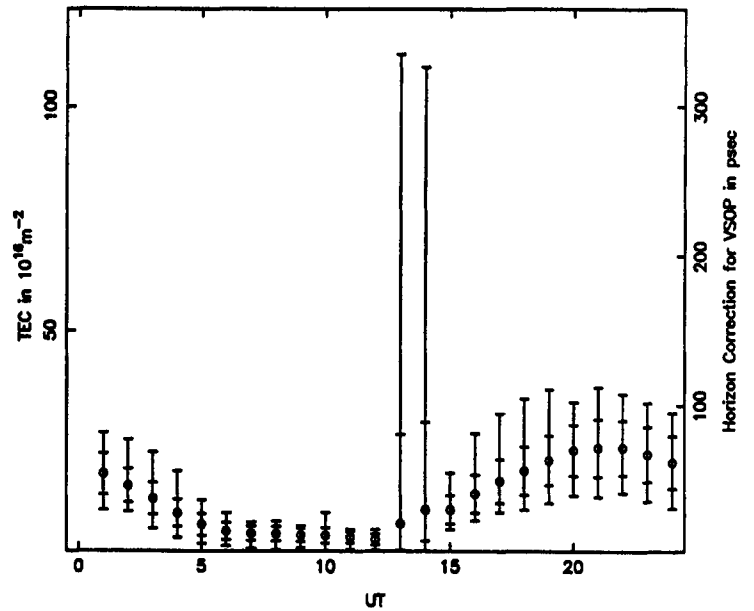
Monthly Averaged Boulder Zenth TEC: February 1983



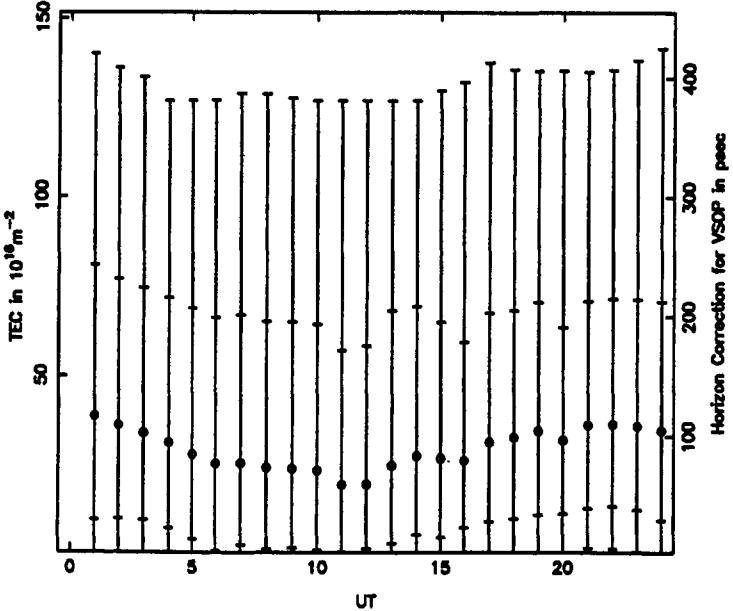
Monthly Averaged Boulder Zenth TEC: March 1983



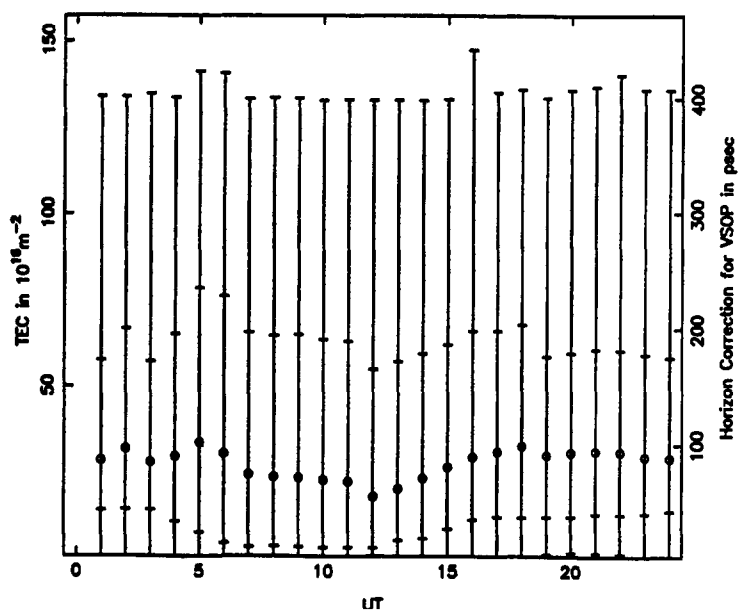
Monthly Averaged Boulder Zenth TEC: April 1983



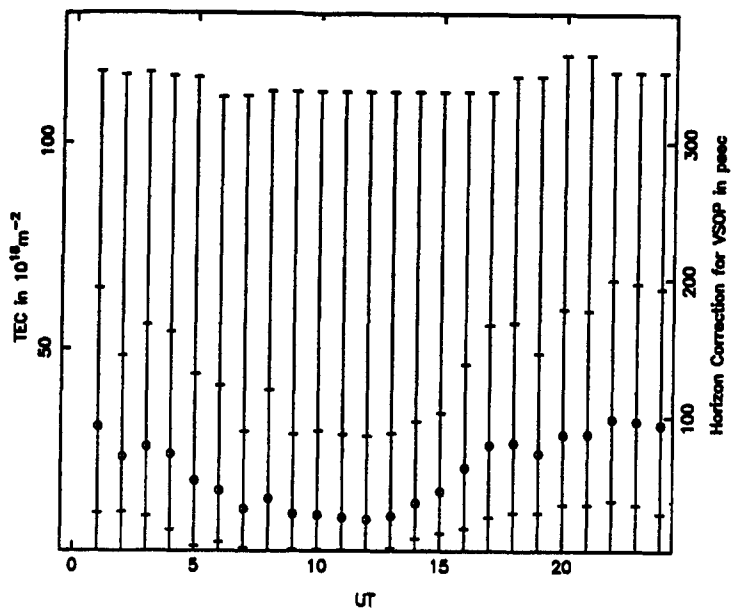
Monthly Averaged Boulder Zenth TEC: May 1983



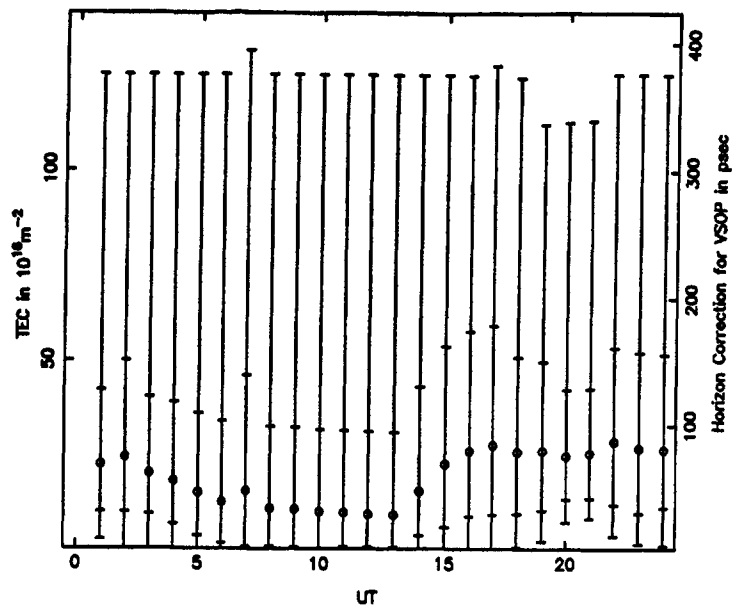
Monthly Averaged Boulder Zenth TEC: June 1983



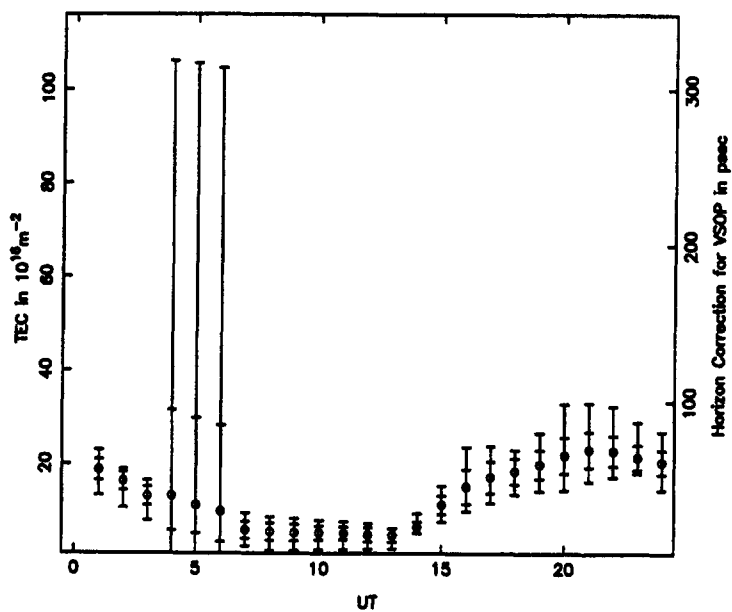
Monthly Averaged Boulder Zentith TEC: July 1983



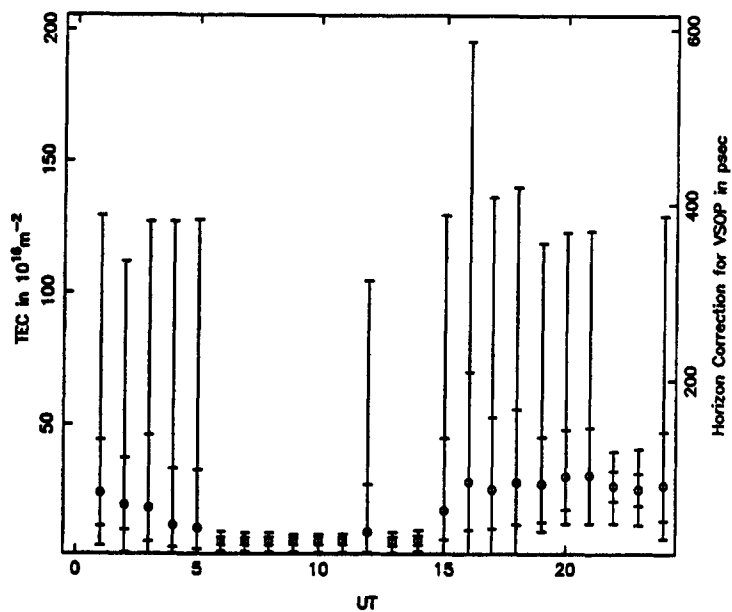
Monthly Averaged Boulder Zentith TEC: August 1983



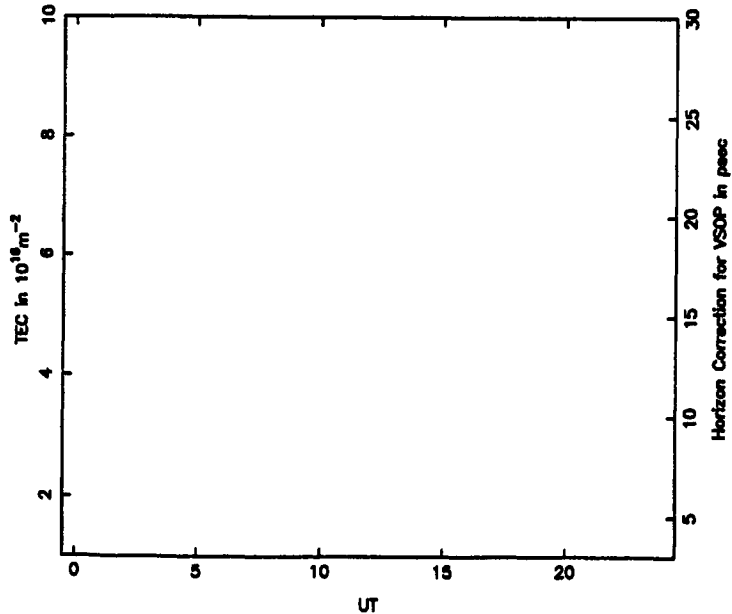
Monthly Averaged Boulder Zentith TEC: September 1983



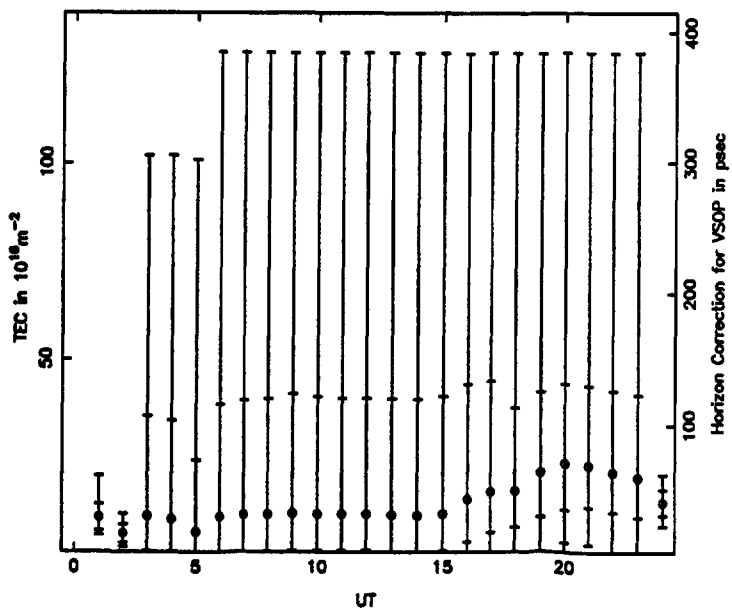
Monthly Averaged Boulder Zentith TEC: October 1983



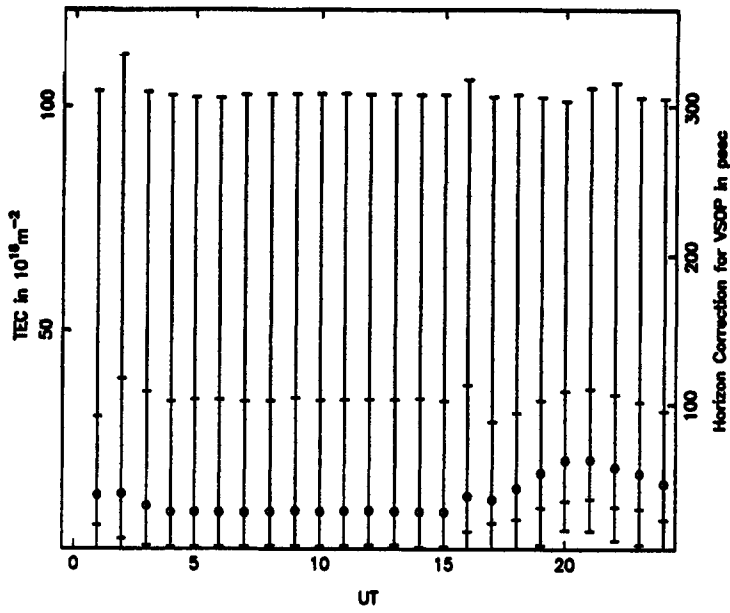
Monthly Averaged Boulder Zentith TEC: November 1983



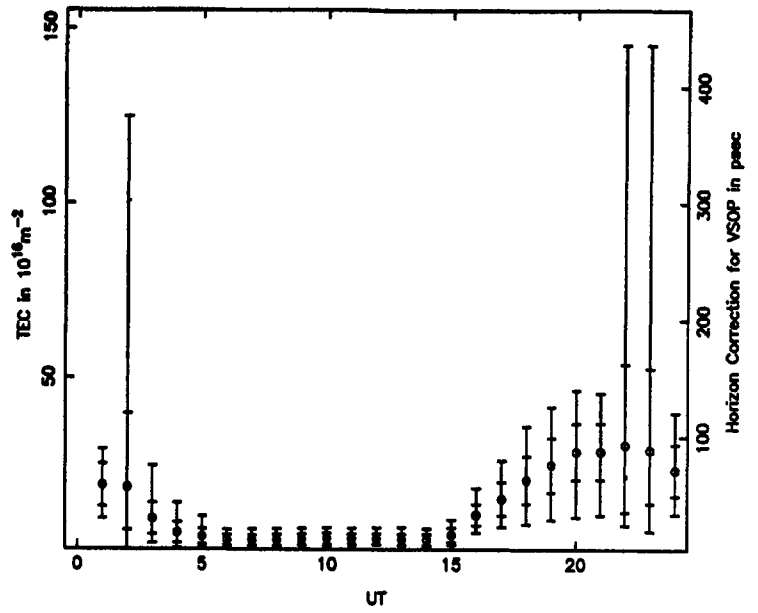
Monthly Averaged Boulder Zentith TEC: December 1983



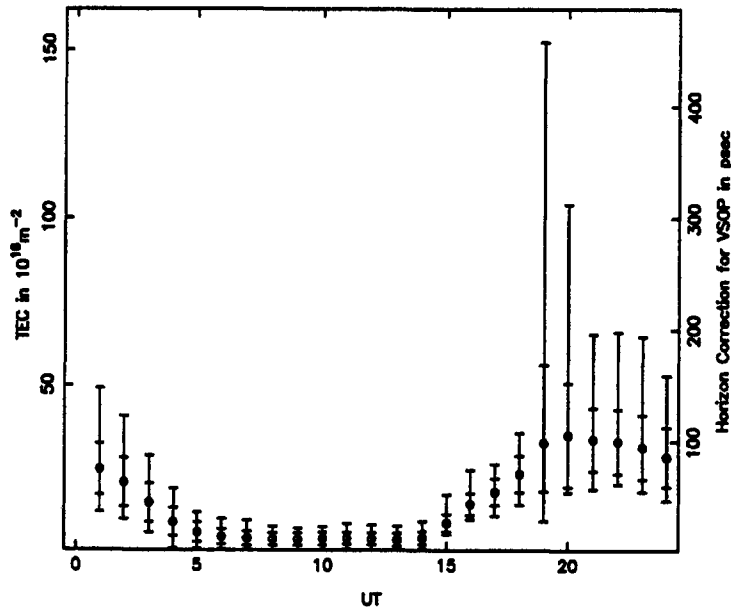
Monthly Averaged Boulder Zenthith TEC: January 1984



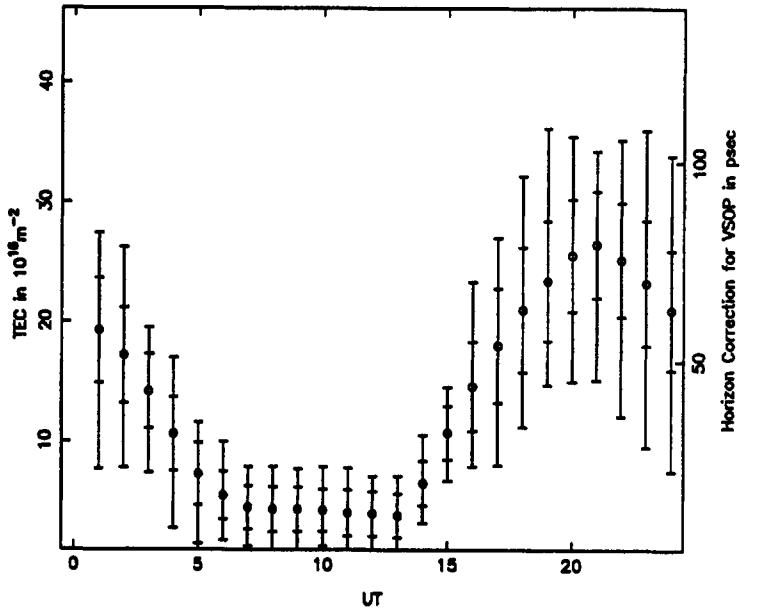
Monthly Averaged Boulder Zenthith TEC: February 1984



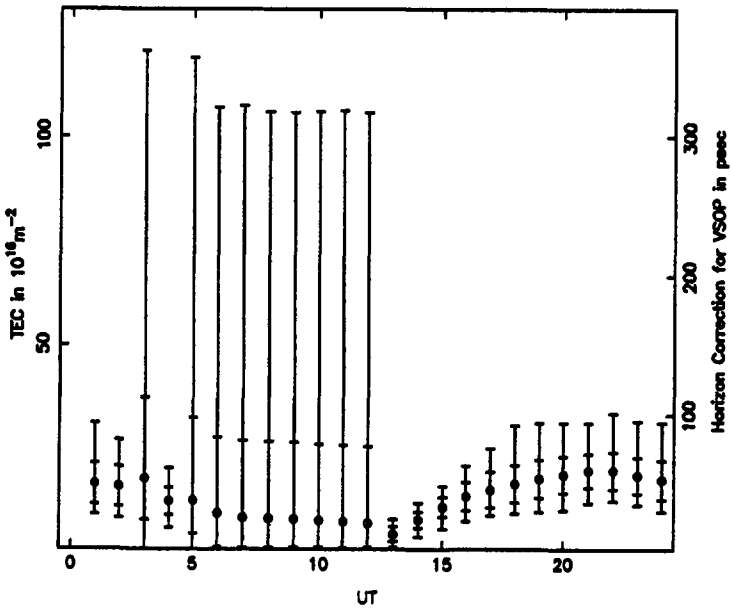
Monthly Averaged Boulder Zenthith TEC: March 1984



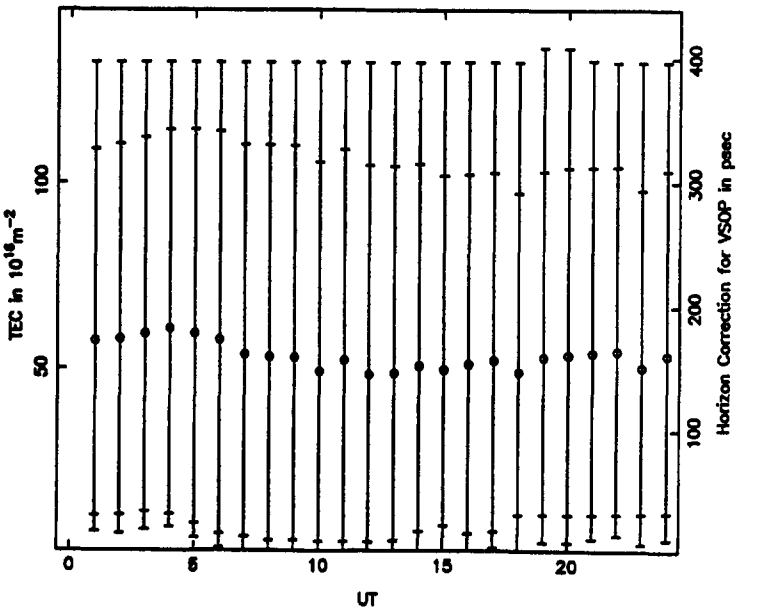
Monthly Averaged Boulder Zenthith TEC: April 1984



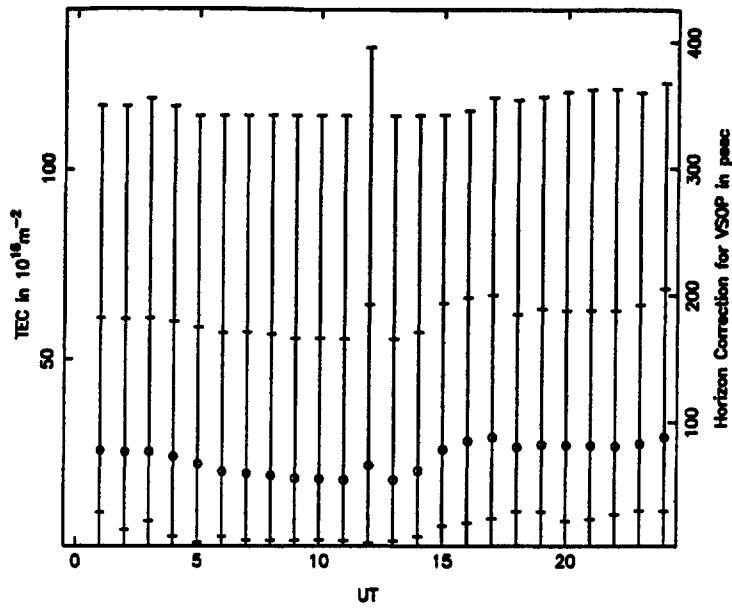
Monthly Averaged Boulder Zenthith TEC: May 1984



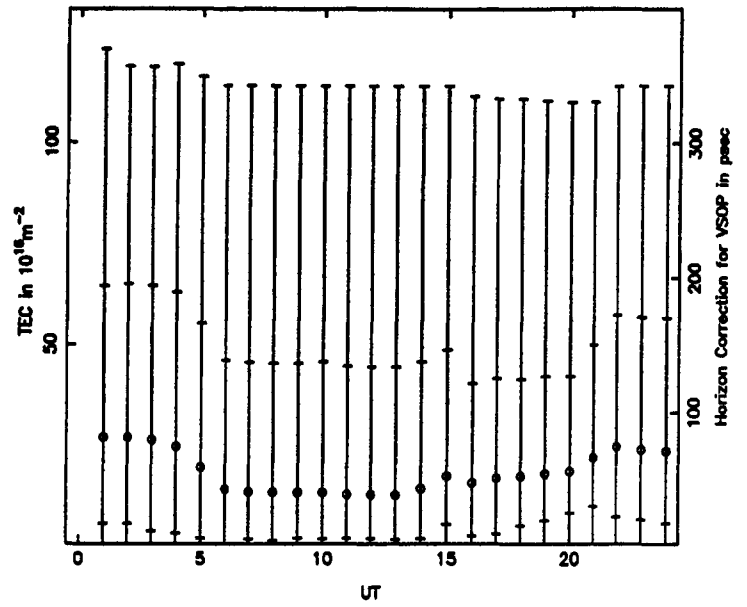
Monthly Averaged Boulder Zenthith TEC: June 1984



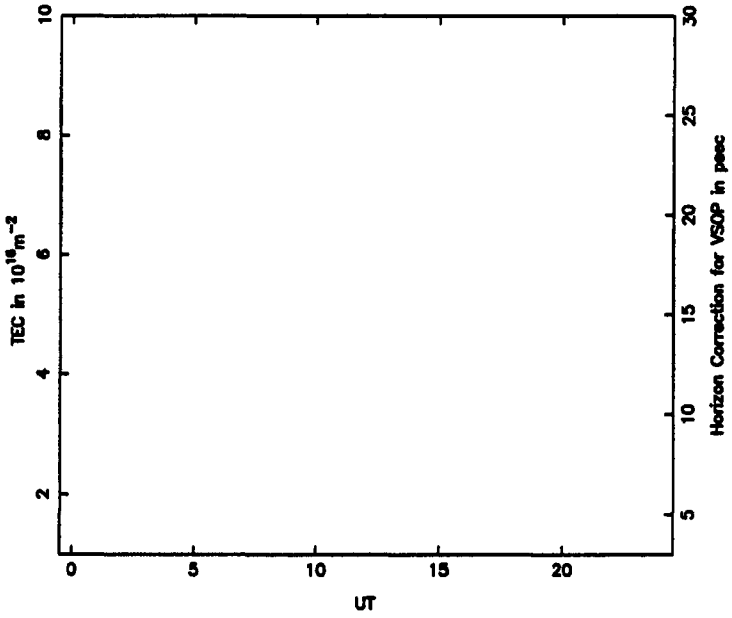
Monthly Averaged Boulder Zentith TEC: July 1984



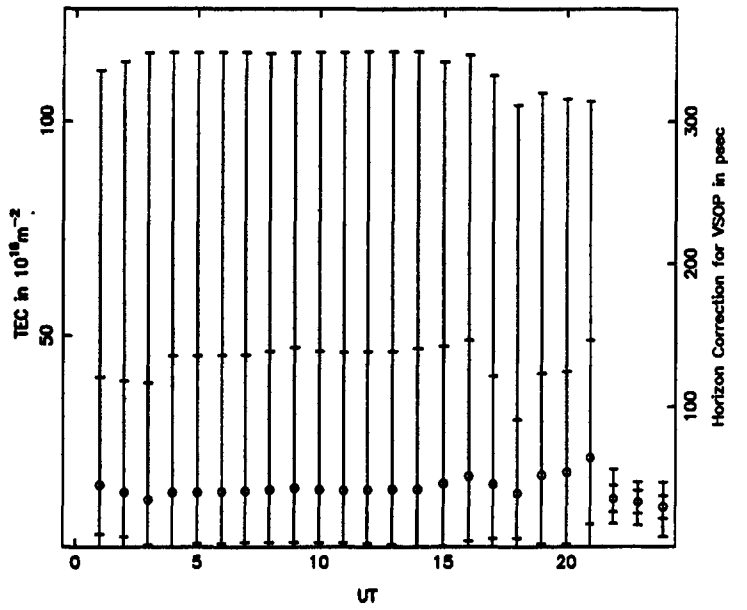
Monthly Averaged Boulder Zentith TEC: August 1984



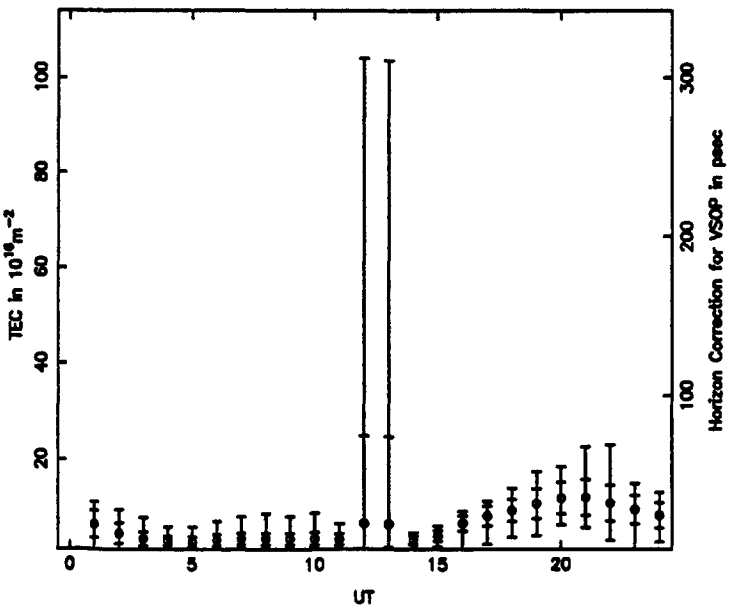
Monthly Averaged Boulder Zentith TEC: September 1984



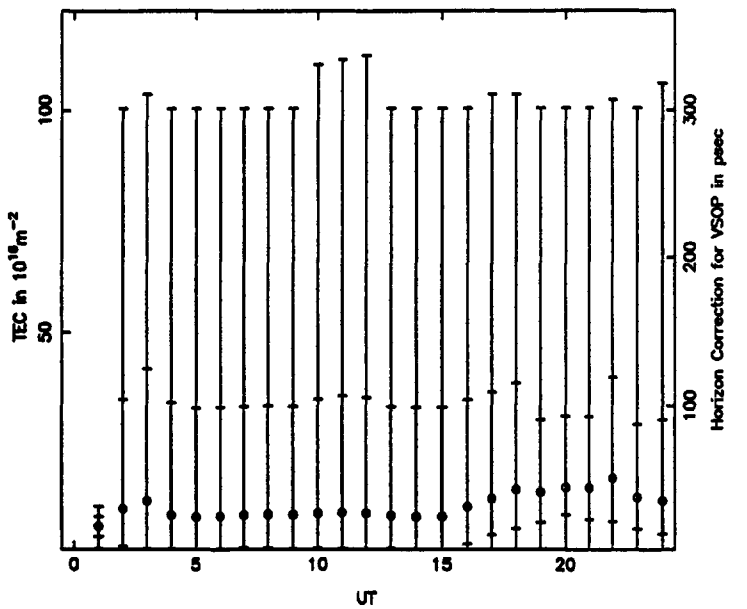
Monthly Averaged Boulder Zentith TEC: October 1984



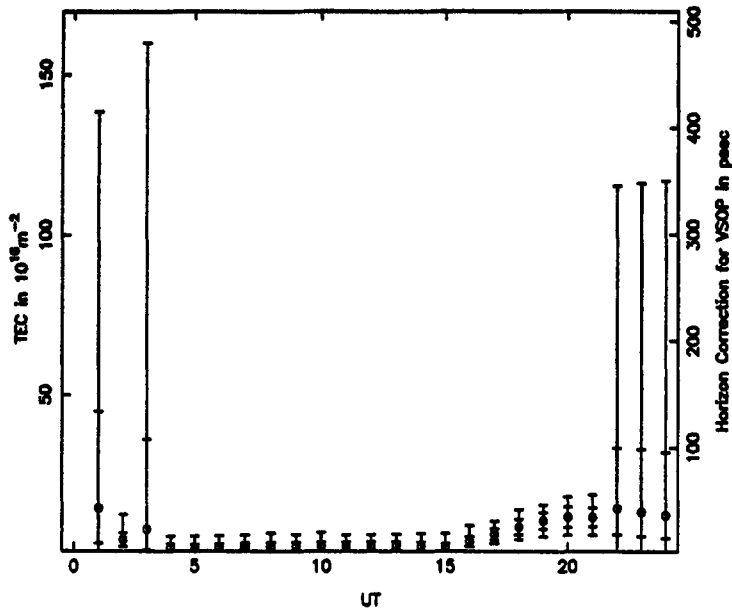
Monthly Averaged Boulder Zentith TEC: November 1984



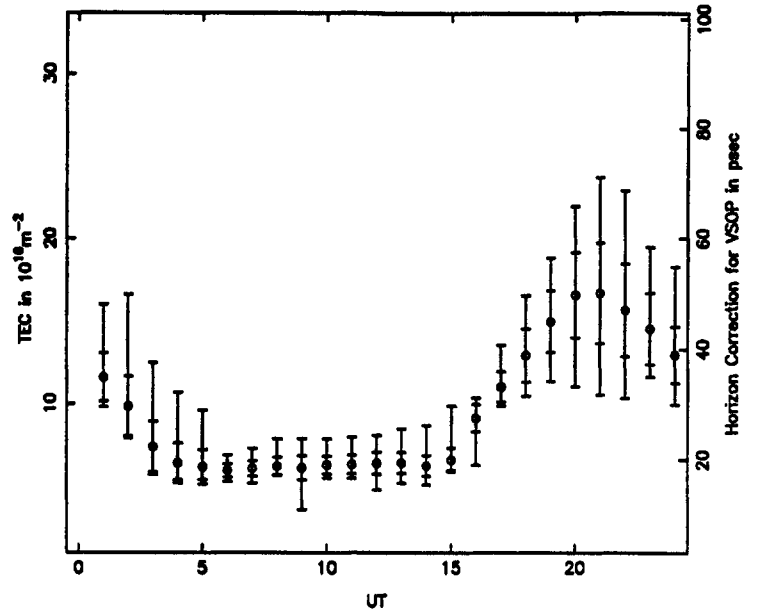
Monthly Averaged Boulder Zentith TEC: December 1984



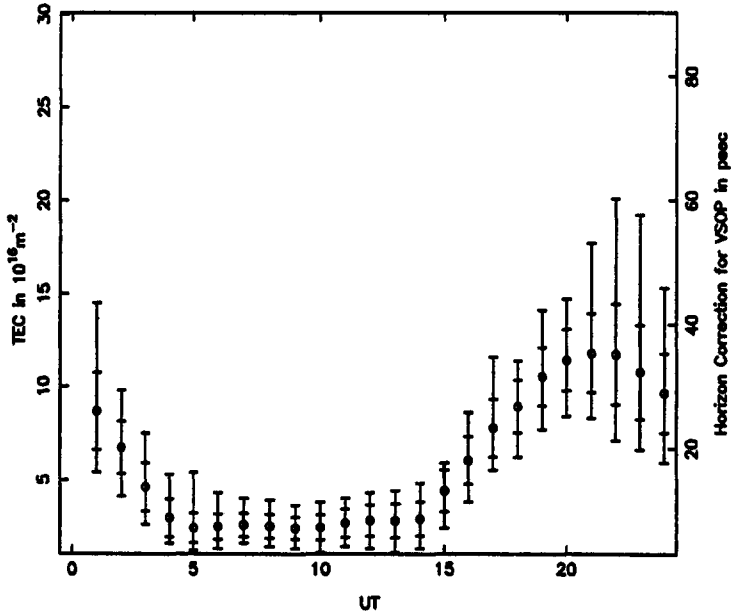
Monthly Averaged Boulder Zenith TEC: January 1985



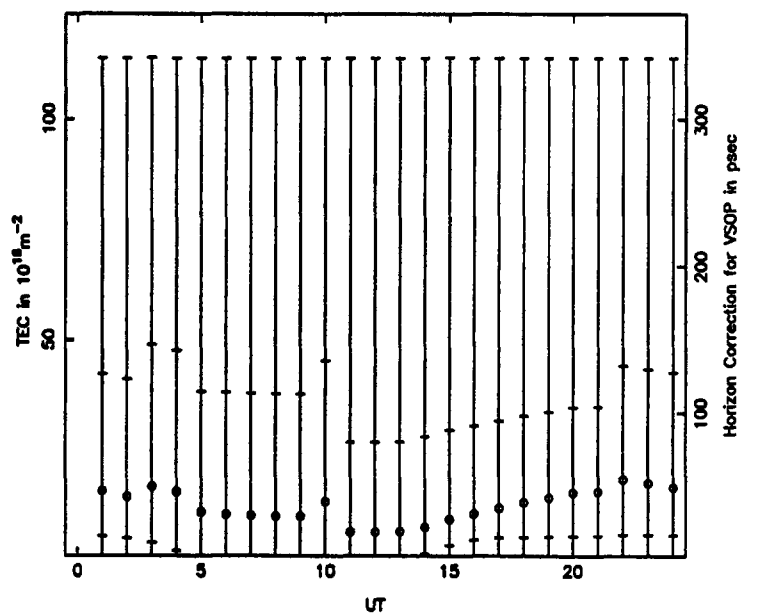
Monthly Averaged Boulder Zenith TEC: February 1985



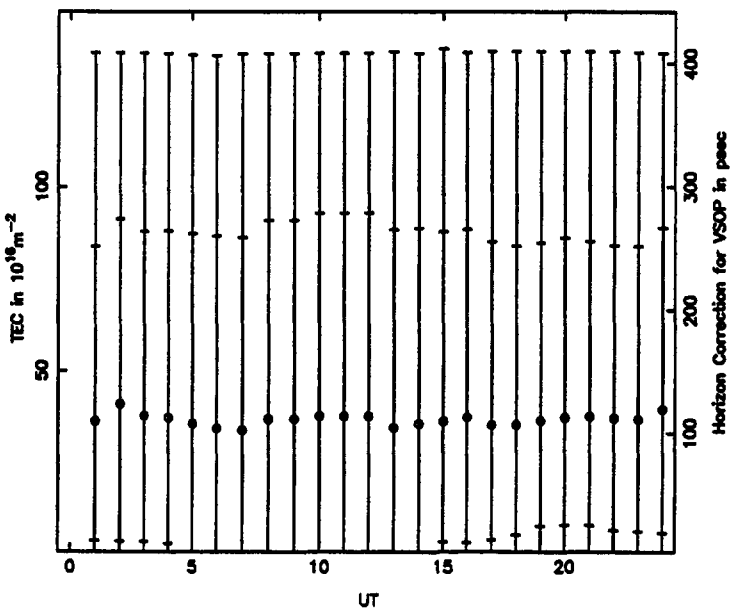
Monthly Averaged Boulder Zenith TEC: March 1985



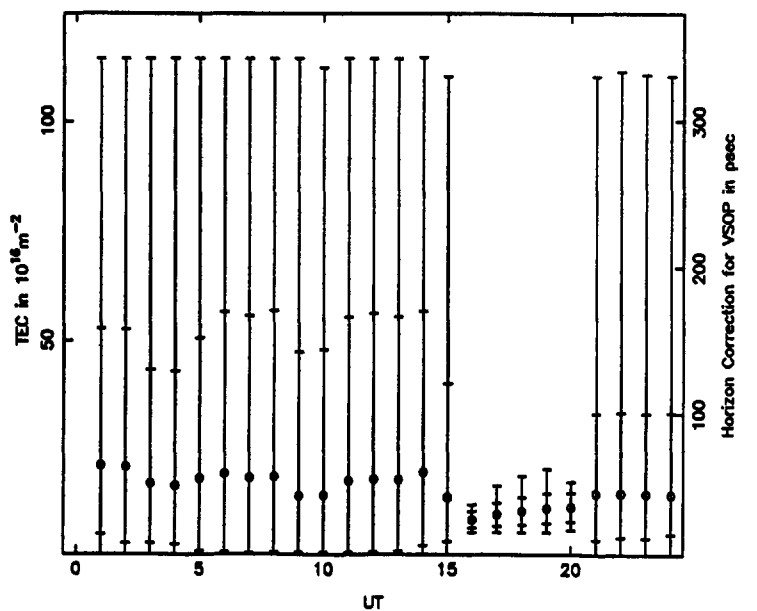
Monthly Averaged Boulder Zenith TEC: April 1985



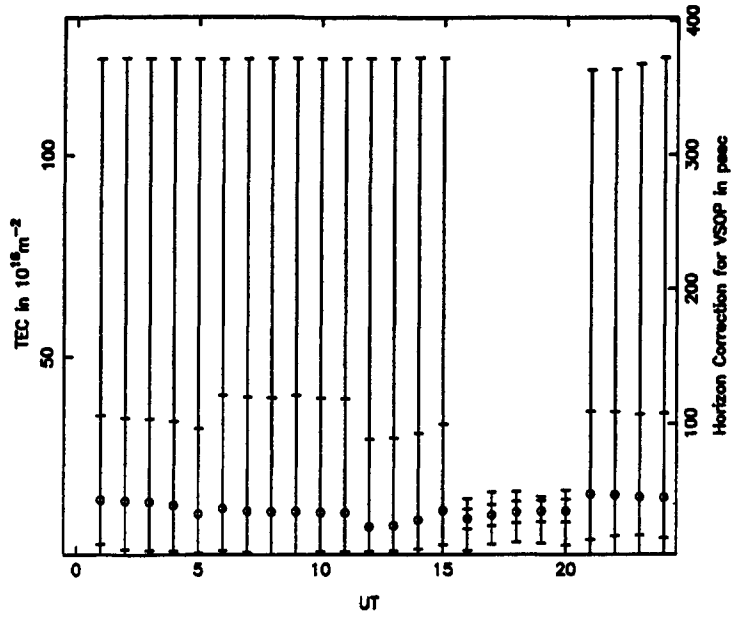
Monthly Averaged Boulder Zenith TEC: May 1985



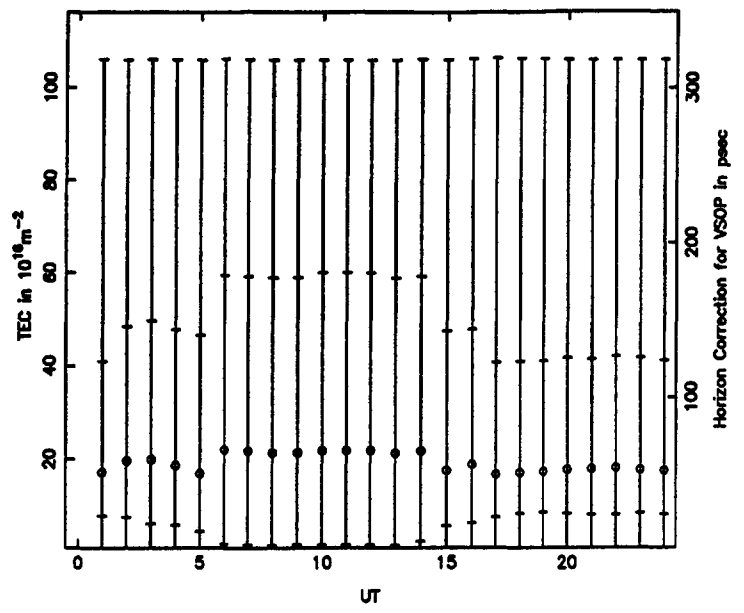
Monthly Averaged Boulder Zenith TEC: June 1985



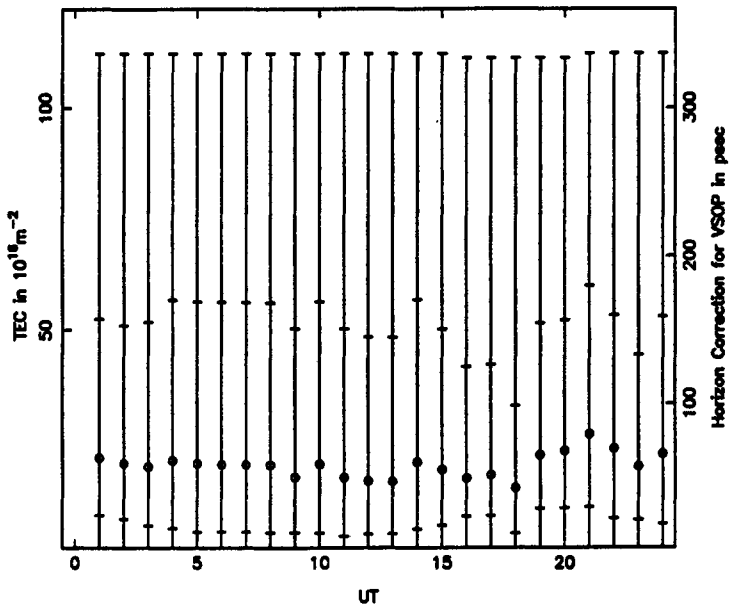
Monthly Averaged Boulder Zentith TEC: July 1985



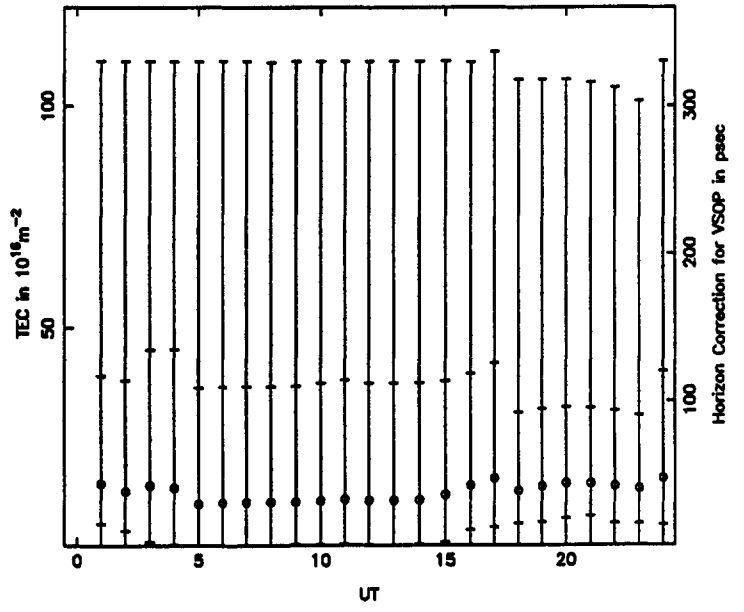
Monthly Averaged Boulder Zentith TEC: August 1985



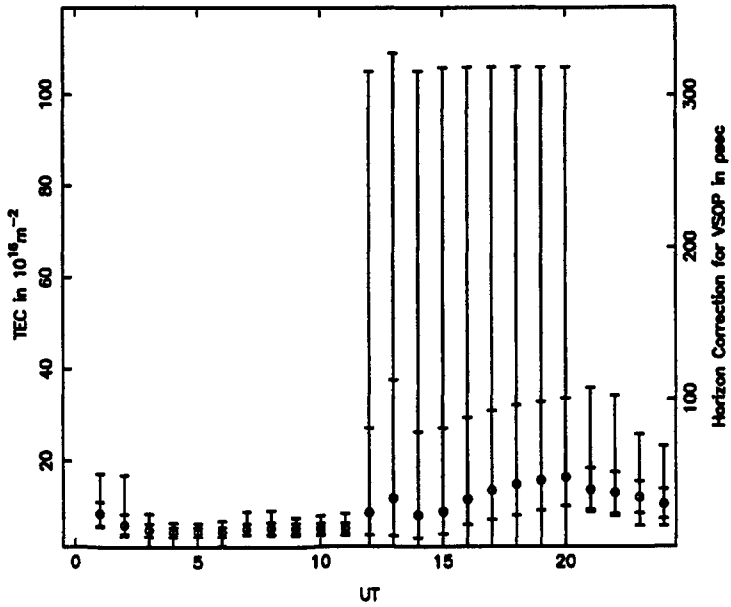
Monthly Averaged Boulder Zentith TEC: September 1985



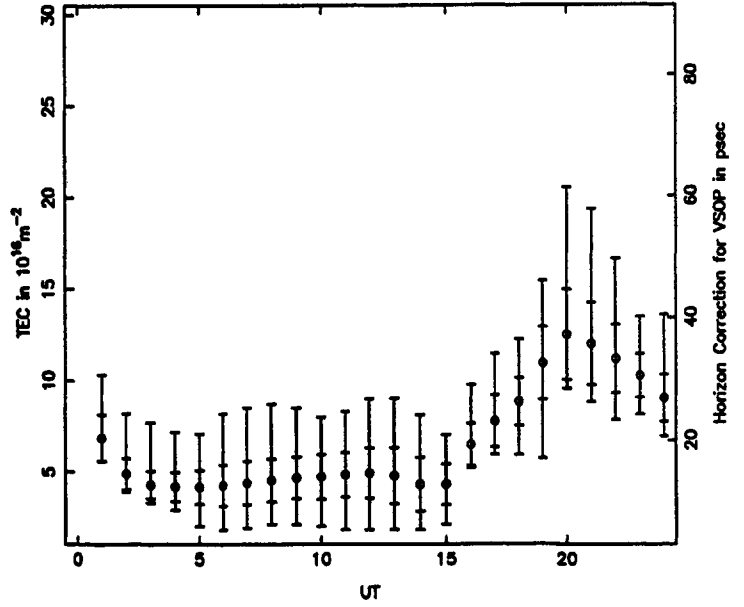
Monthly Averaged Boulder Zentith TEC: October 1985



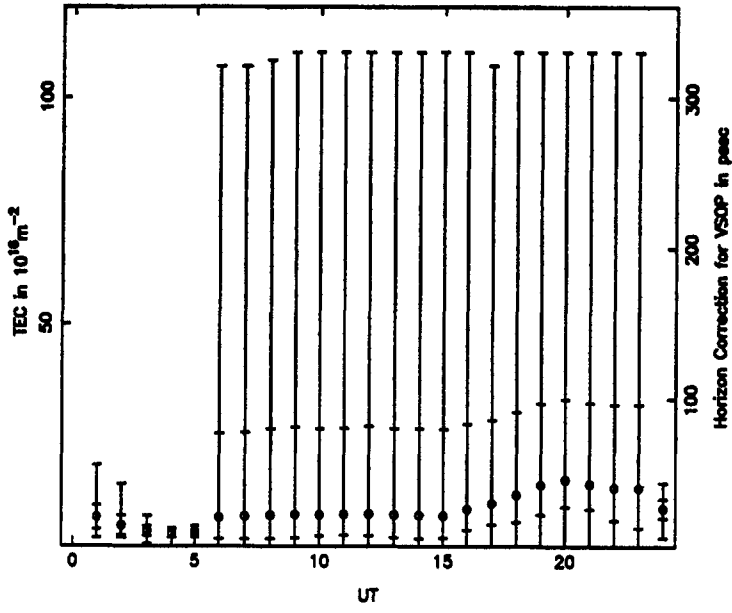
Monthly Averaged Boulder Zentith TEC: November 1985



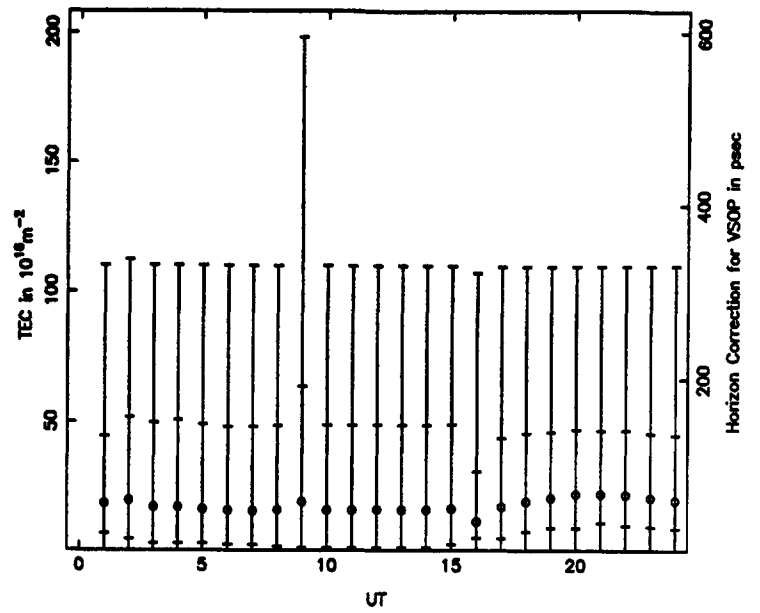
Monthly Averaged Boulder Zentith TEC: December 1985



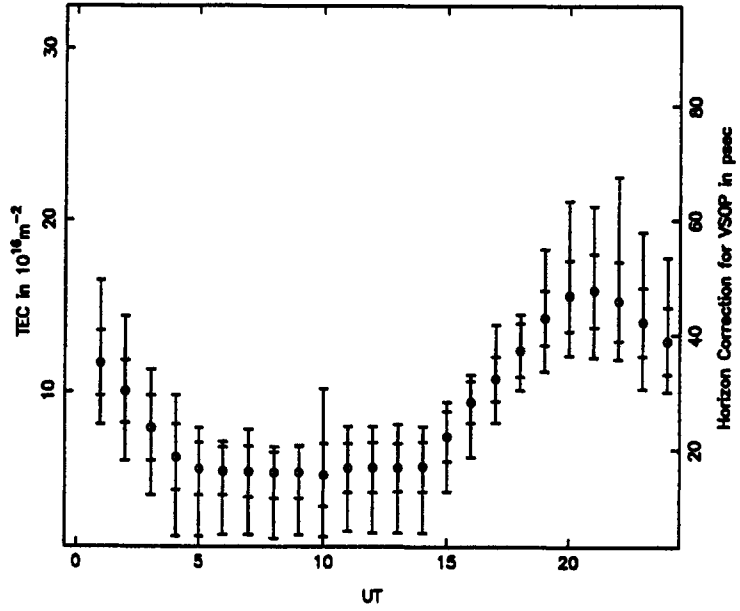
Monthly Averaged Boulder Zentith TEC: January 1986



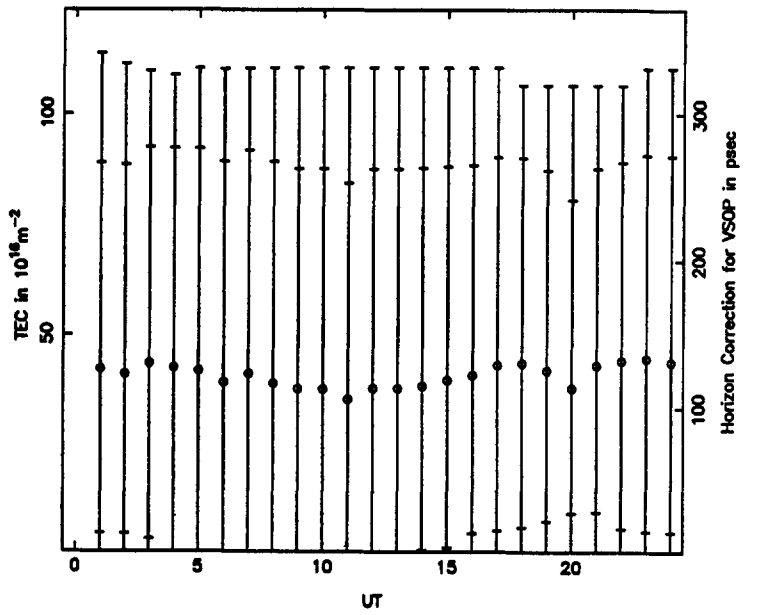
Monthly Averaged Boulder Zentith TEC: February 1986



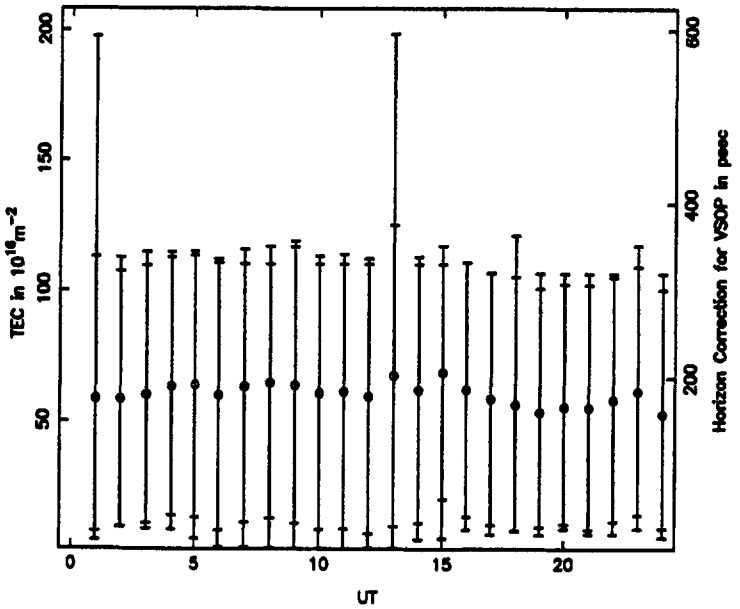
Monthly Averaged Boulder Zentith TEC: March 1986



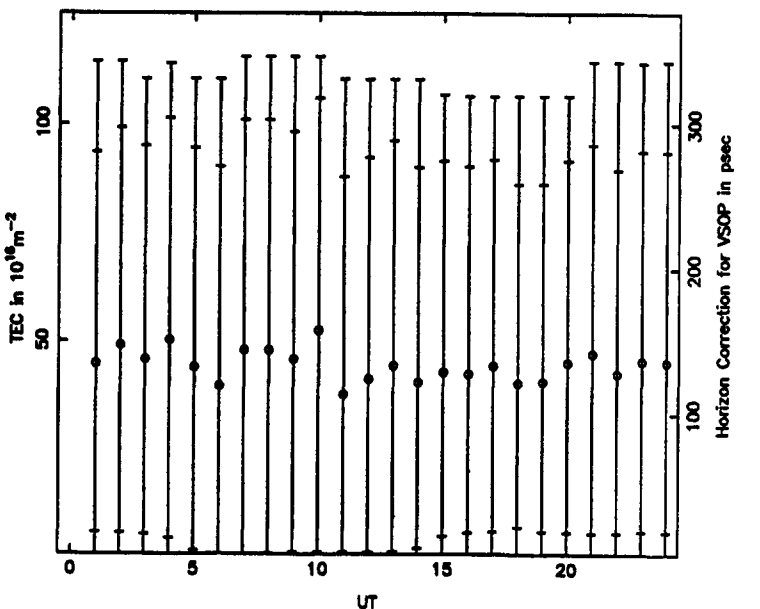
Monthly Averaged Boulder Zentith TEC: April 1986



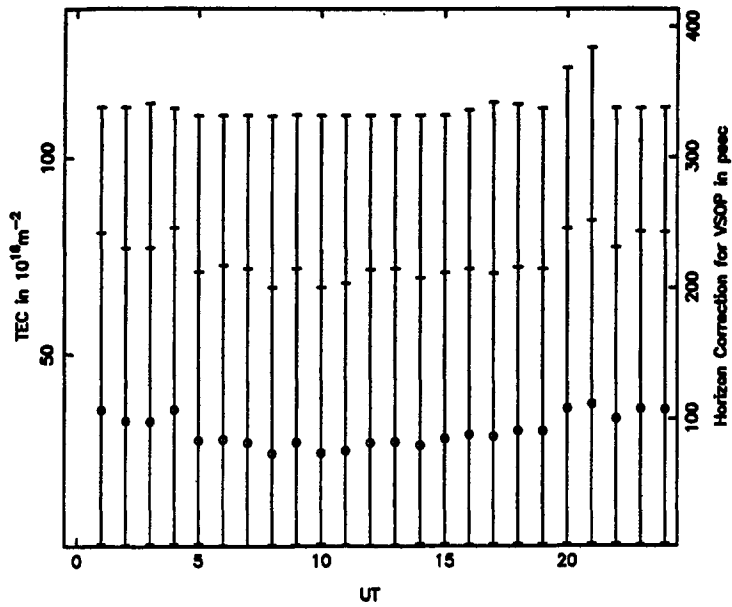
Monthly Averaged Boulder Zentith TEC: May 1986



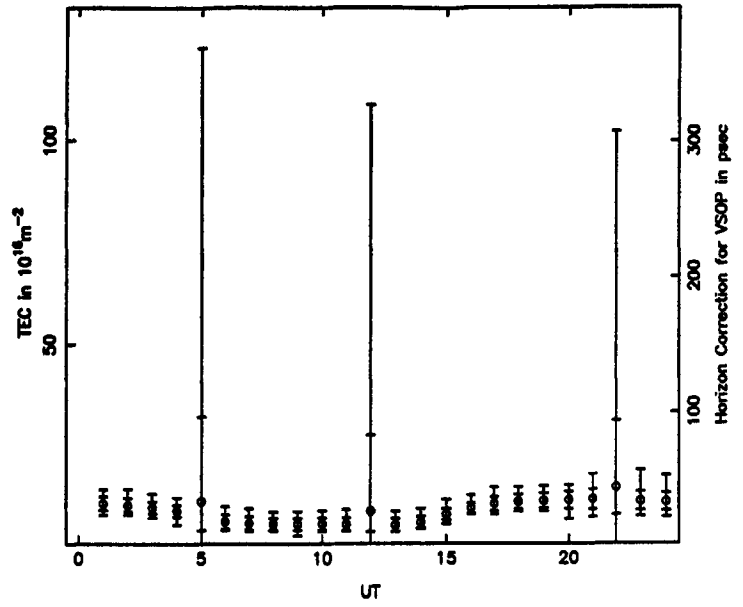
Monthly Averaged Boulder Zentith TEC: June 1986



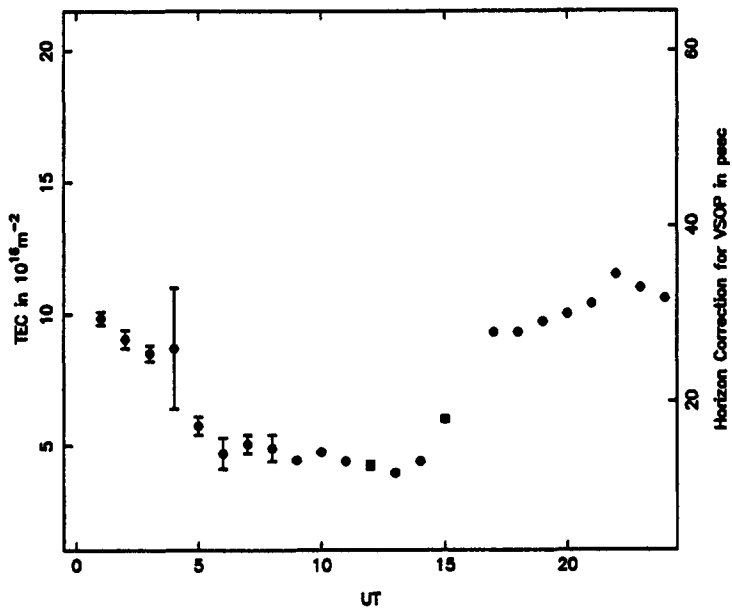
Monthly Averaged Boulder Zenith TEC: July 1986



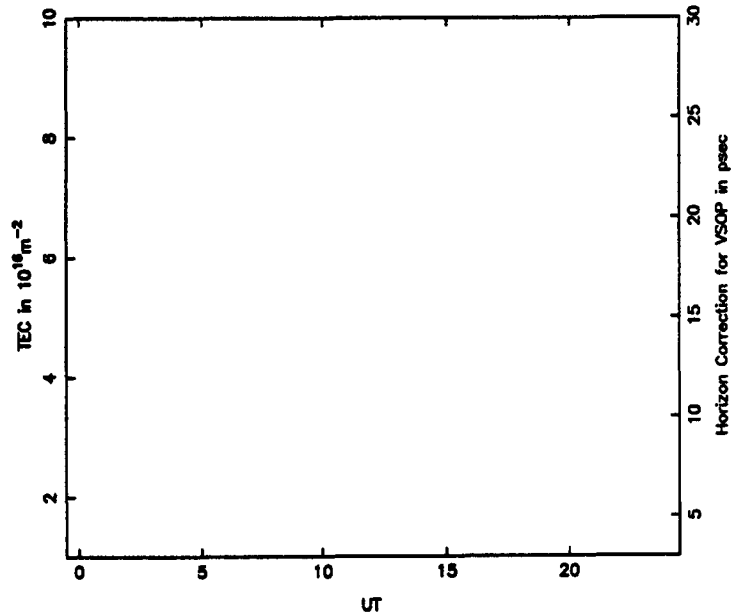
Monthly Averaged Boulder Zenith TEC: August 1986



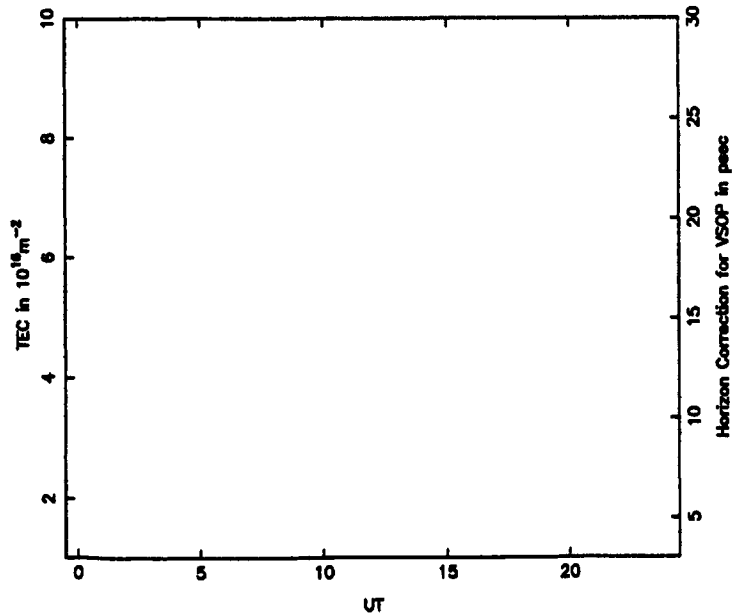
Monthly Averaged Boulder Zenith TEC: September 1986



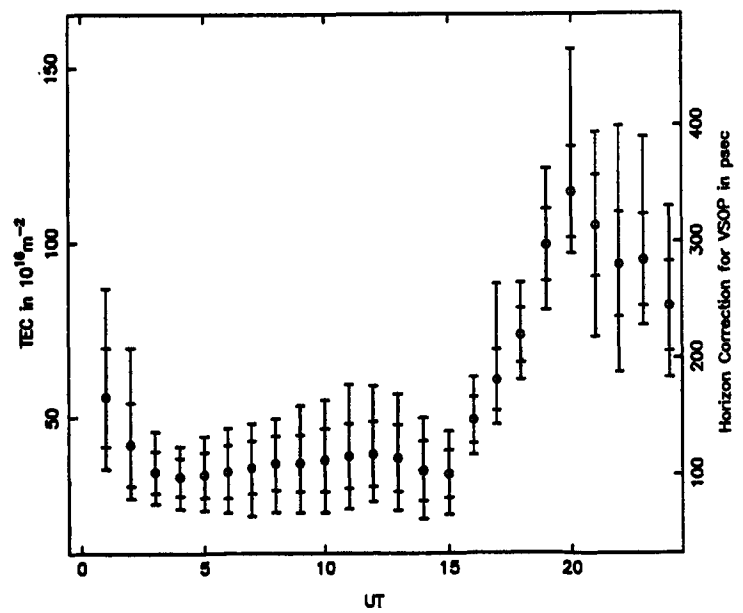
Monthly Averaged Boulder Zenith TEC: October 1986



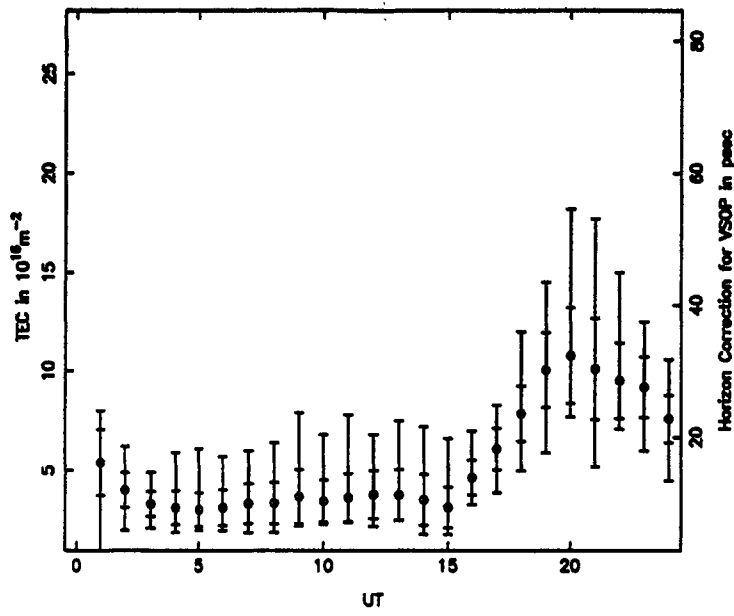
Monthly Averaged Boulder Zenith TEC: November 1986



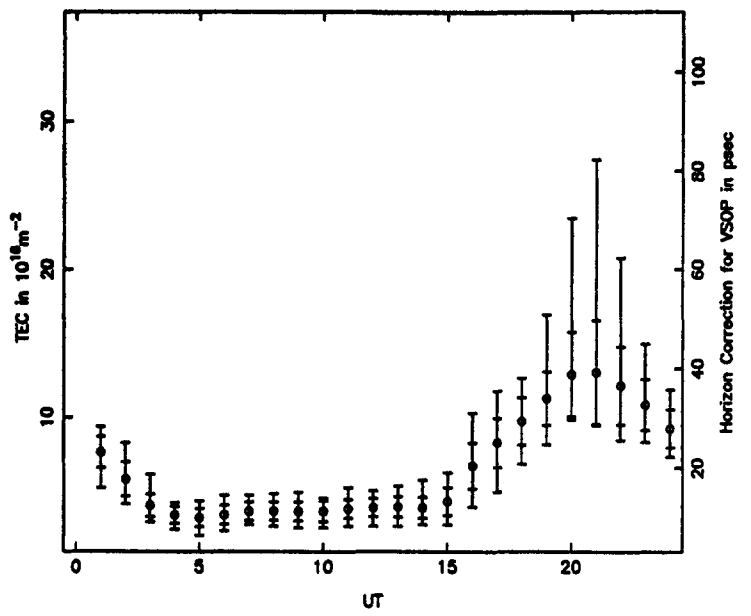
Monthly Averaged Boulder Zenith TEC: December 1986



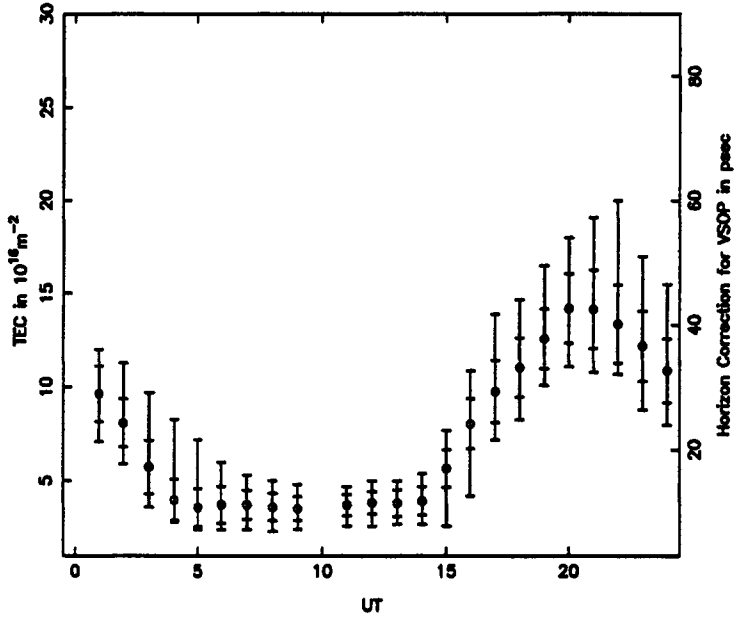
Monthly Averaged Boulder Zentith TEC: January 1987



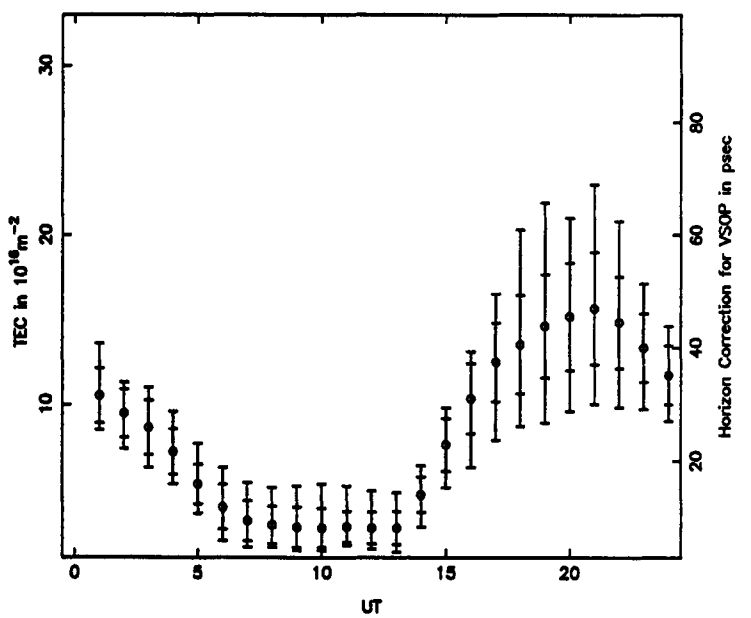
Monthly Averaged Boulder Zentith TEC: February 1987



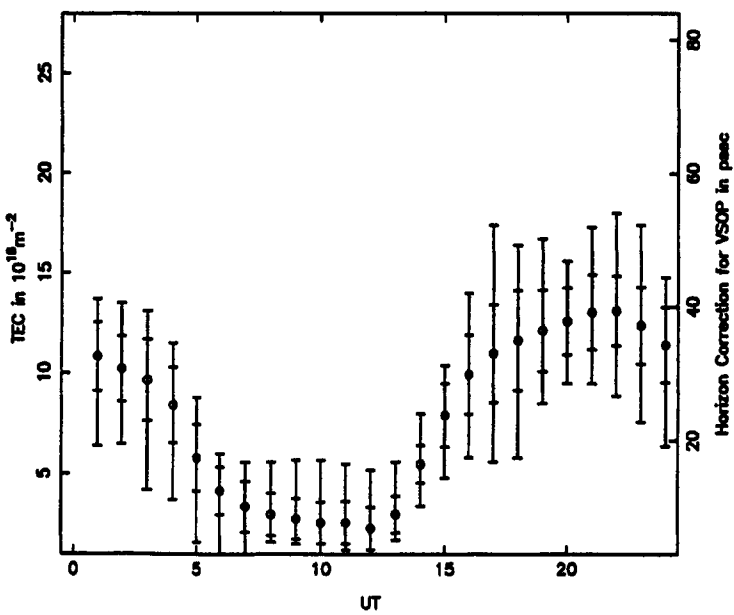
Monthly Averaged Boulder Zentith TEC: March 1987



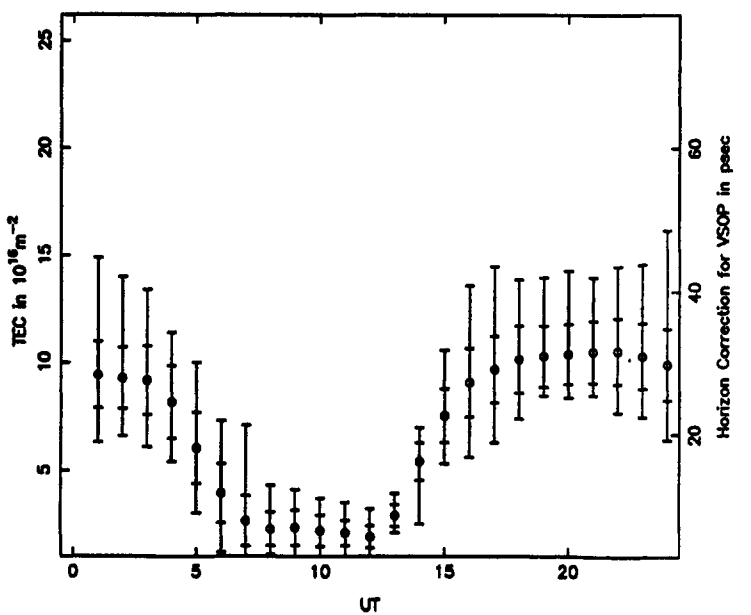
Monthly Averaged Boulder Zentith TEC: April 1987



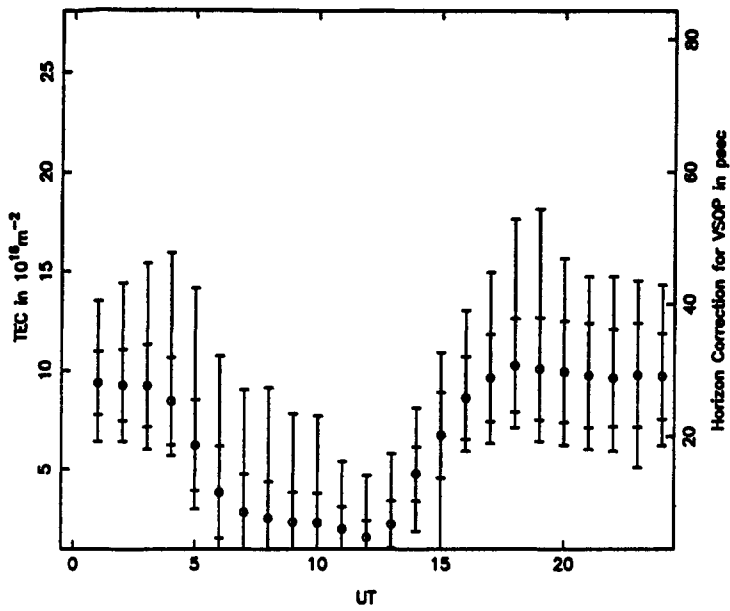
Monthly Averaged Boulder Zentith TEC: May 1987



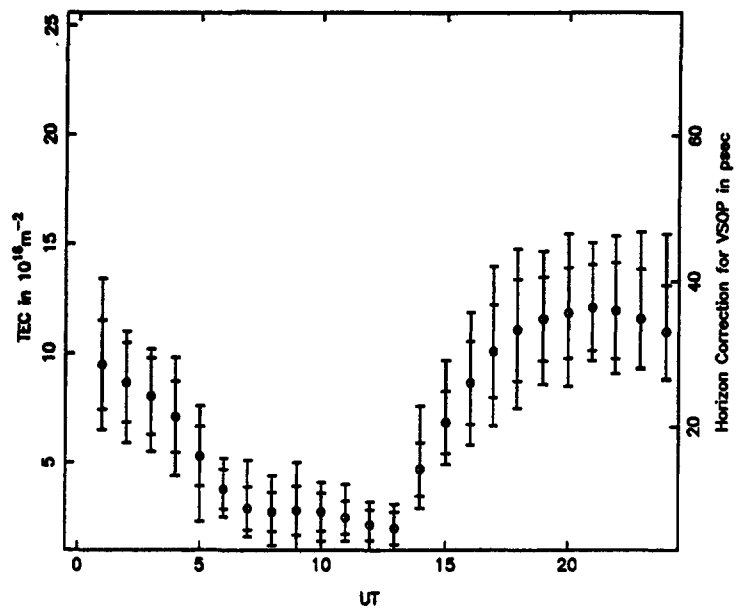
Monthly Averaged Boulder Zentith TEC: June 1987



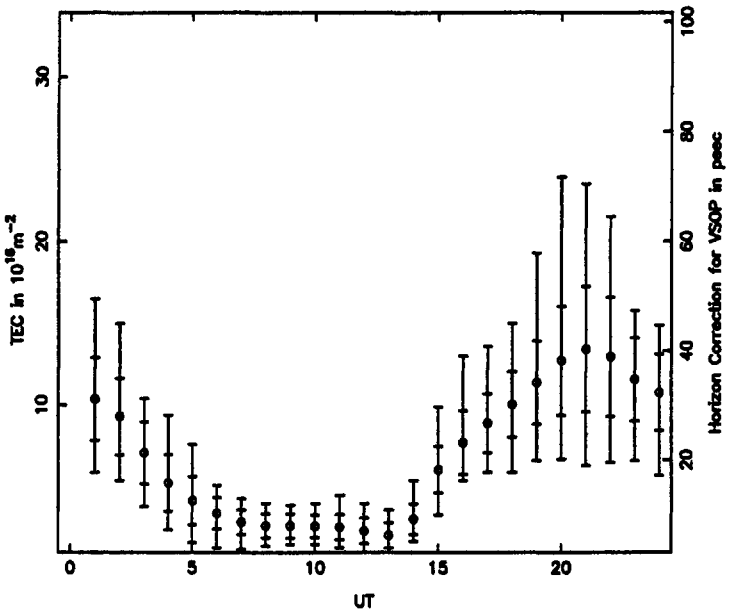
Monthly Averaged Boulder Zenith TEC: July 1987



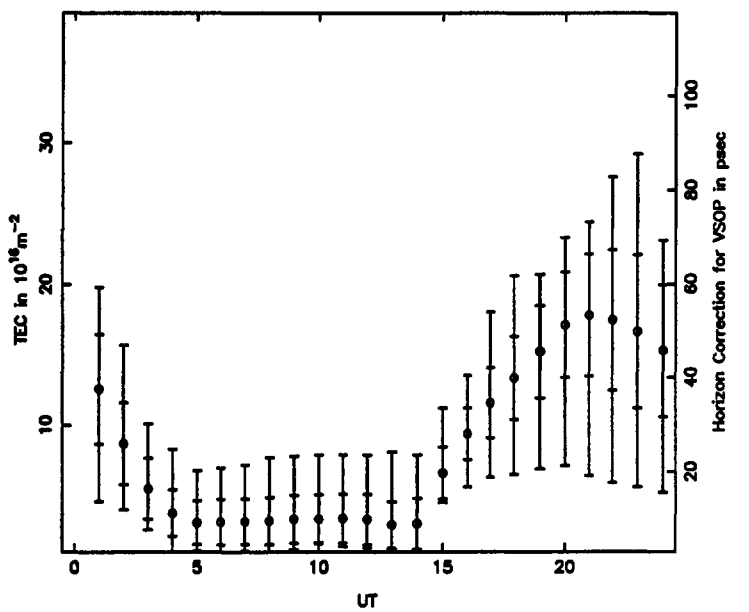
Monthly Averaged Boulder Zenith TEC: August 1987



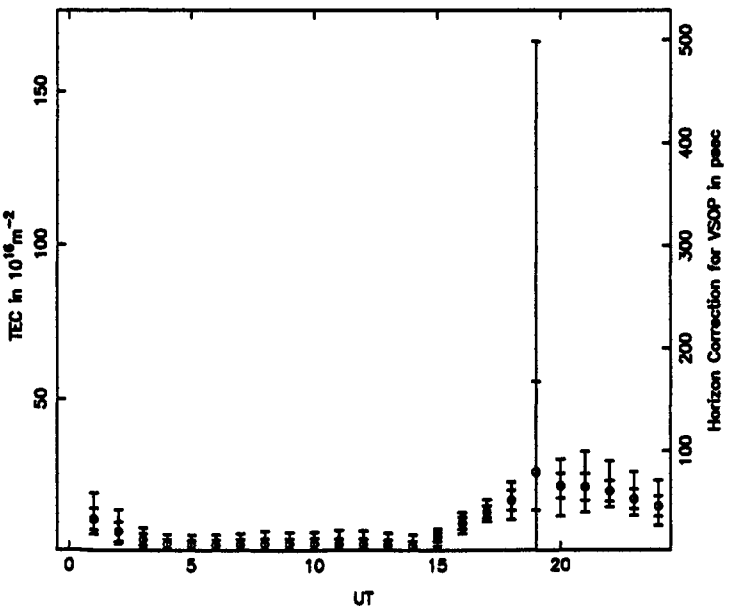
Monthly Averaged Boulder Zenith TEC: September 1987



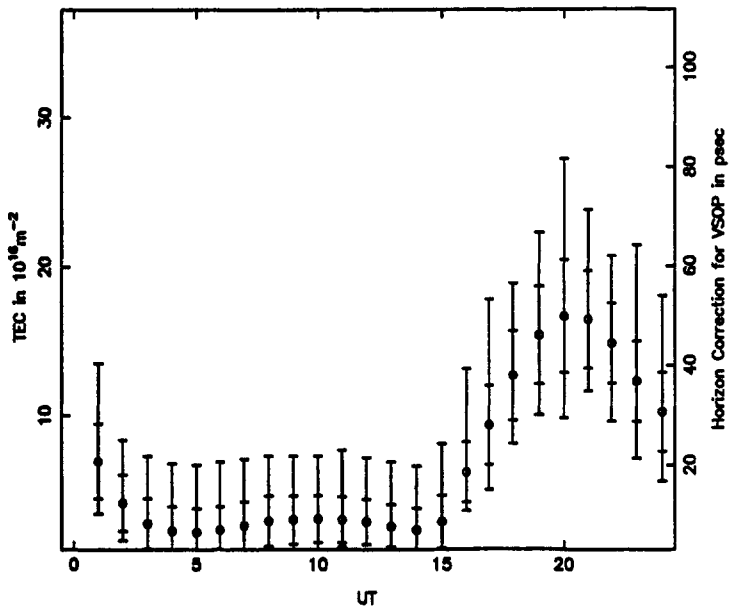
Monthly Averaged Boulder Zenith TEC: October 1987



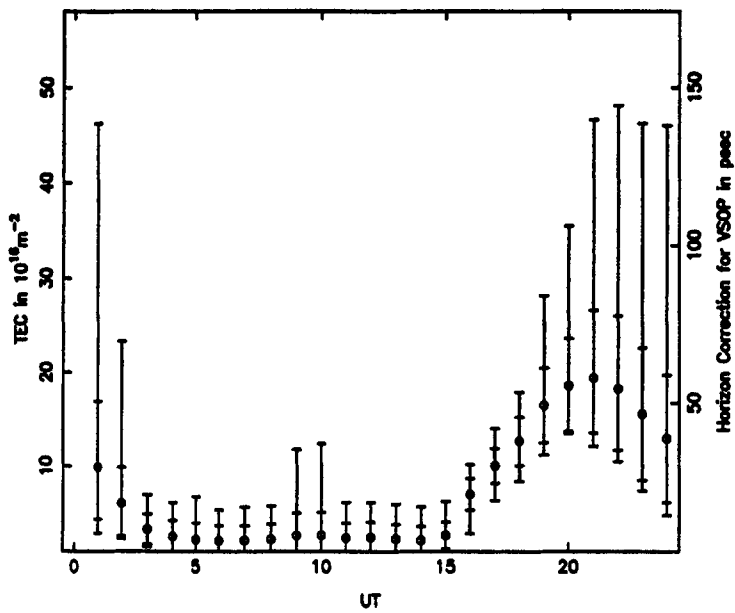
Monthly Averaged Boulder Zenith TEC: November 1987



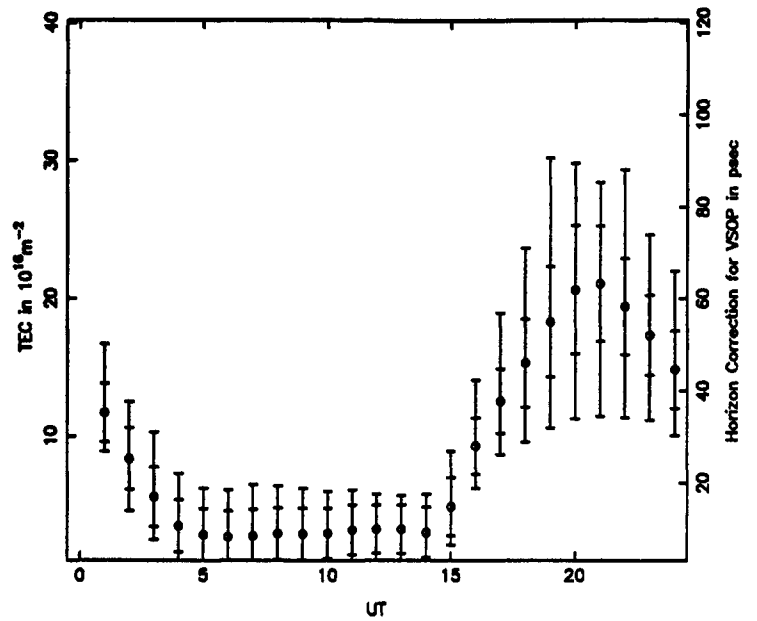
Monthly Averaged Boulder Zenith TEC: December 1987



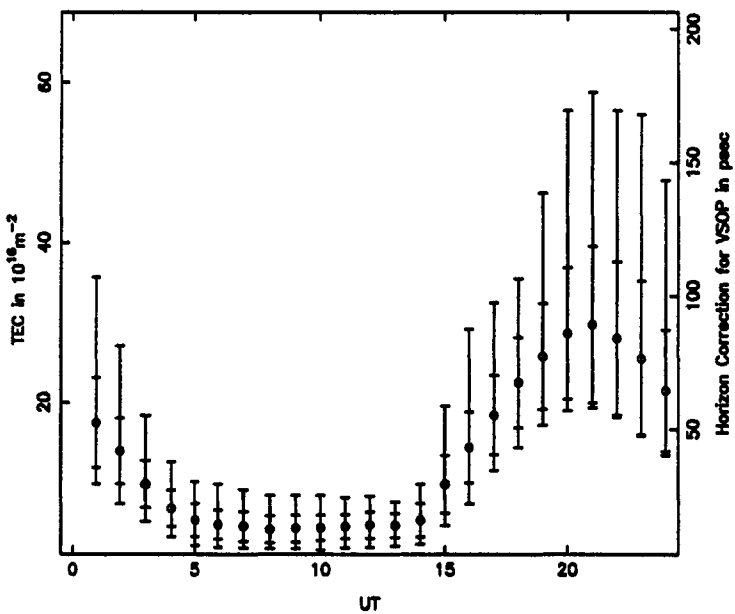
Monthly Averaged Boulder Zenthith TEC: January 1988



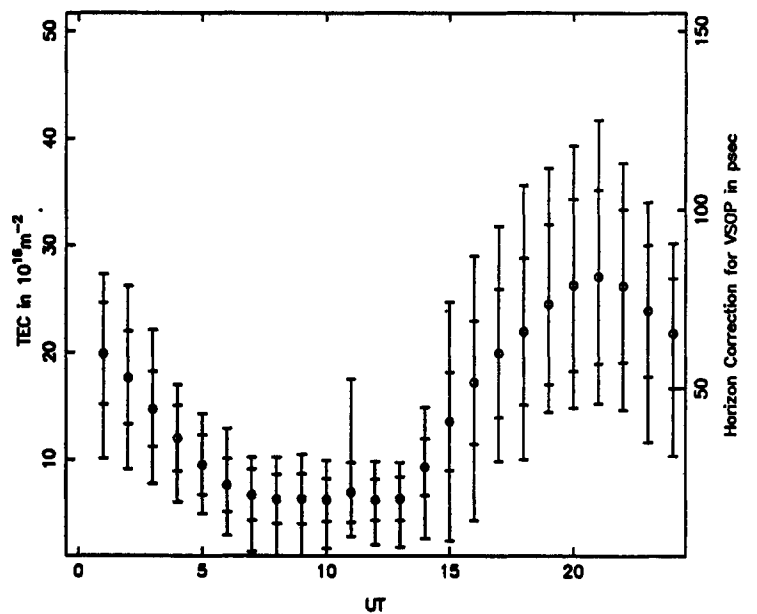
Monthly Averaged Boulder Zenthith TEC: February 1988



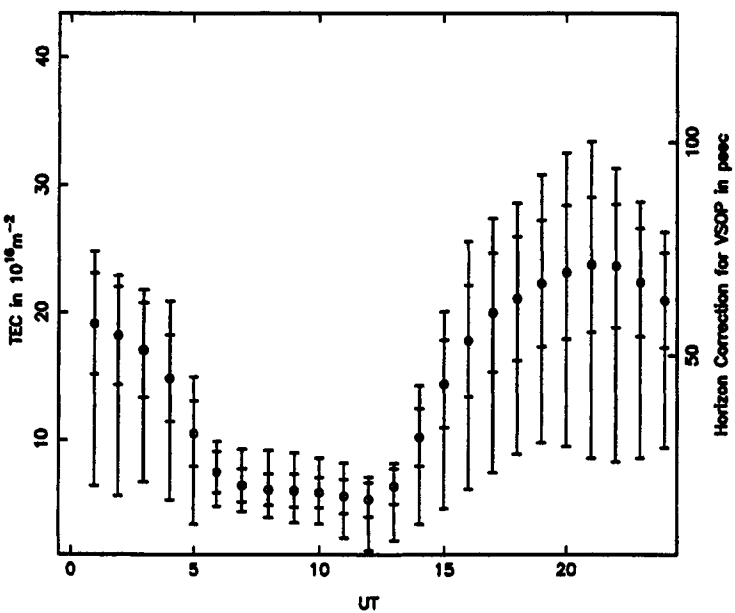
Monthly Averaged Boulder Zenthith TEC: March 1988



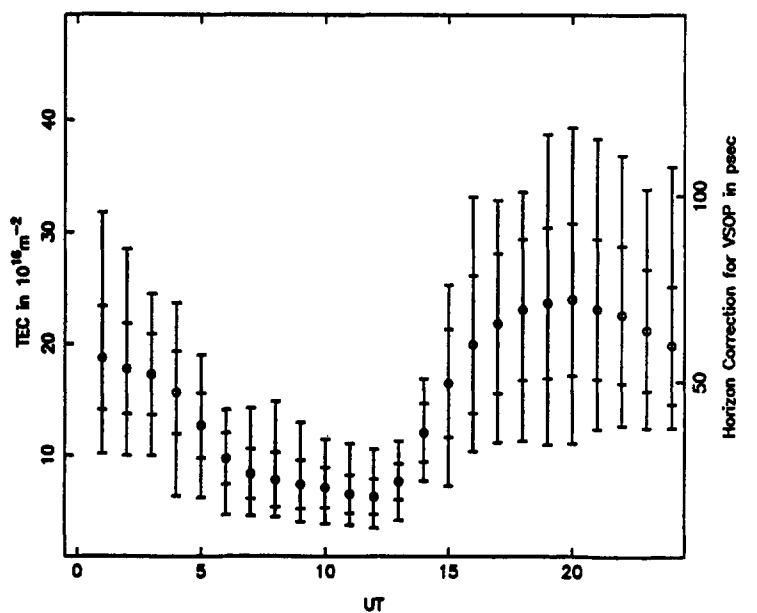
Monthly Averaged Boulder Zenthith TEC: April 1988



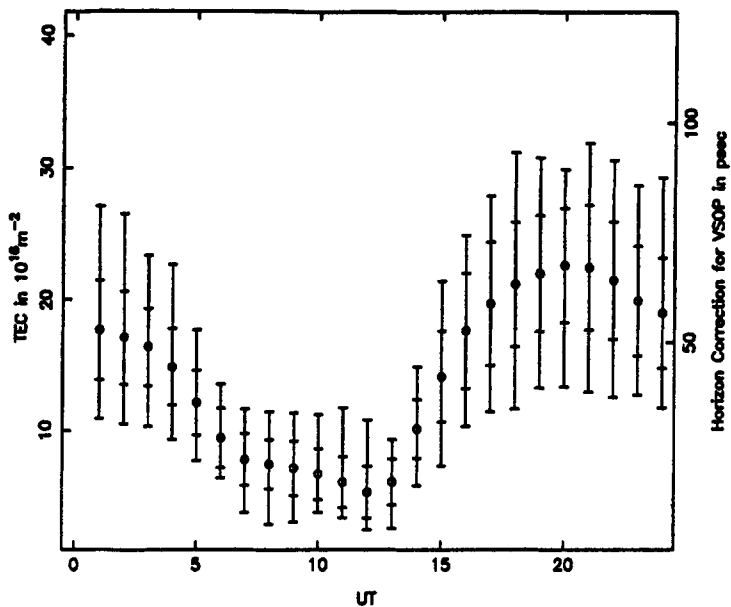
Monthly Averaged Boulder Zenthith TEC: May 1988



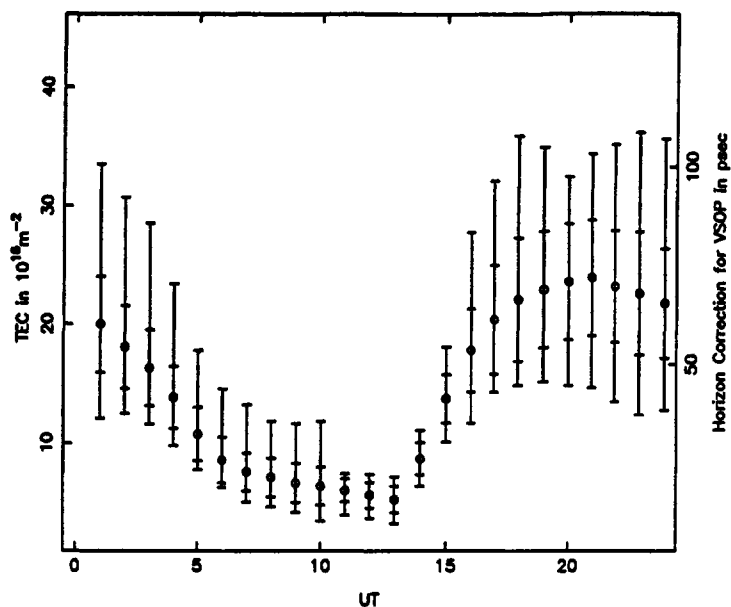
Monthly Averaged Boulder Zenthith TEC: June 1988



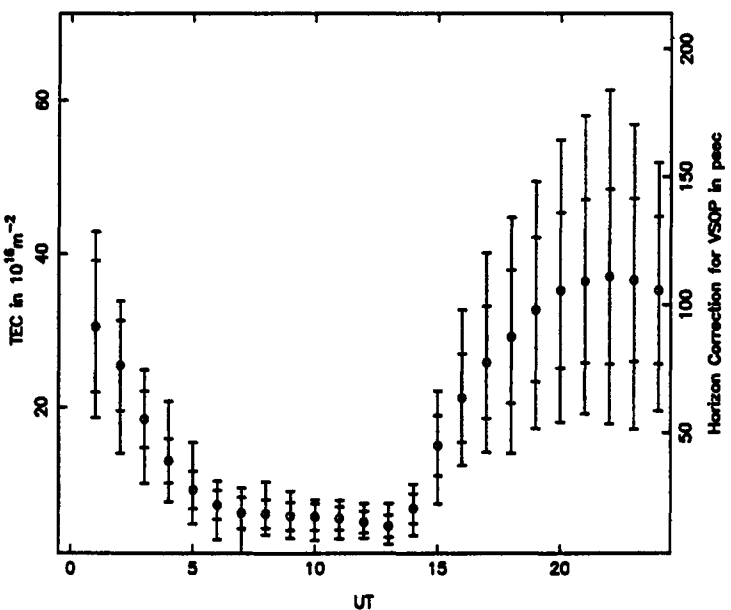
Monthly Averaged Boulder Zentith TEC: July 1988



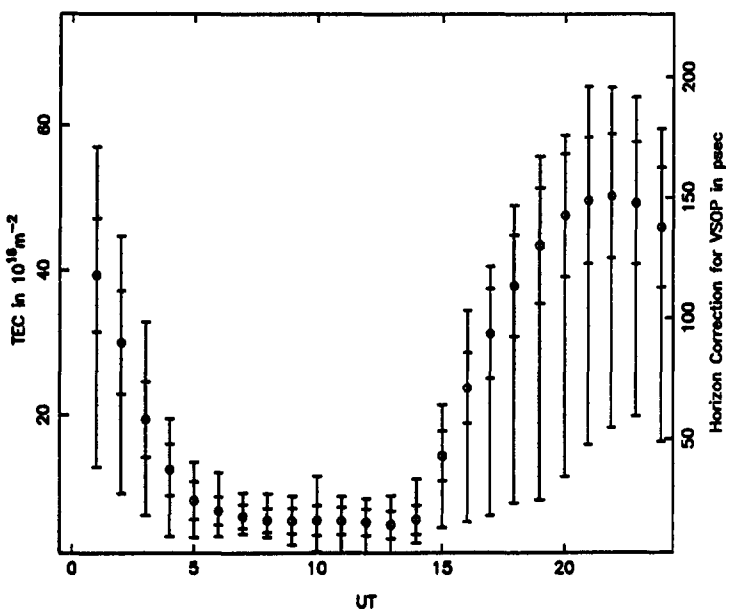
Monthly Averaged Boulder Zentith TEC: August 1988



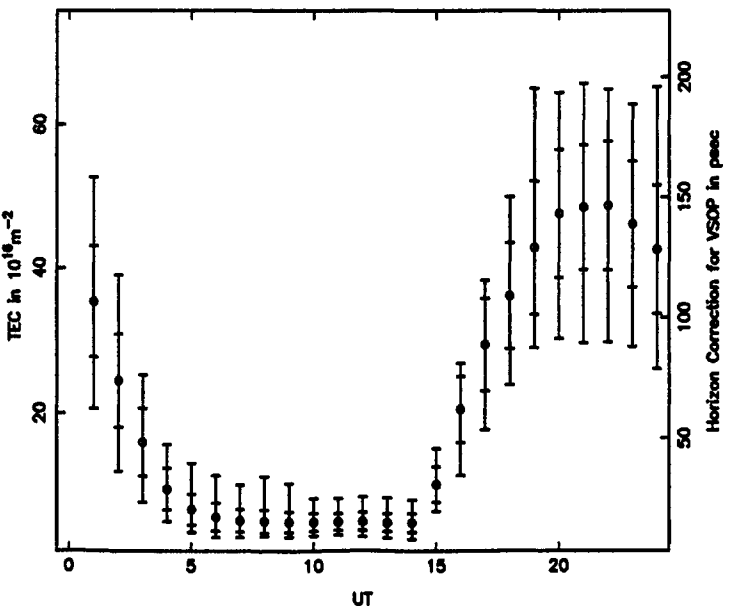
Monthly Averaged Boulder Zentith TEC: September 1988



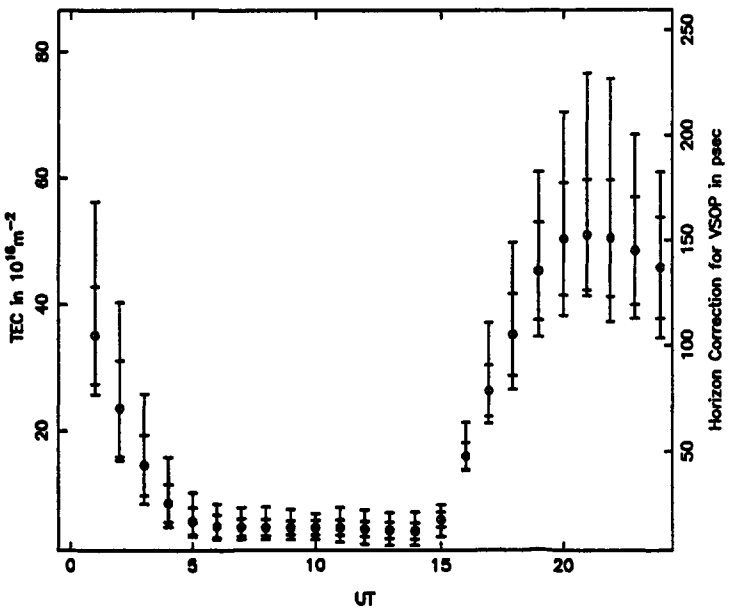
Monthly Averaged Boulder Zentith TEC: October 1988



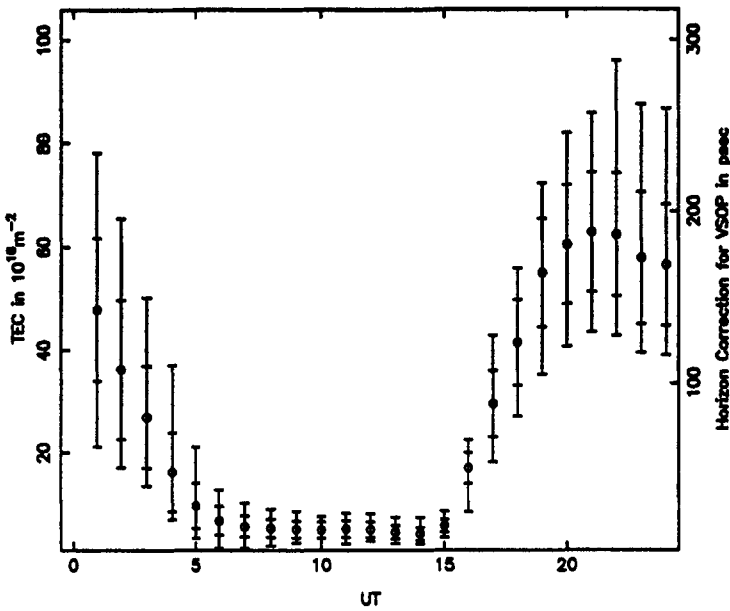
Monthly Averaged Boulder Zentith TEC: November 1988



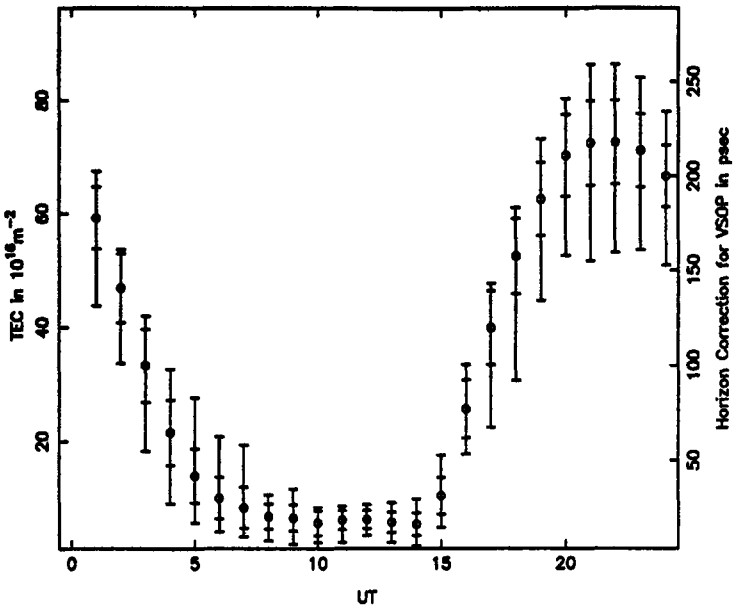
Monthly Averaged Boulder Zentith TEC: December 1988



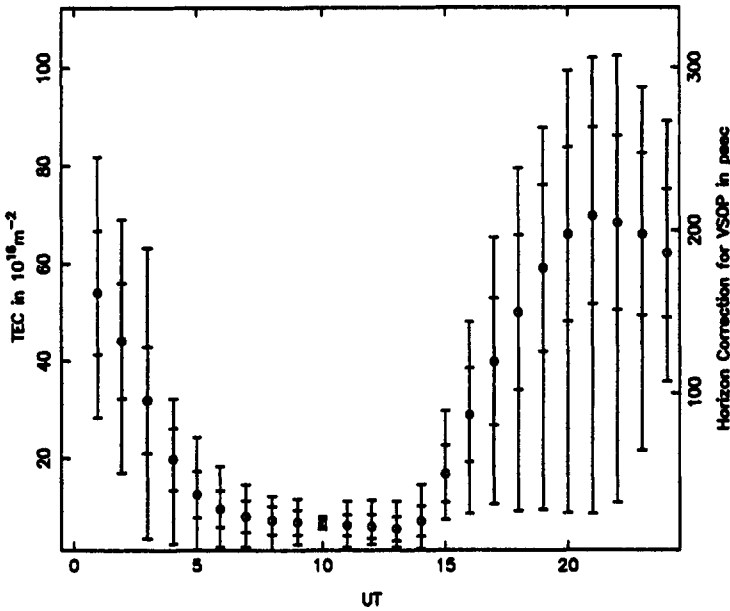
Monthly Averaged Boulder Zenthith TEC: January 1989



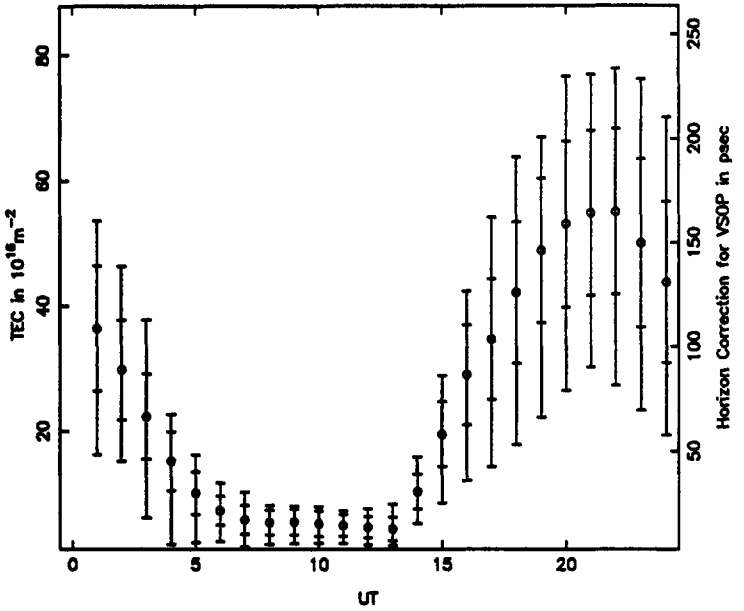
Monthly Averaged Boulder Zenthith TEC: February 1989



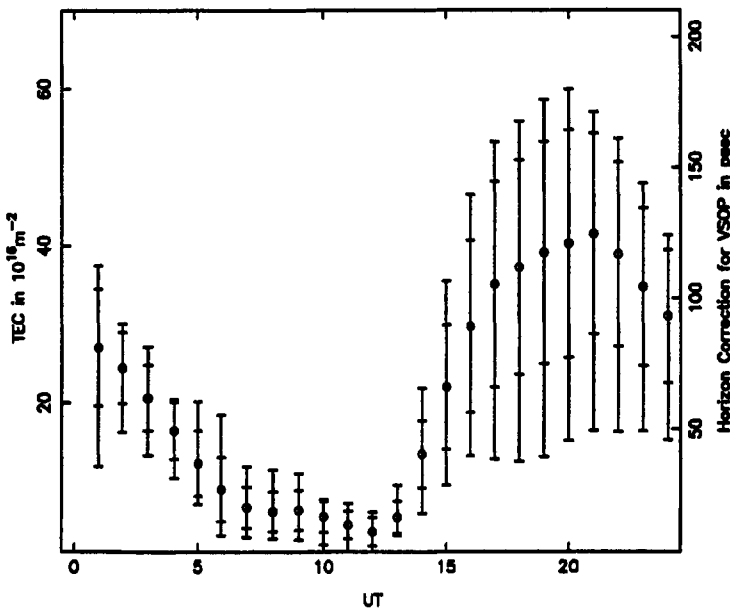
Monthly Averaged Boulder Zenthith TEC: March 1989



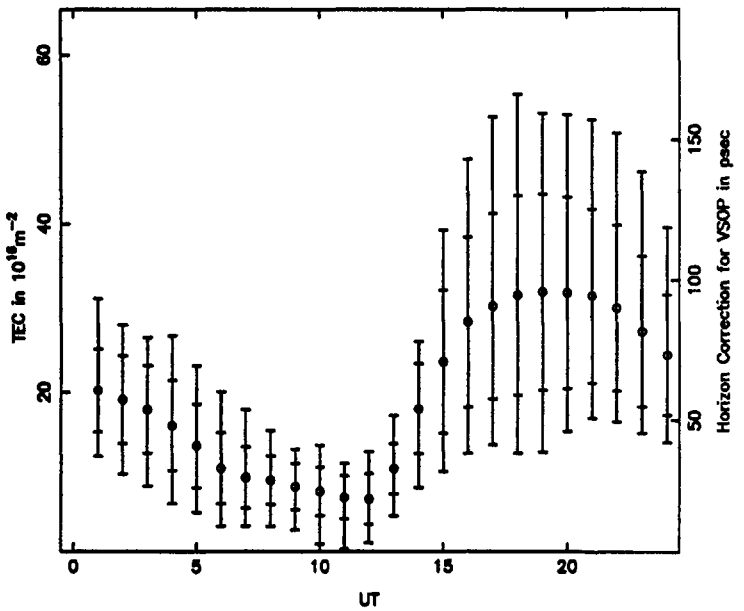
Monthly Averaged Boulder Zenthith TEC: April 1989



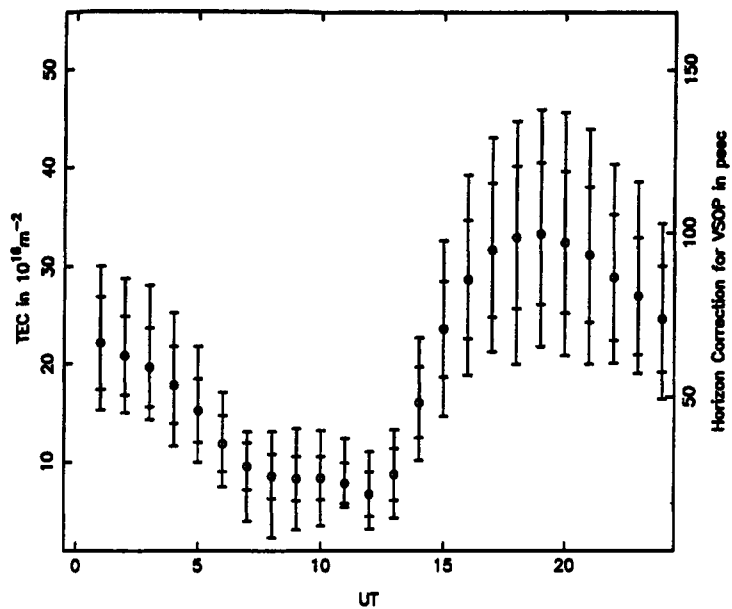
Monthly Averaged Boulder Zenthith TEC: May 1989



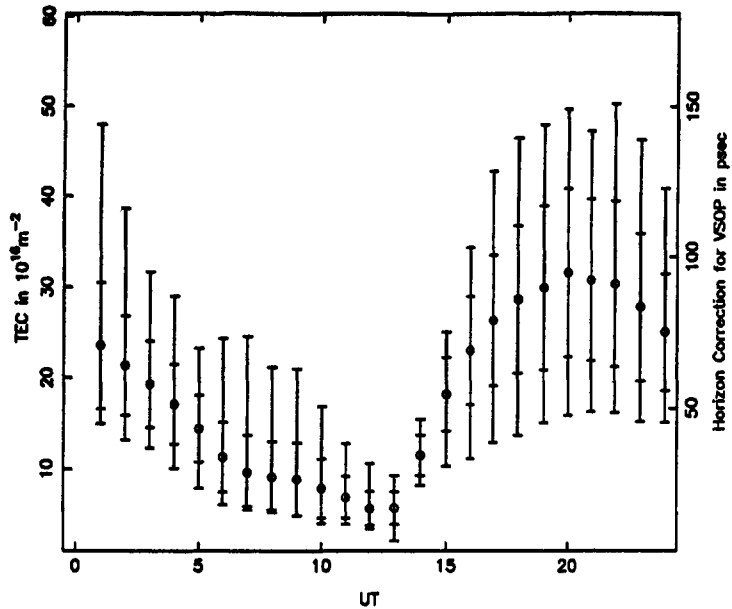
Monthly Averaged Boulder Zenthith TEC: June 1989



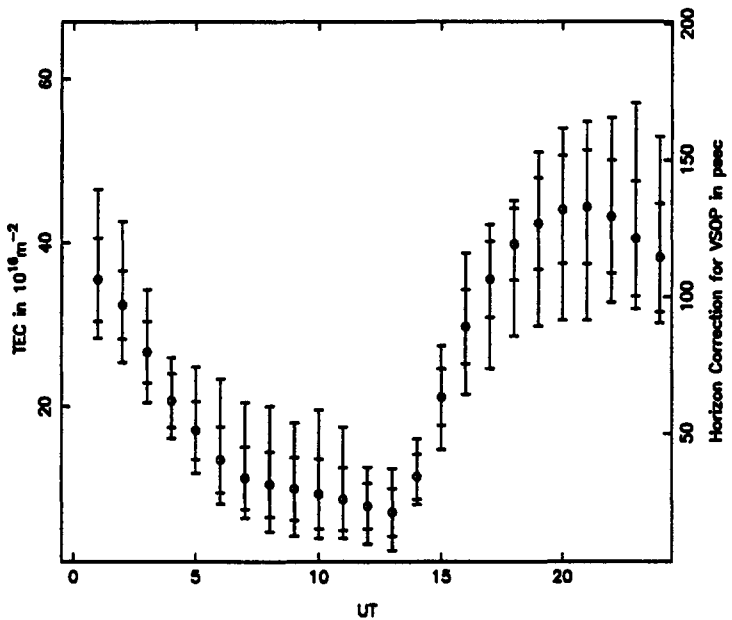
Monthly Averaged Boulder Zenith TEC: July 1989



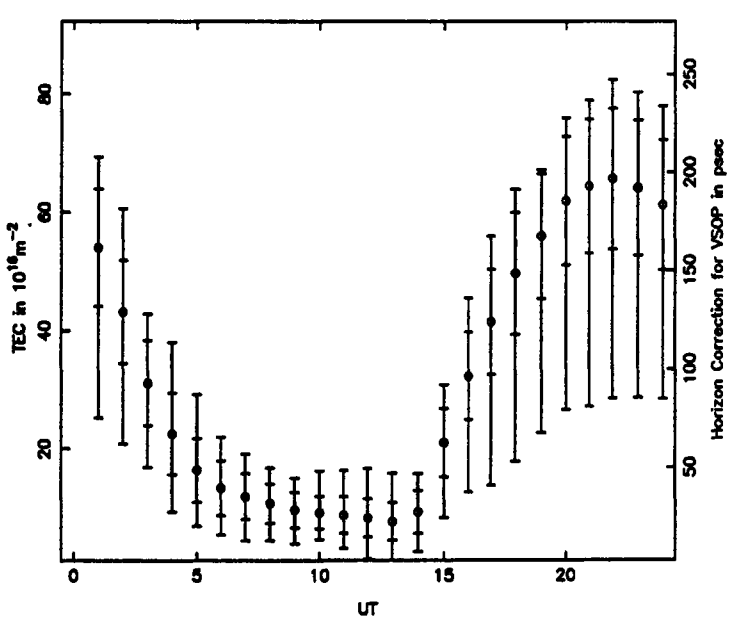
Monthly Averaged Boulder Zenith TEC: August 1989



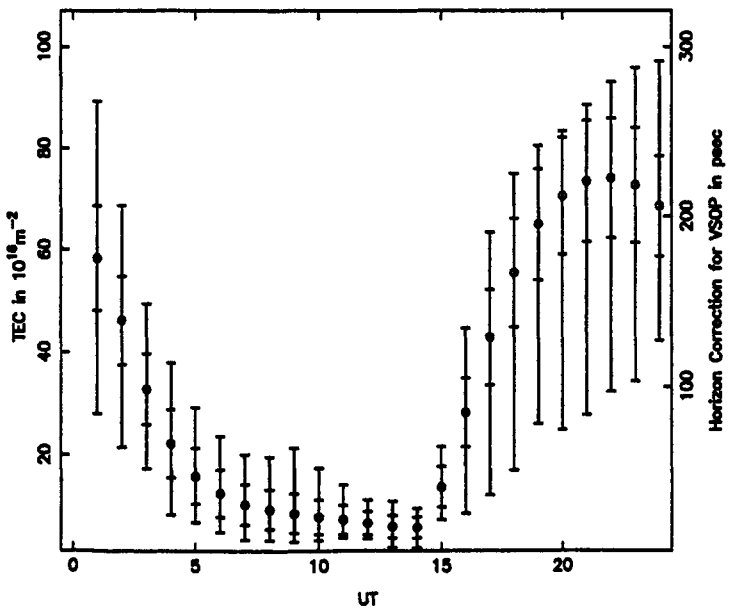
Monthly Averaged Boulder Zenith TEC: September 1989



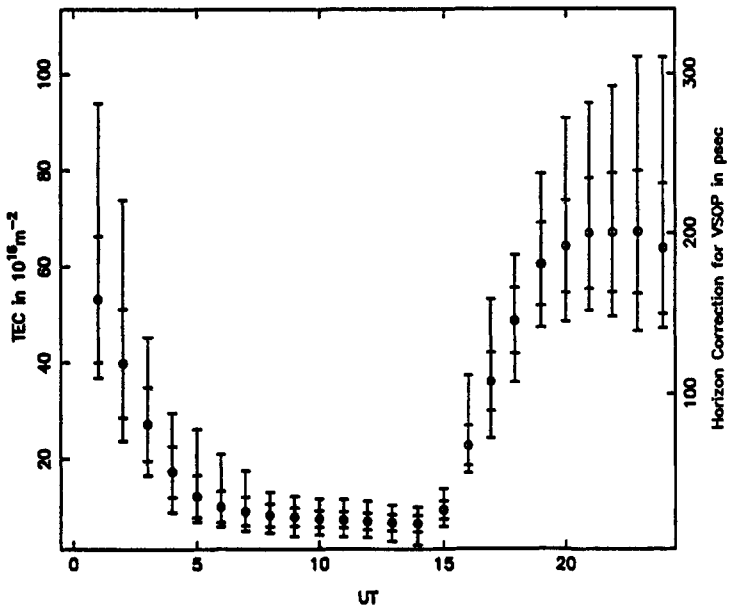
Monthly Averaged Boulder Zenith TEC: October 1989



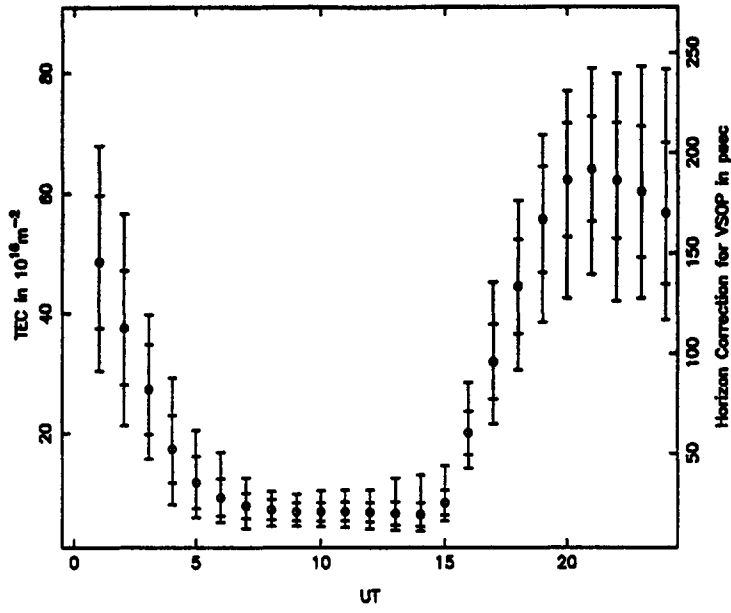
Monthly Averaged Boulder Zenith TEC: November 1989



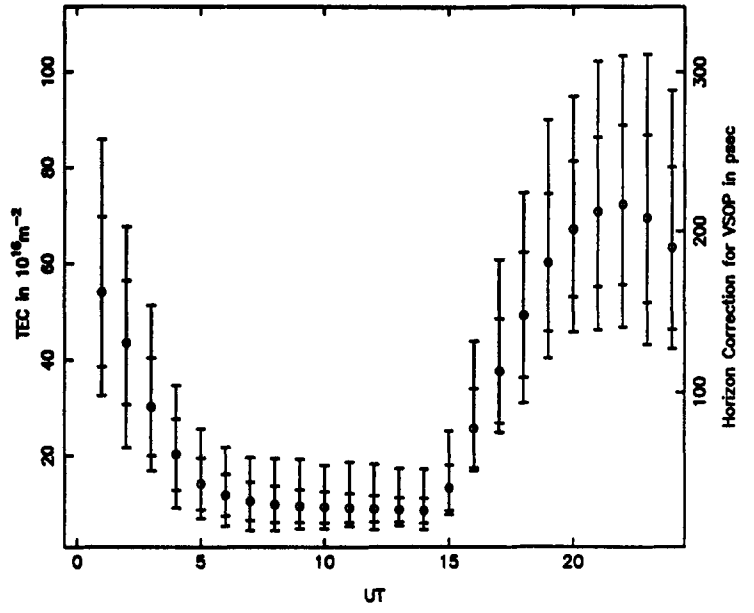
Monthly Averaged Boulder Zenith TEC: December 1989



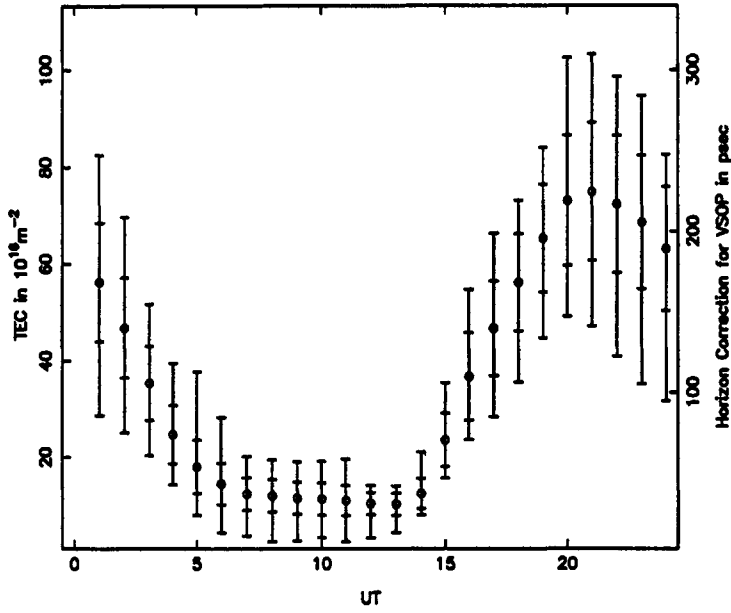
Monthly Averaged Boulder Zenith TEC: January 1990



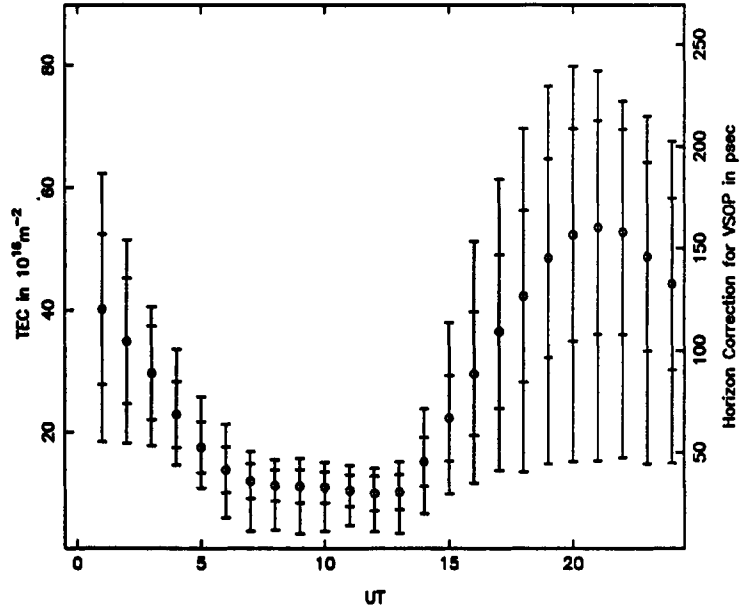
Monthly Averaged Boulder Zenith TEC: February 1990



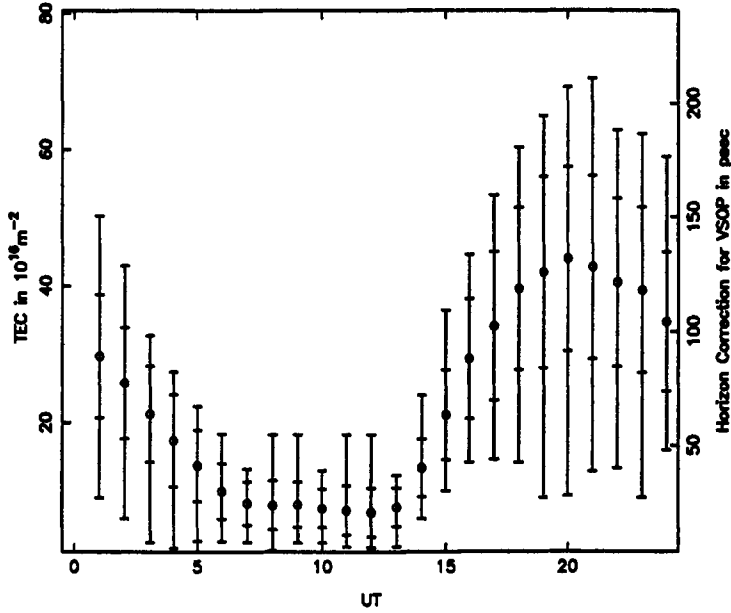
Monthly Averaged Boulder Zenith TEC: March 1990



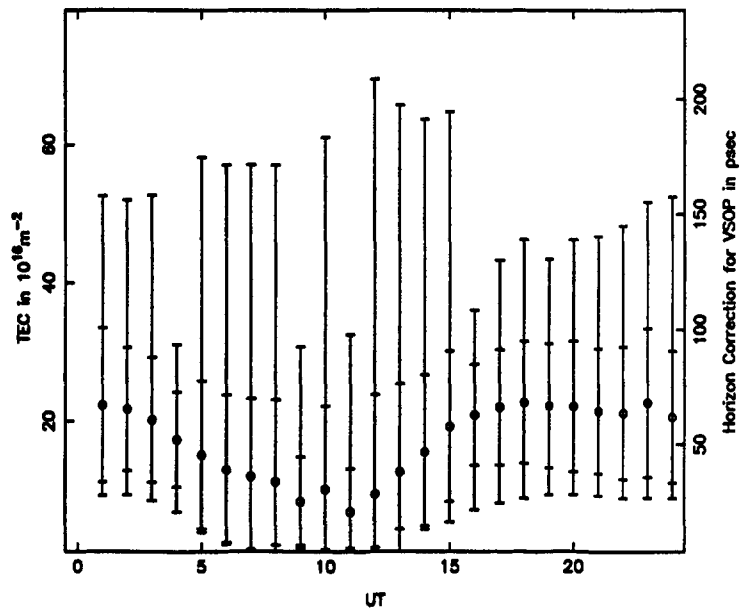
Monthly Averaged Boulder Zenith TEC: April 1990



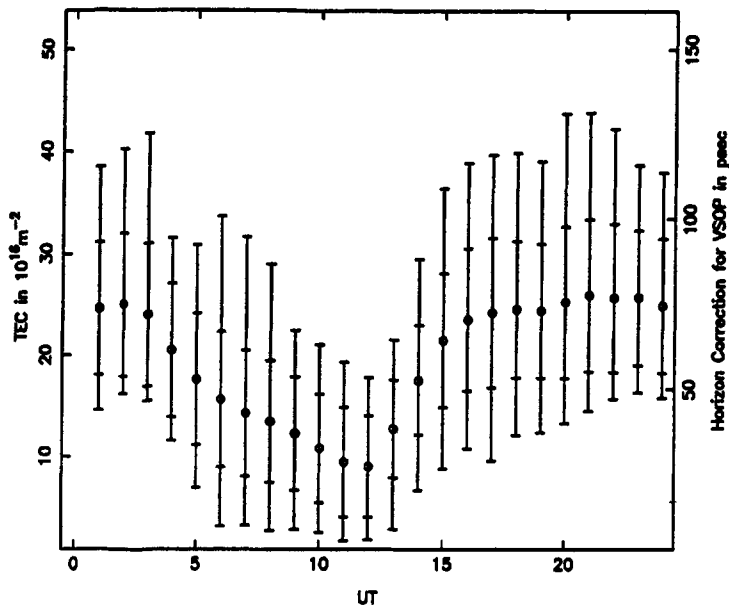
Monthly Averaged Boulder Zenith TEC: May 1990



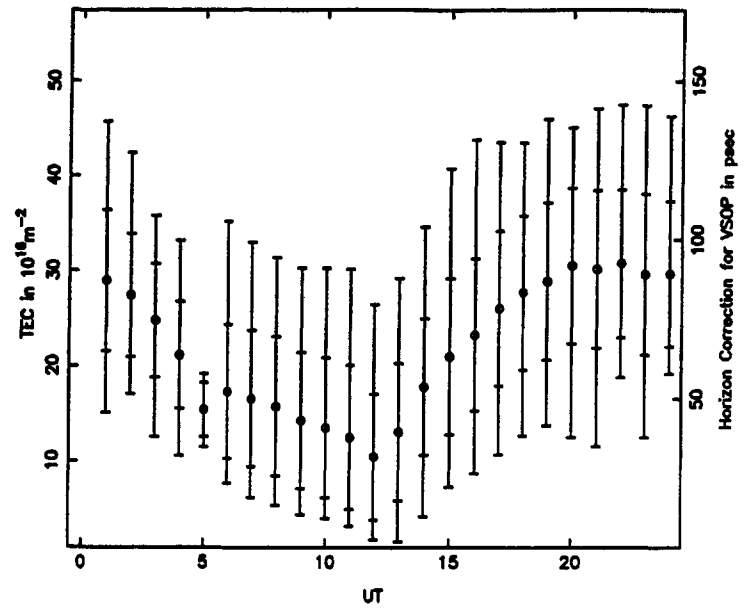
Monthly Averaged Boulder Zenith TEC: June 1990



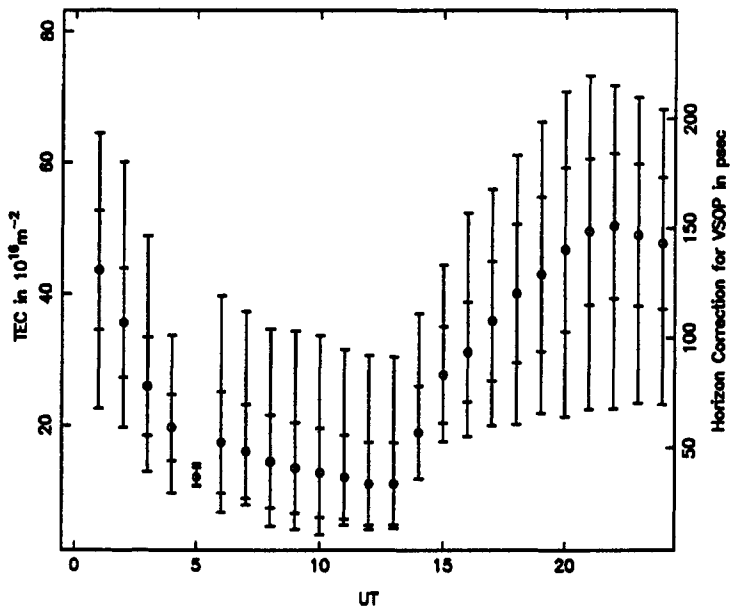
Monthly Averaged Boulder Zentith TEC: July 1990



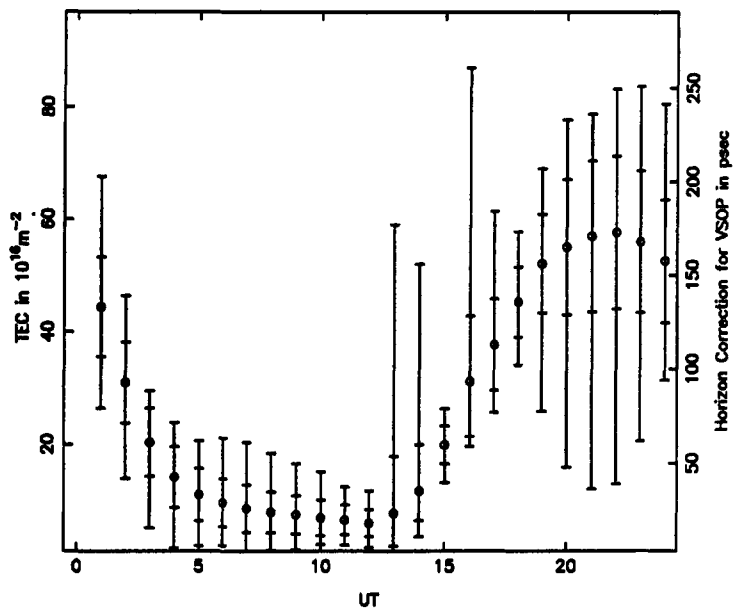
Monthly Averaged Boulder Zentith TEC: August 1990



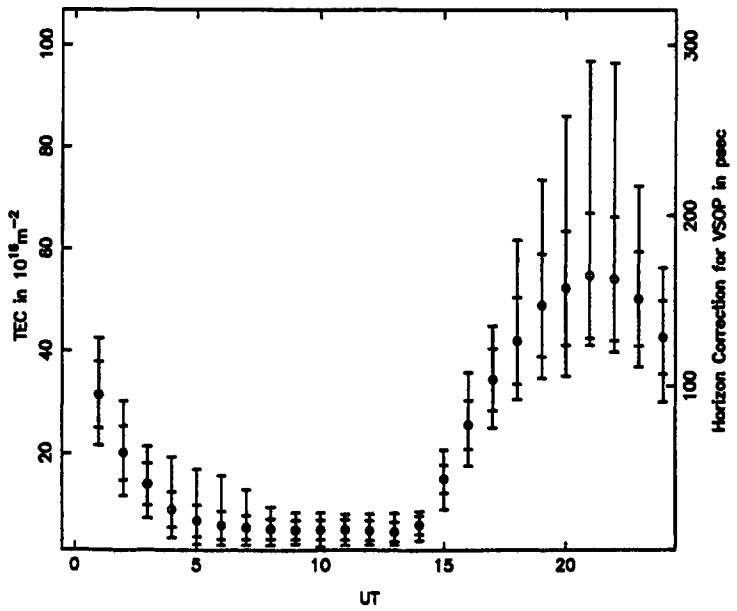
Monthly Averaged Boulder Zentith TEC: September 1990



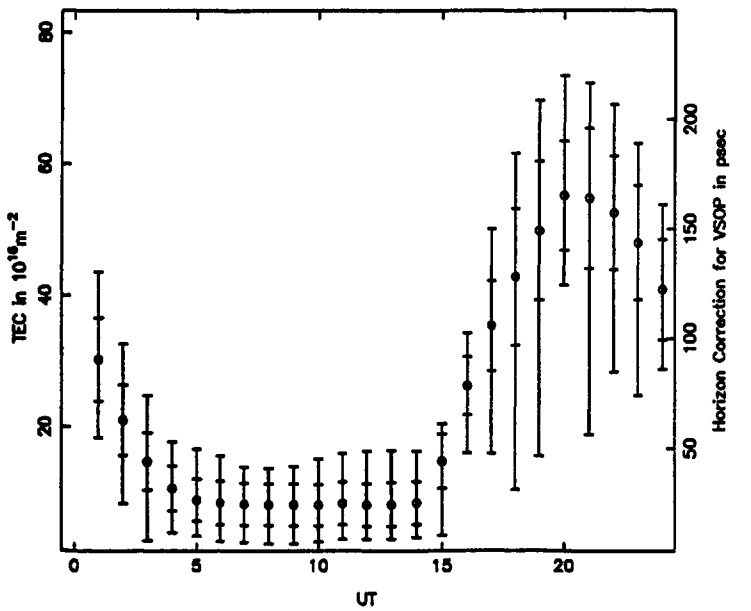
Monthly Averaged Boulder Zentith TEC: October 1990



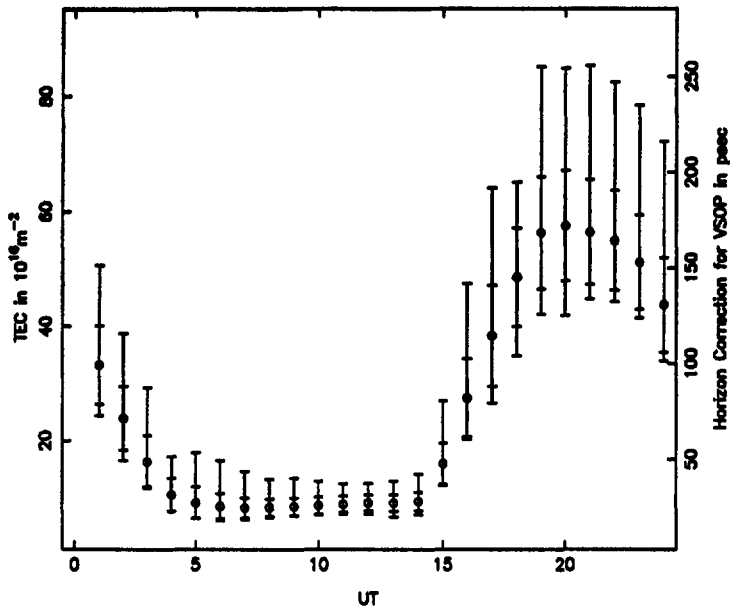
Monthly Averaged Boulder Zentith TEC: November 1990



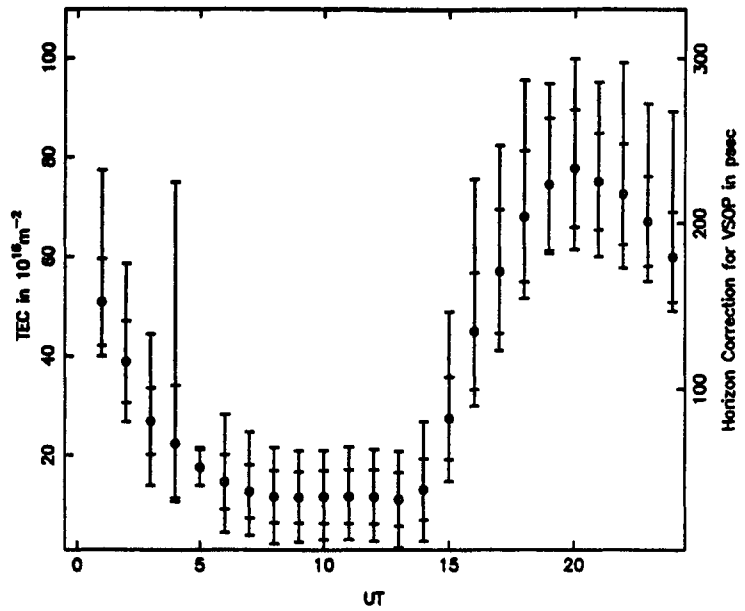
Monthly Averaged Boulder Zentith TEC: December 1990



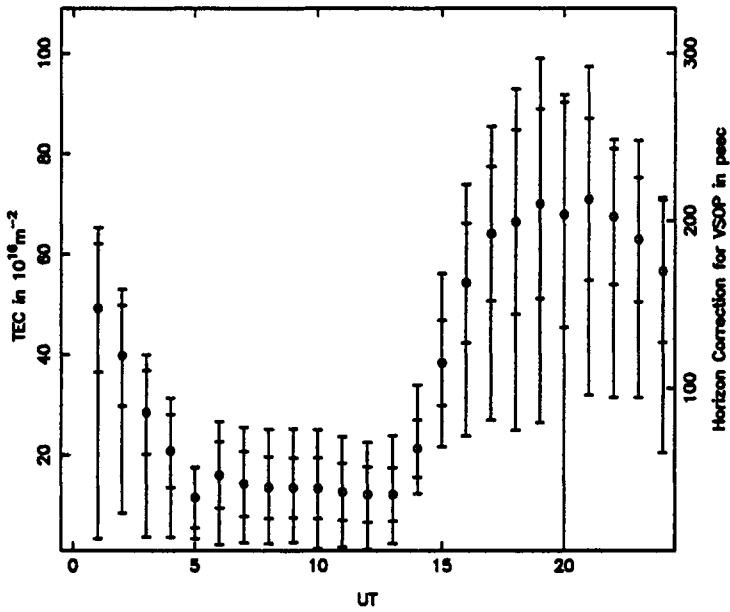
Monthly Averaged Boulder Zentith TEC: January 1991



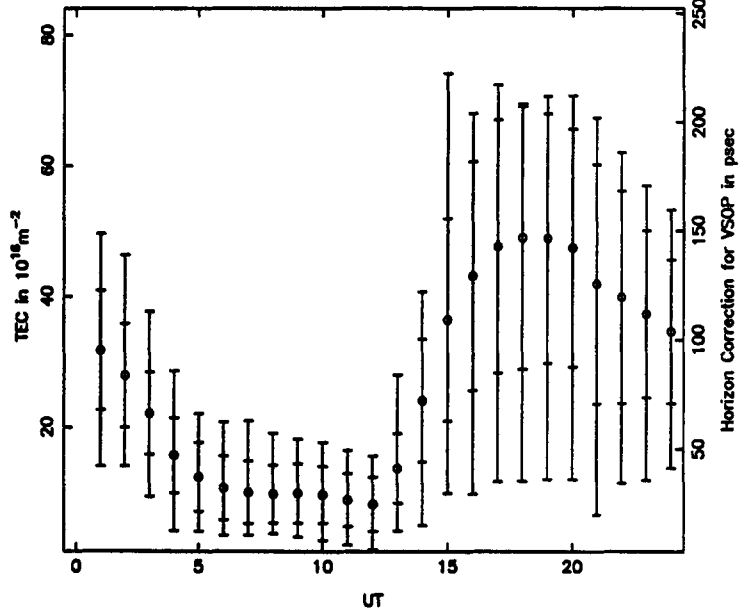
Monthly Averaged Boulder Zentith TEC: February 1991



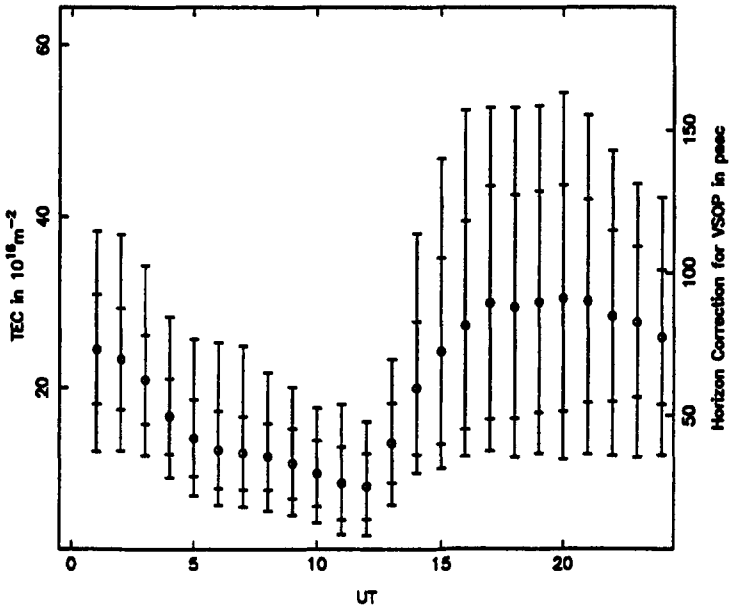
Monthly Averaged Boulder Zentith TEC: March 1991



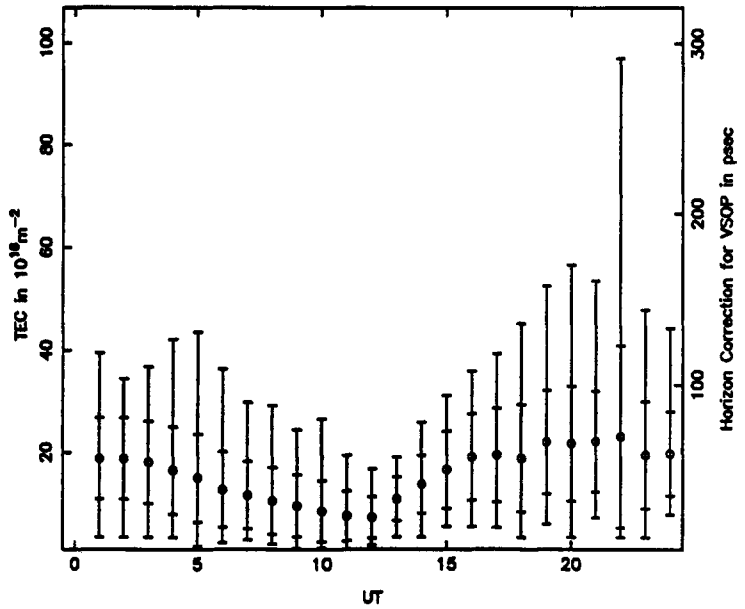
Monthly Averaged Boulder Zentith TEC: April 1991



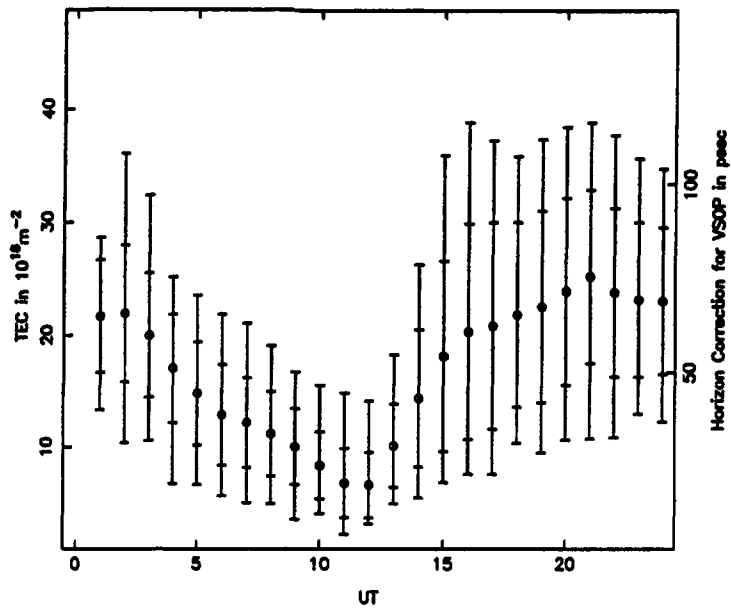
Monthly Averaged Boulder Zentith TEC: May 1991



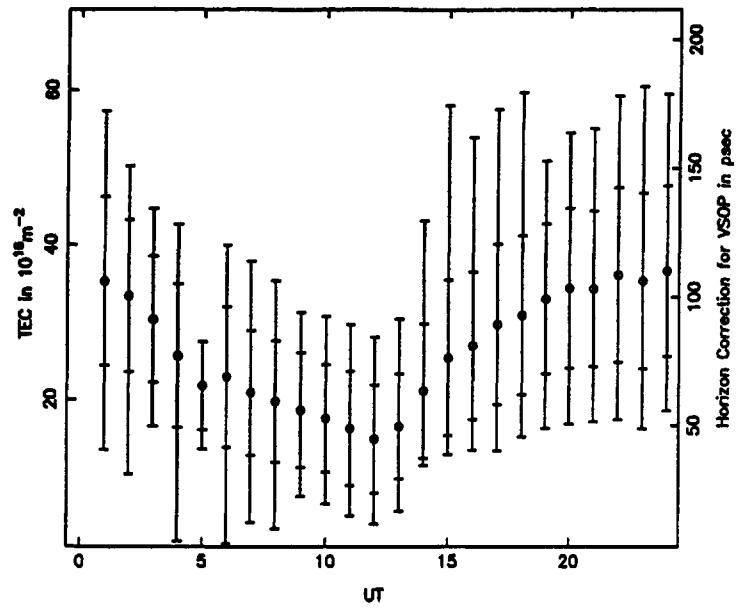
Monthly Averaged Boulder Zentith TEC: June 1991



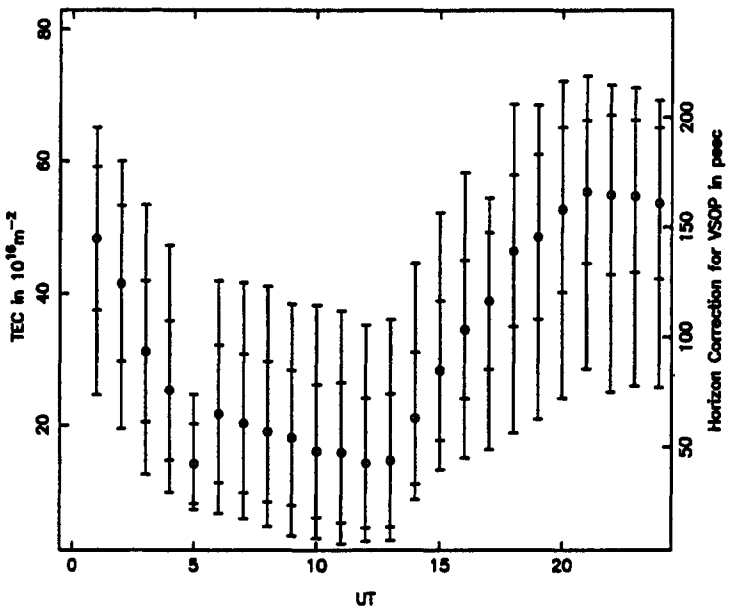
Monthly Averaged Boulder Zentith TEC: July 1991



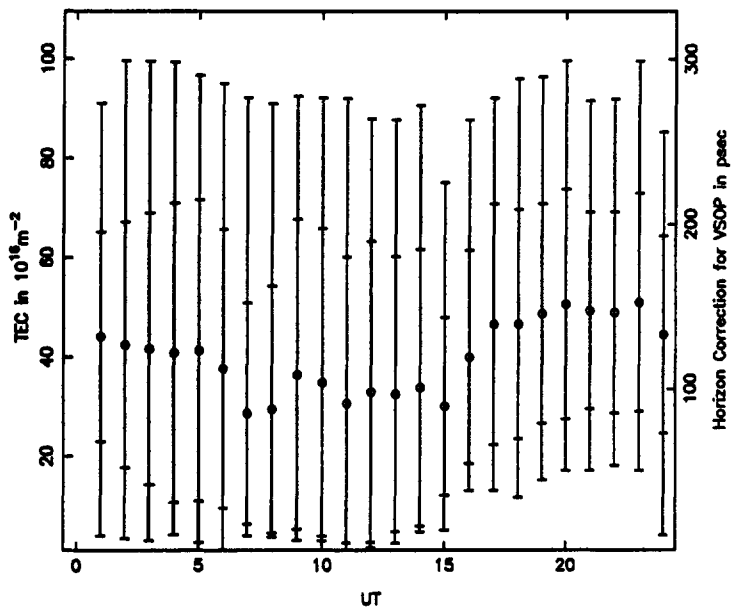
Monthly Averaged Boulder Zentith TEC: August 1991



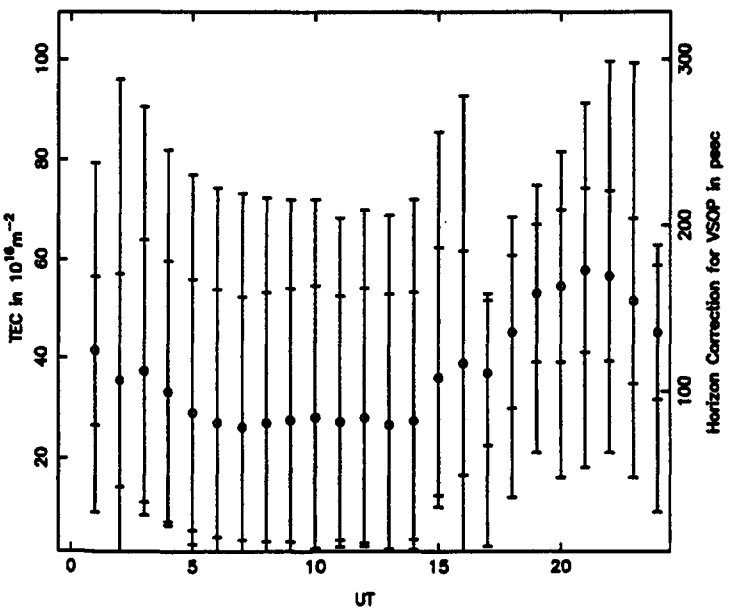
Monthly Averaged Boulder Zentith TEC: September 1991



Monthly Averaged Boulder Zentith TEC: October 1991



Monthly Averaged Boulder Zentith TEC: November 1991



Monthly Averaged Boulder Zentith TEC: December 1991

